ABSTRACT

Taiping pluton is an N-S elongated pluton located in the Bintang batholith. This batholith together with Main Range batholith, represent most of the granitoid within the Main Range granite province of Peninsular Malaysia. The Taiping amphibole-bearing melagranite, also known as the Buloh Pelang granite was briefly studied before. It is only recently, ultrapotassic "durbachite" type characteristics are found in these rocks. Taiping melagranite can be described as K-Mg rich, megacrystic to porphyritic, coarse grained, dark colored granite. Petrographic examination shows the rocks contain granite felsic mineral proportion with high amount of biotite, amphiboles (actinolite) with pyroxene relics and traces of pyroxene. The melagranite also contain mutliple mafic microgranular enclaves of various sizes. Most melagranite samples are ultrapotassic and intermediate in SiO_2 composition while showing high MgO and Cr. They are also high in certain incompatible elements (Ba, Zr, Rb, Th) and LREE. In general, the melagranite geochemistry is comparable to the Central European durbachite suite. The "durbachite" type melagranite petrogenesis is believed to be complex, requiring a crustal component and enriched lithospheric mantle source. The enrichment process could have been contributed by a previous subduction event. The Taiping pluton itself is located in the Sibumasu plate (which subducted under the Indochina plate before the collision) and U-Pb zircon dating results (218 ± 1.3 Ma) indicate that they are emplaced during the Triassic Sibumasu-Indochina collision (200 – 220 Ma), when most of the Main Range granite province are emplaced. To fit into the current tectonic model, I believe a minor episode of extension could have occurred during early contraction. As the plates continue to converge, compressive tectonic regime was re-established.

ABSTRAK

Pluton Taiping yang memanjang U-S terletak di Batholith Bintang. Batholith ini bersama-sama dengan batholith Banjaran Utama, mewakili kebanyakan granit dalam wilayah granit Banjaran Utama di Semenanjung Malaysia. Granit gelap amfibol Taiping, juga dikenali sebagai granit Buloh Pelang, telah dikaji secara ringkas sebelum ini. Ia hanya baru-baru ini, ciri-ciri ultrapotassic "durbachite" dijumpai dalam batu-batu ini. Granit gelap Taiping boleh digambarkan sebagai granit yang menunjukkan tekstur porphyritic dan megacrystic, kaya dengan K dan Mg, berbutir kasar dan berwarna gelap. Petrografi menunjukkan batu-batu itu menyerupai granit dengan biotit yang banyak dan mengandungi amfibol dan piroksen surih. Granit gelap ini juga mengandungi pelbagai "mafic microgranular enclaves" yang berlainan saiz. Kebanyakan sampel granit gelap adalah ultrapotassic dan mempunyai komposisi SiO_2 serdehana dan MgO dan Cr yang tinggi. Sampel-sampel juga menunjukkan nilai yang tinggi dalam kebanyakan "incompatible elements" (Ba, Zr, Rb, Th) and LREE. Secara umum, geokimia granit gelap boleh dibandingkan dengan kumpulan durbachite Eropah tengah. Petrogenesis granit gelap jenis durbachite ini dipercayai sangat kompleks, ia memerlukan sumber kerak dan lithosphere mantel yang diperkayakan. Proses pengayaan boleh disumbangkan oleh peristiwa subduksi sebelumnya. Pluton Taiping terletak di atas plat Sibumasu (mengalami subduksi ke bawah plat Indochina sebelum perlanggaran) dan keputusan U-Pb zirkon (218 ± 1.3 Ma) menunjukkan mereka terbentuk semasa perlanggaran Sibumasu-Indochina lewat Triassic (200 – 220 Ma), semasa kebanyakan granit di wilayah granit Banjaran Utama terbentuk. Untuk dimuatkan ke dalam model tektonik semasa, kami percaya satu episod pemanjangan yang kecil boleh berlaku semasa perlanggaran awal. Rejim tektonik mampatan akan ditubuhkan semula apabila perlanggaran bersambung.

TABLE OF CONTENTS

List of Figures

List of Tables

List of Appendices

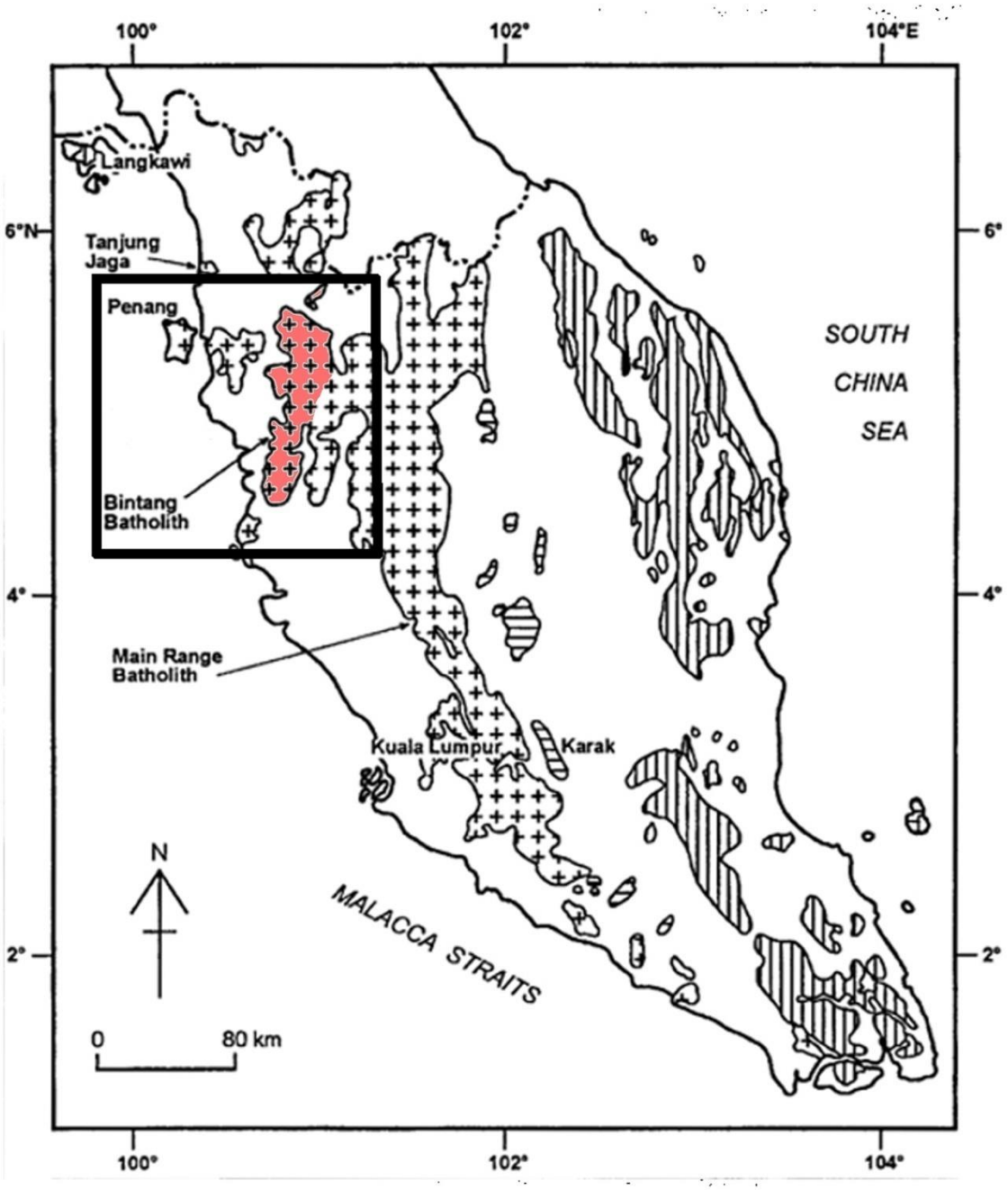

This map shows the outline of granitoid in Peninsular Malaysia. Bintang batholith (shaded in red) (which houses the study pluton and its melagranite) is located within the black box. Map is adapted from Ghani (2000).

CHAPTER 1: INTRODUCTION

1.1 Aims and objectives of the study

This research is primarily focused on the Taiping pluton's amphibole-bearing melagranite (within the Bintang batholith), an unusual granitoid that contains multiple I-type characteristics which deviates from the typical S-type Main Range granite province (Liew, 1983). Ghani et al. (2013) have previously suggested Main Range granite province contain both I- and S-type granitoid. Below are the research objectives:

1. To report petrography and geochemistry of the melagranite
2. To review the I-S classification for the melagranite
3. To correlate and compare the melagranite with the typical Main Range granite
4. To deduce the possible source and tectonic setting for the melagranite

1.2 Research structure

This thesis consists of six chapters where Chapter 1 will provide plain introduction by discussing about the research objectives, general geographical information and general geology of Peninsular Malaysia. Chapter 2 will discuss about the previous literatures on the research area (Taiping pluton) and other research works related to this research, namely ultrapotassic classification and European durbachite research. Field observation and research methodology will be explained in the next chapter which is Chapter 3 while Chapter 4 will discuss about the petrography of both melagranite and enclaves. Chapter 5 will present the melagranite and enclaves geochemical data, including comparison with European durbachite and Peninsular

Malaysia Main Range granite. The thesis is ended with Chapter 6, which gives the discussion to the questions brought up by the objectives in Chapter 1. A full summary about this research is also included in the same chapter.

1.3 Physiography

Malaysia covers a land area of about 329,847 km^2, consisting of the Peninsular Malaysia which lies on the southeastern end of Asia, and the states of Sabah and Sarawak in the northwestern coast of Borneo Island. The two regions are separated by the South China Sea. Peninsular Malaysia, covering 132,090 km^2, is bounded by a border with Thailand to the north and Singapore in the south. Peninsula Malaysia contains numerous mountain ranges running parallel from north to south along the peninsula. Most mountains are mainly composed of granite, but exposed outcrops are rare due to heavy tropical forest.

The main mountain range is the Titiwangsa Mountains, which divides the peninsula into east and west coasts. The Bintang mountain range is located on the west of Titiwangsa Mountains. Bintang Mountains runs from southern Thailand in the north to the general south of Perak. The currently inactive Bokbak fault (a prominent fault in Peninsular Malaysia) crosses the northern Bintang mountain range. Fig. 1.1 shows the terrain map for Bintang mountain range.

The particular Bintang mountain range section of interest is primarily located in Perak state. The state of Perak covers an area of 21,035 km^2; it is the second largest Malaysian state in the Malay Peninsula, and the fourth in the whole of Malaysia. Most of the mountain area is covered by heavy tropical rainforest. Only part of the forest has been cleared to cultivate commercial plants.

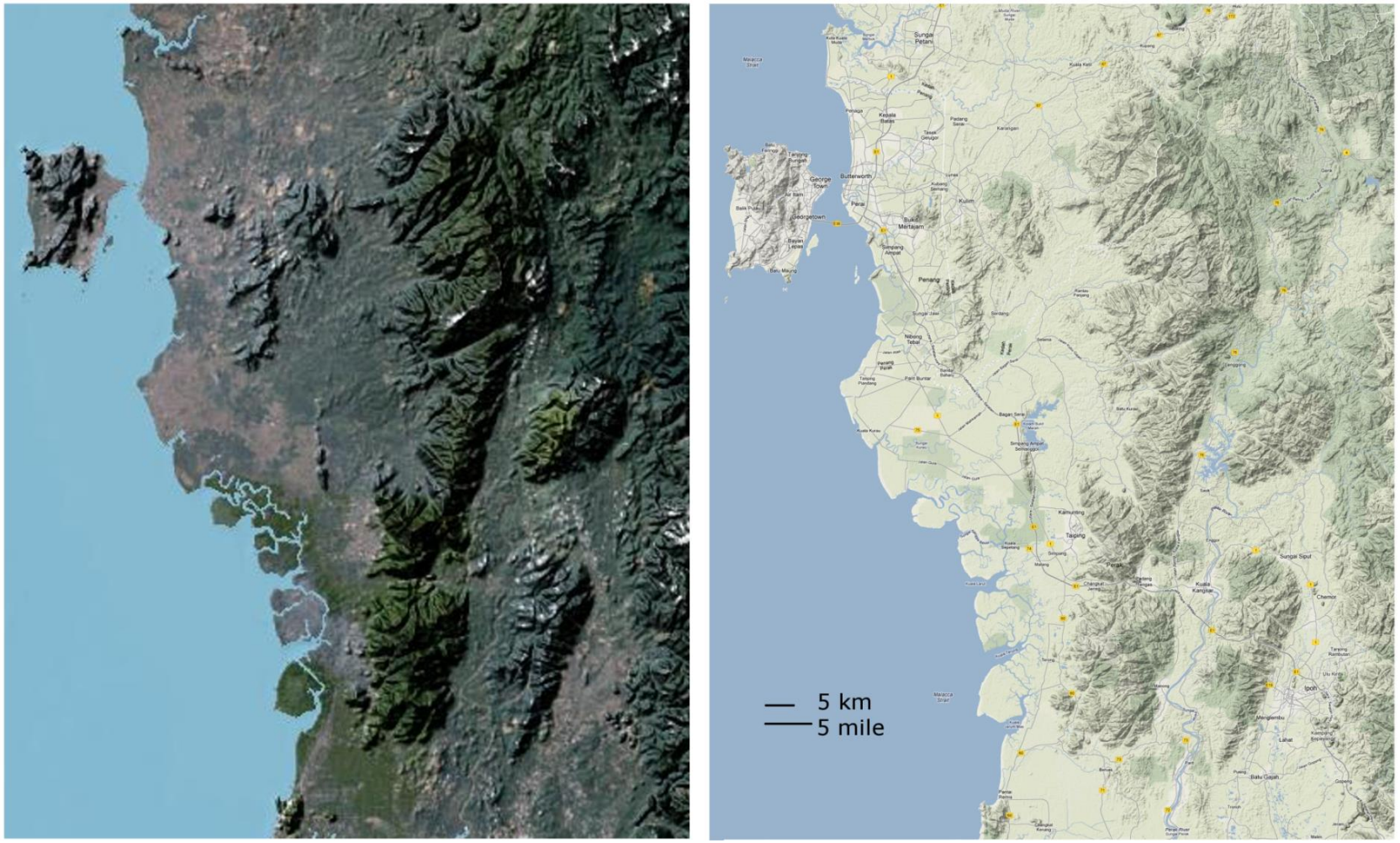

Fig. 1.1: Terrain Map of Bintang batholith

Peninsular Malaysia L7030 series 1:50000 topographic maps that cover the Taiping pluton area are: 3462, 3463 and 3464 (Southern part of Taiping and Bubu pluton); 3465 (mainly Selama pluton); 3466, 3566 and 3565 (Northern part of Taiping pluton and Damar pluton). My research area is mainly located within the Taiping pluton area covered by these maps.

1.4 Location and accessibility

Taiping pluton, an elongated intrusion that makes up the bulk of the Bintang mountain range (Bintang batholith) is located at the state of Perak. The batholith is very close to the Main Range batholith; the distance between the two batholiths varies from 10 to 30 km. The southern section of Taiping pluton starts at Beruas town, and extends northwards to Selama pluton, another pluton in the Bintang batholith (the contact is believed to be parallel with Sungai Ijok and Sungai Termelong). The North-South Expressway cut through the southern pluton.

The northern section of Taiping pluton starts near Gerik town and extend northwest towards Baling town. There are numerous tar roads around the northern pluton section. Well exposed outcrops are sometimes found along the roadside and large boulders are found in nearby drainage basins connected by the roads. Main tar roads around the batholith is shown in Fig. 1.2

Fig. 1.2: Map showing roads around the batholith

1.5 General geology

Generally, Southeast Asia comprises of a collage of allochthonous continental fragments and volcanic arcs joined together by suture zones, which represent the presence of ancient ocean basins that once separated the fragments/arcs. It is suggested that the Southeast Asia continental pieces were derived from the ancient southern hemisphere supercontinent Gondwana (Metcalfe, 1988). They were gradually assembled during Late Paleozoic to Cenozoic by convergent tectonic activity, which ended with present day continuing collision of India with Asia and Australia with Southeast Asia (Metcalfe, 2013).

1.5.1 General geology of Bintang batholith area

The Main Range province granite is formed in a terrain dominantly composed Paleozoic formations (Cobbing et al., 1992). For the Bintang batholith, there are at least five main sedimentary rocks of different ages surrounding the batholith:

1. Cambrian to Devonian Baling Group
2. Silurian to Permian Kinta Limestone
3. Carboniferous to Permian Kati Formation
4. Triassic Semanggol Formation
5. Tertiary Lawin basin

Paleozoic stratigraphy is summarized in Table 1.1. Locations of the sedimentary basins are shown in Fig. 1.4. Baling group is generally located at the north and west of the batholith, while Kati formation, Kinta Limestone and Lawin basin is located at the east and south of the batholith. Semanggol formation is located at the west of the batholith.

Table 1.1: Paleozoic stratigraphy around the Bintang Batholith

Period	Bintang Batholith area				
Permian					
Carboniferous				Kinta Limestone	Kati Fm.
Devonian					
Silurian	**Baling Group**	Bendiang Riang Fm.		Kroh Fm.	
Ordovician		Lawin Tuff	Gerik Fm.		
Cambrian		Papulut Quartzite (?)			

Adapted from Lee (2009)

The Baling Group starts with the undated Papulut Quartzite at its base. This basal sequence is succeeded by thick variably bedded turbidites of the Gerik Formation (Lee, 2009). The sequence is followed by Bendiang Riang Formation, which contains phyllite and metamorphosed limestone (Lee, 2009). Also included in the group is the Lawin Tuff, an acid rhyolitic crystal tuff of possible Ordovician to Early Silurian age (Lee, 2009). The volcanic rocks are found interbedded with Baling group units and is faintly visible (Lee, 2009).

The Kroh Formation, formed around the same time as the Baling Group, has a conformable contact with the Papulut Quartzite. It contains black carbonaceous shale, siliceous mudstone with chert, subordinate lenses of arenite and calcareous rocks commonly recrystallized to hornfels, metaquartzite and pseudo sparite (Lee, 2009). The age of this formation as determined from fossil study is from Upper Ordovician to Lower Devonian (Burton, 1986).

Kinta Limestone is found in plenty around Kinta valley, where they are well studied. The deposition of limestone appears to be nearly continuous from Silurian to

Permian with no evidence of a Devonian orogeny (Lee, 2009). Kati Formation, occur between the Bintang and Kledang ranges, are made up of metamorphosed reddish brown to purplish carbonaceous shale, siltstone, mudstone and rare sandstone with minor conglomerate and lenses of carbonaceous limestone (Lee, 2009). A probable Carboniferous to Permian age is assigned and they are interpreted to be equivalent to Kubang Pasu Formation (Hutchison, 2007; Lee, 2009).

Semanggol Formation, named after Gunung Semanggol, is made up of argillaceous-arenaceous rocks of Upper Middle Triassic (Ladinian) to Lower Upper Triassic age (Carnian) (Burton, 1973). Bintang batholith granitoid magma is believed to have intruded around the same time. Semanggol formation is divided by Burton (1973) into three informal members: chert, rhythmite (sediment or sedimentary rock layers which are deposited with clear periodicity and regularity) and conglomerate members.

The Lawin Basin contains the youngest sedimentary rock in the Bintang batholith area. The basin deposit comprises of poorly graded sediments ranging from sand, grit, gravel and boulders (Raj et al., 2009). Majority of the materials are believed to have a granitic source (Raj et al., 2009). The deposition of Lawin basin is proposed to have occurred during the Tertiary (Jones, 1970).

1.5.2 Granites in Peninsular Malaysia

The granite province of Southeast Asia can be subdivided into (a) Eastern (East Peninsular Malaysia), (b) Main Range (South Thailand-West Peninsular Malaysia), and (c) Northern (Northern Thailand) and Western (Southwest Thailand–East Myanmar) granite provinces (Fig. 1.4) (Cobbing et al., 1992; Ghani et al., 2013). The Eastern and Main Range Granite provinces are found in Peninsular Malaysia, separated by the Bentong–Raub suture (Metcalfe, 2000, 2013). The Eastern granite province consists of Permian to Mid-Triassic I-type granitoids which includes gabbro, diorite, tonalite and

monzogranite (Cobbing et al., 1992; Ghani et al., 2013). The Late Triassic to Early Jurassic Main Range Granite is mainly granite to granodiorite (Ghani et al., 2013).

Basically, ignoring several tiny outlying plutons, Main Range granite province can be classified into two major batholiths, the larger Main Range batholith and the smaller Bintang batholith. The typical granite facies of Main Range batholith is described as texturally coarse to very coarse grained megacrystic biotite-muscovite granite and the mineralogy is high Al-biotite, muscovite and Mn-rich garnet (Ghani, 2000). Enclaves present within the granite province were thought to be of metasedimentary origin (Cobbing et al., 1992). Besides plutonic rocks, felsic volcanic rocks are also found within the Main Range granite province. Genting Sempah complex is one of the best known volcanic complexes, and it contains rhyodacite and orthopyroxene rhyodacite (Ghani, 2000).

The main study area, Taiping pluton is located within Bintang batholith. Besides Taiping pluton, Selama pluton, Damar pluton, and Bubu pluton (which will be shown in Fig. 2.1 and discussed in the next chapter) are important plutons that make up the Bintang batholith (Bintang batholith granitoid outline and surrounding sedimentary rocks are shown Fig. 1.4). The batholith houses several kinds of granite and the unique amphibole-bearing melagranite is one of them. The said melagranite is the main focus of this study and it primarily resides within Taiping pluton. This particular granite deviates from the Main Range granite province typical granite facies, where amphiboles are absent and aluminosilicate, muscovite and garnet are more common.

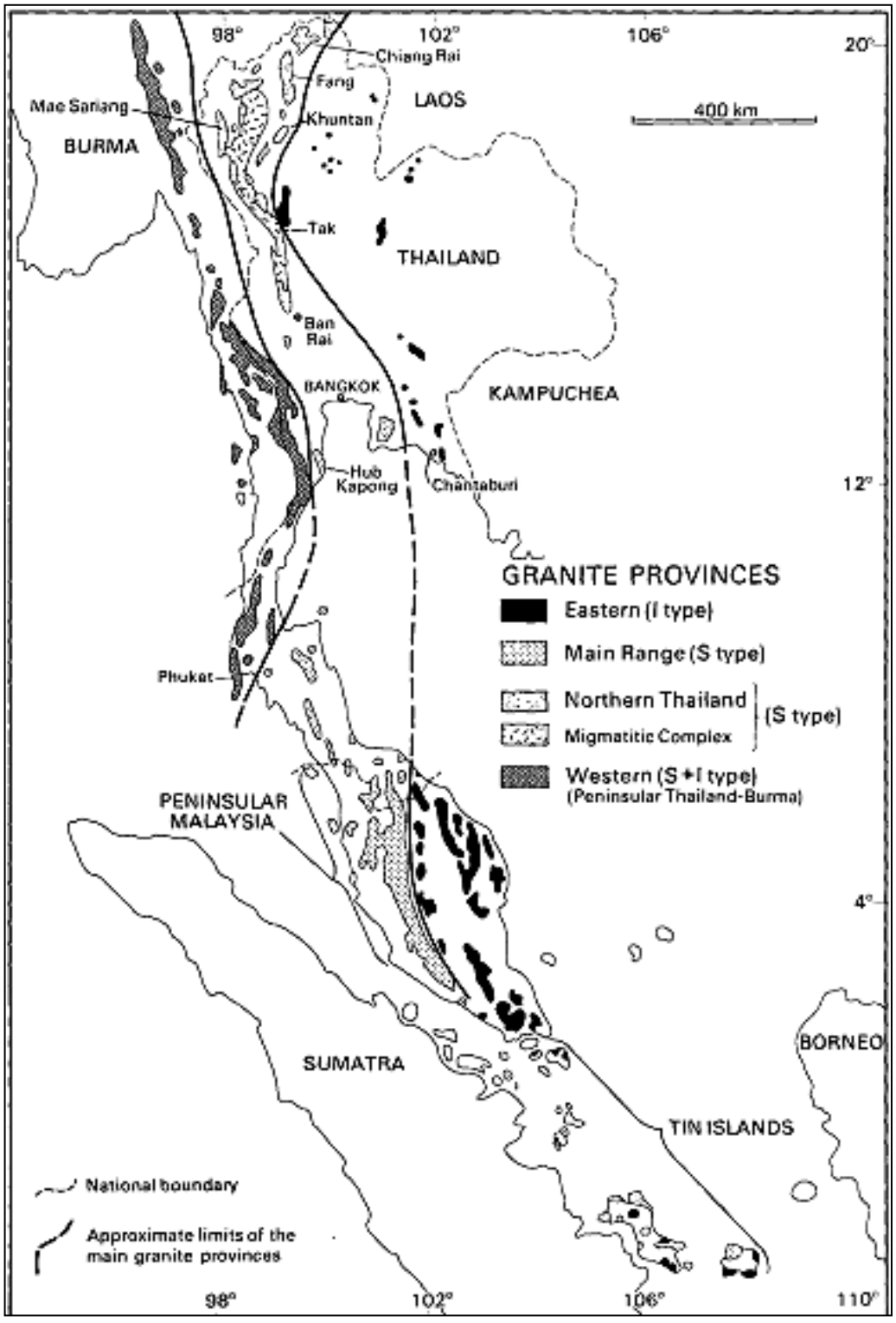

Fig. 1.3: Granite provinces around Peninsular Malaysia, adapted from Cobbing et al. (1992)

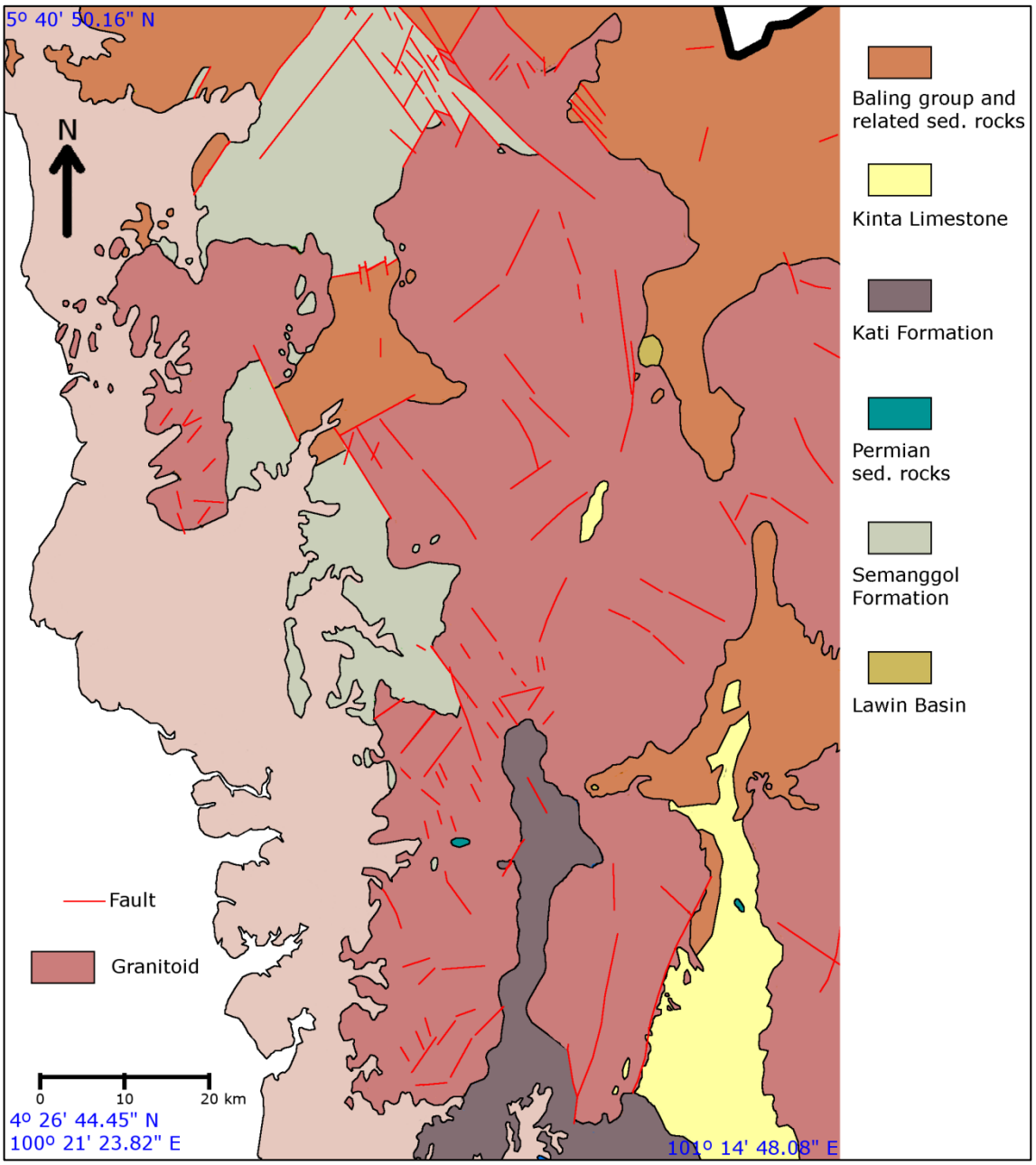

Fig. 1.4: Bintang batholith granitoid outline and surrounding sedimentary rocks

CHAPTER 2: LITERATURE REVIEW

2.1 Introduction

This chapter will discuss the previous findings on Taiping pluton as well as theoretical contribution on ultrapotassic classification, durbachite, enclaves and granite geochemical classification (I-S classification).

2.2 Taiping pluton

Taiping pluton is a long and narrow intrusion which nearly occupies the entire batholith. Cobbing et al. (1992) sketch on Fig. 2.1 show the location of Taiping pluton. It is present in two separate bodies, the fault controlled northern section and the southern section (Cobbing et al., 1992). It is in contact with Damar, Selama, Bubu, Kledang and Chenderoh plutons (Cobbing and Mallick, 1987; Cobbing et al., 1992).

Liew (1983) was the first to study the granitoid from this pluton. His sampling is limited (only 4 samples from the southern part of the pluton) and he described these granites as porphyritic sphene-amphibole-biotite granodiorite. Liew (1983) mineral chemistry suggests the biotites are low aluminum biotite while the amphiboles are actinolite or actinolitic hornblende.

Kumar (1985) pointed out these granitoid hosted enclaves and have megacrystic feature. Point counting results show that the overall rock is quartz monzodiorite (old term: adamellite) in mode while the matrix alone is tonalite and relatively mafic with a medium grain size. Kumar (1985) found allanite present among the accessory minerals, traces of clinopyroxene and clinopyroxene-amphibole enriched enclaves in the granite.

He also noted the amphiboles may occur as discrete coarse grains or as cluster of fine granules and plagioclases show oscillatory zoning with calcic andesine cores.

Cobbing and Mallick (1987) and Cobbing et al. (1992) did a thorough study of Taiping pluton. They reported three types of the granitoid in the area:

1. Buloh Pelang granite (Fig. 2.2) the main unit within the pluton. Described as extremely distinctive coarse, K-feldspar porphyritic to megacrystic biotite-amphibole melagranite
2. Maxwell Hill granite, the smaller unit found around Maxwell Hill. Described as K-feldspar megacrystic tourmaline-bearing microgranite
3. Granite of transitional type, between Buloh Pelang and Maxwell. Difficult to distinguish in the field, and occur near to Maxwell Hill granite

Cobbing and Mallick (1987) and Cobbing et al. (1992) division of Taiping pluton suggest that the pluton itself is very complex and Liew (1983) and Kumar (1985) study may only represent particular rock type/types.

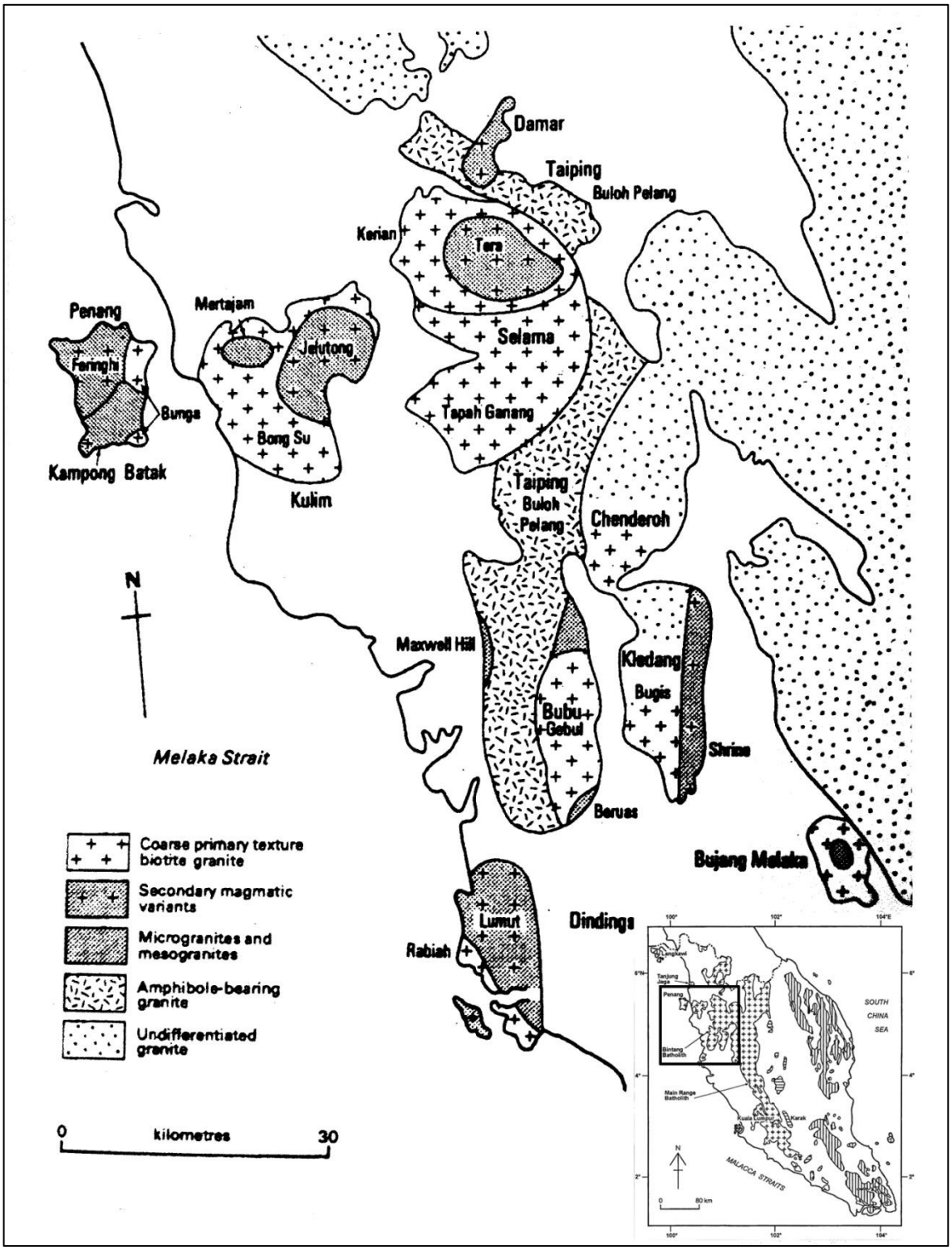

Fig. 2.1: The pluton division in Bintang batholith. Bottom right: Location of Bintang batholith in Peninsular Malaysia. Adapted from Cobbing et al. (1992)

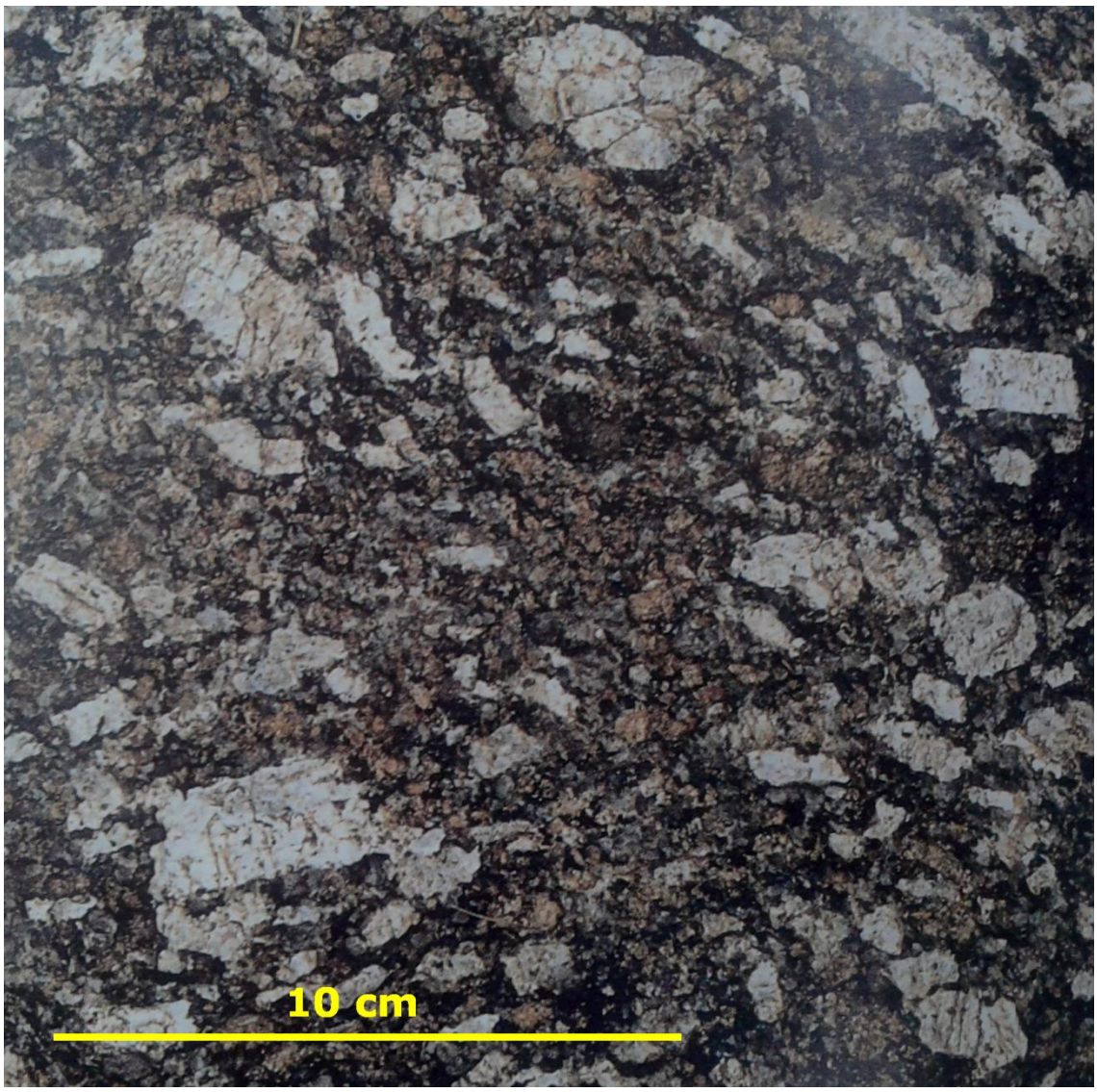

Fig. 2.2: Primary textured granite with tabular K-feldspar megacryst, Buloh Pelang unit. Adapted from Cobbing et al., 1992

2.2.1 Buloh Pelang granite

Cobbing and Mallick (1987) pointed out that the Buloh Pelang granite (Fig. 2.2) normally carry 10% biotite and contain amphiboles with pyroxene cores but mafic content up 25% have been reported on the eastern side of the pluton.

Cobbing et al. (1992) reported the amphiboles are found to contain relic pyroxene cores. Sphene, allanite, zircon and apatite are found as accessory minerals. Microcline, plagioclase and quartz form an allotriomorphic granular texture in which plagioclase is found in single euhedral crystals. Microcline is anhedral towards both plagioclase and quartz and has reaction rims against enclosed and adjacent plagioclase while quartz is subhedral or anhedral in connected grain clusters.

Cobbing et al. (1992) also suggest that cataclastic deformation increases towards the eastern margin of the pluton, where quartz and biotite becomes totally re-crystallized while plagioclase are broken and deformed.

2.2.2 Microgranular enclaves in Taiping pluton

Kumar (1985) did a study on the enclaves at two quarries near Taiping (the quarries are believed to house either the Maxwell Hill granite or the Transitional type granite). He described the enclaves as clinopyroxene-amphibole enriched enclaves. The enclaves are generally large (the largest found was about 30cm). The shape of enclaves is usually ovoid or angular-irregular. Biotite rims can be seen around the enclaves and ore mineral (such as pyrite) may be developed at the enclave granitoid contact. Rare megacrysts might occur in some enclaves. Kumar believed the amphibole-rich character of the granitoid in that region is provided by the enclaves (magma mixing).

The mafic components in the enclaves are commonly actinolitic hornblende, biotite and salite (formula: $(Mg,Fe)_2Si_2O_6$; describing a diopside with more magnesium than iron). The felsic components are quartz, K-feldspar and andesine. Amphiboles in

enclaves typically occur in rounded clusters. Pyroxenes may exceed amphibole in some samples and it is common to find pyroxene rims around the amphibole. Direct replacement of pyroxenes by biotite is frequently observable. At enclave-host contact, pyroxenes are stable and found coarsened. Accessory minerals such as apatite needles are abundant and sphene commonly occurs as shapeless sieved grains.

2.3 Ultrapotassic classification

This section will discuss the previous literature on ultrapotassic classification and durbachite, as our study suggest presence of such characteristics. The term "ultrapotassic" is generally used to describe plutonic/volcanic rocks which have high K_2O content, incompatible elements, K_2O/Na_2O ratio, Mg number, Ni and Cr. Foley et al. (1987) introduced an ultrapotassic definition using the major elements chemical screen K_2O> 3 wt. %, MgO> 3 wt. % and K_2O/Na_2O> 2 for whole rock analyses.

Foley et al., (1987) and Foley (1992) divided ultrapotassic rocks filtered from their chemical screen into four groups based on their geochemical characteristics: (1) lamproites; (2) kamafugites; (3) plagioleucitites; (4) transitional groups. The fourth group, transitional group, has higher crustal contamination and includes "special" granitic rocks such as durbachite and vaugnerite. Literature on durbachite will be discussed below since our petrographic study on Taiping amphibole-bearing melagranite suggests possible similarities.

2.3.1 Durbachite

Durbachites was first described and found in Black Forest, Germany by Sauer (1893). Later, Holub (1989) studied similar rock from other areas and improved on the previous description. He reported durbachitic rocks from Vosges Mountain of East

France and Molabnubian zone of the Bohemian Massif in Central Europe. It is said that the main bodies of durbachitic rocks are distributed in the Molabnubian Zone: Trebic massif, Milevsko massif, Zelnava massif and Rastenberg massif (Fig. 2.3). Durbachite bodies are often found in two linear NNE-trending zones.

Holub (1989) suggest durbachite suite geochemistry typically ranges from mafic to acidic and often display enrichment in LREE. On mineralogy, he found high proportions of Mg-rich biotite and light-green amphibole within those rocks. Cognate xenoliths that have been found in durbachite often contain amphibole pseudomorphs after phenocrysts of pyroxene and olivine.

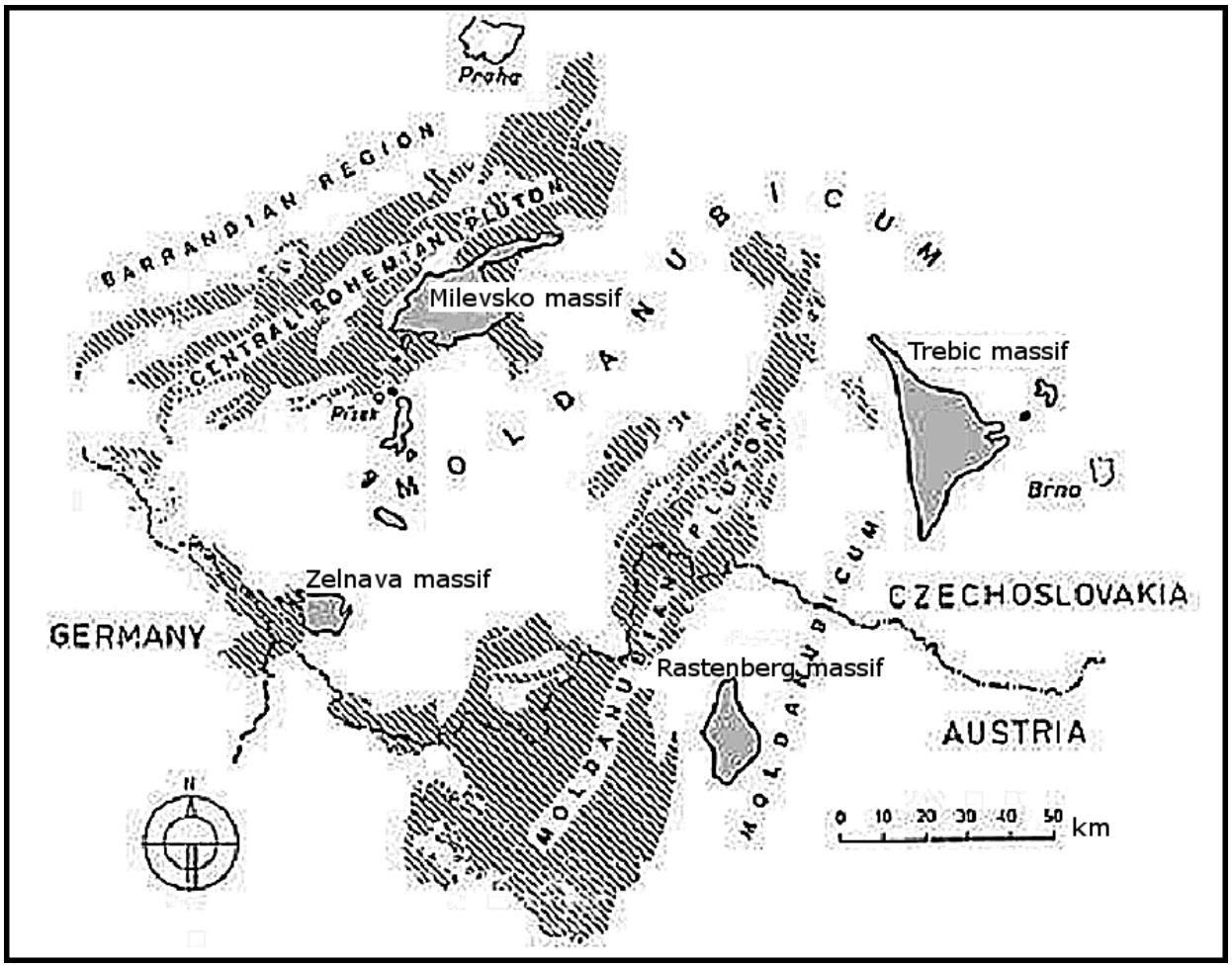

Fig. 2.3: Distribution of the main bodies of durbachitic rocks (dark) in the Moldanubian part of the Bohemian Massif, central Europe. Adapted from Holub, 1989

Holub (1997) studied the trace elements pattern of the Bohemian massif ultrapotassic rocks. Durbachite can be characterized by very high Rb/Sr (0.7 to 1.2), low contents of Na, Ca and Sr as well as a weak negative Eu-anomaly. Durbachite are exceptional as they display high contents of incompatible elements (namely K, Rb, Th) despite their relatively primitive nature in respect to Mg, Cr and Ni. He argued that the mantle source that formed the durbachites have undergone depletion (indicated by low Na, Ca, Sr, high Mg/Ca and relatively high Si) before re-enriched by hydrous fluid.

Janousek et al. (2000) studied various intrusions in the Bohemian area. Among them is a durbachitic intrusion, Certovo Bremeno suite (Milevsko massif). The intrusion is described as a porphyritic amphibole-biotite to biotite granite. The accessory minerals are apatite, zircon, titanite, allanite and opaque minerals. Plagioclase is a relatively homogeneous andesine, with rare oligoclase rims and fracture infillings. Mafic microgranular enclaves (MME) are common on the granite. They are mainly metaluminous with intermediate SiO_2 content. Trace elements show high Zr, Cr, Ni and ΣREE (elevated LREE).

Ferre and Leake (2001) suggested that the distinctive magnesian and potassic character of durbachites and vaugnerites justifies the use of specific terms instead of the IUGS generic terms, such as melagranite, melasyenite or meladiorite. Vaugnerite are Mg-K meladiorites but durbachites are even more magnesian and potassic equivalents which range from melasyenites to melagranites and sometimes even to ultramafic types.

Janousek and Holub (2007) did a case study on the Moldanubian zone of the Bohemian Massif. Durbachite geochemistry can be divided to mafic and more acidic. Mafic durbachite (typically below 63 wt. % SiO_2) are highly magnesian (MgO: 7 to 9 wt. %, mg#: ~70), rich in Cr (450 to 600 ppm) as well as in U, Th, LILE (K_2O: 6 to 8 wt. %, Ba: 2000 to 2750 ppm, Rb: 350 to 400 ppm, Cs: 15 to 25 ppm). The more acidic members (typically SiO_2: 63 to 66 wt. %) are unusually rich in MgO (> 3 wt. %) and Cr

(>200 ppm) compared to common granitic suite. From trace elements and REE data analysis, they concluded durbachitic rock require derivation from anomalous mantle sources contaminated by mature crustal material.

Kotkova et al. (2010) reviewed mafic durbachitic rocks (SiO_2: 56.45 wt. %) from Trebic massif in Bohemian area while doing U-Pb age determination on them. Durbachite there typically features a magmatic fabric with abundant large phenocrysts of alkali feldspar and rarer plagioclase phenocrysts. Reported primary phases are: K-feldspar, plagioclase, quartz, biotite and hornblende, and accessory phases are: zircon, apatite, rutile and titanite. Amphiboles have actinolite hornblende in the core and actinolite in the rim. Small pyroxene relics are present among the amphibole. MME are present and typically contain high amount of amphibole and biotite.

Von Raumer et al. (2013) suggested durbachite-vaugnerite rocks could represent possible geodynamic marker in the central European Variscan orogen. Durbachite-vaugnerite rocks in the region are believed to be derived from enriched mantle source and geochronological work show most of them formed around 335 to 340 Ma. Concluding from various durbachite-vaugnerite study observations in the region, Von Raumer et al. (2013) suggest their presence can be interpreted as a geodynamic marker for a prominent late-collisional melting event within the enriched sub-continental mantle underneath the Variscan orogen.

2.4 I-S classification

This well known geochemical classification was first introduced by Chappell and White (1974), while studying granitoids in Berridale-Kosciusko region of the Lachlan Fold Belt (LFB). The I- and S-type are given to the two contrasting granitoid in the area, separated according to their petrographic, geochemical and isotropic properties

(Table 2-1). The classification system was well accepted outside of LFB (Chappell and White, 2001) and was applied to Peninsular Malaysia granite province (Liew, 1983).

Chappell and White (1974) interpreted I-type granite as being derived from igneous source while S-type granites are derived from sedimentary sources. I- and S-types have distinctive petrographic feature which reflect their difference in chemical composition. I-type granites typically contain hornblende and accessory sphene, while S-type granites are commonly found with muscovite and aluminosilicates xenoliths.

Classifying granites into I-S type (Chappell and White, 1974) appears to be difficult sometimes because overlap between the types might occur. Chappell and White (1992) managed to re-invent classification by introducing the ACF diagram (a ternary diagram, where A= Al – Na – K, C= Ca, F= Mg + Fe). This diagram is based on the relationship between chemical composition and mineral composition for both I- and S-type granites. The ACF diagram (Fig. 6.2) is able to show clear separation between I- and S-type granite of the Kosciuko Batholith and also successfully discriminates between hornblende-bearing and hornblende free I-type granite. However, the correlation precision of the ACF diagram is strongly affected by the quality of the data.

Chappell and White (2001) reviewed Chappell and White (1974) classification. They point out that the main minerals for both types from the 1974 publication remain correct for the LFB even though some of the chemical criteria that distinguished I-and S-type granites are unsatisfactory. One of the issues is the sodium limit. With more data in hand, they believed sodium (Na) role in discriminating between the granite types is overstressed. Samples from the entire LFB show that about 12.1 % of S-type granites (751 samples) lie above the sodium limit of 1974 and 20.4 % of I-type granites (1217 samples) lie under the limit. Since sodium is highly mobile during alteration, primary magmatic features could be obscured.

Chappell and White (2001) LFB I- and S-type granite data show significant overlaps for isotopic composition of both types. This suggests not all granites are exclusively originated from I- or S-type source. Chappell and White (2001) proposed that derivation from range of source rocks comprising various proportions of igneous and sedimentary material could cause this.

Clemens et al. (2011) work on experimental and theoretical perspective suggests transitional I-S type rocks are possible. The degree of inherited I-type or S-type character will depend on the clay content in the protolith. Clemens et al. (2011) also point out that the I-S dichotomy in granite typology is unlikely to reflect simple igneous versus sedimentary source.

These findings on I-S classification are important to understand the role of geochemistry in the petrogenesis of Main Range granite province. The problem within the I-S classification itself (overlap between types, simplification of granite source) and its uniqueness to LFB suggests this classification might not be the best for the Main Range granite province. Similar opinion has been previously addressed in Ghani (2000).

Table 2.1: Geochemical properties of I- and S-types from Chappell and White (1974)

I-types	S-types
Relatively high sodium, Na_2O normally >3.2% in felsic varieties, decreasing to >2.2% in more mafic types	Relatively low sodium, Na_2O normally <3.2% in rocks with approximately 5% K_2O, decreasing to <2.2% in rocks with approximately 2% K_2O
A/CNK <1.1 and CIPW normative diopside or <1% normative corundum	A/CNK > 1.1 and >1% CIPW normative corundum
Broad spectrum of compositions from felsic to mafic types	Relatively restricted in composition to high SiO_2
Regular inter-element variations within plutons; linear/near-linear variation diagrams	Variation diagrams more irregular

Adapted from Chappell and White (2001)

CHAPTER 3: FIELD STUDY AND RESEARCH METHODOLOGY

3.1 Introduction

All field samples in this study were personally collected by the author, except for the core samples, they are obtained with the courtesy of Prof. Mohd Mokhtar bin Saidin from Centre for Global Archeology Research, University of Sains Malaysia, Penang and Assoc. Prof. Zuhar Zahir bin Tuan Harith from Department of Geoscience and Petroleum Engineering, PETRONAS University of Technology, Perak. The core samples are originally used for a meteorite impact study. Geochemical analysis was carried out by commercial laboratory (ACME analytical laboratories) in Canada.

3.2 Field study

The amphibole-bearing melagranite is located in Taiping pluton, Bintang batholith, within the Perak state. One of the prominent peaks in the study area is Maxwell hill (1250 m). Outcrops are more common at higher elevation and are fairly uncommon at low elevation as most of granitoid are covered by red laterite or weathered granitoid. At lower elevation, fresh granite is usually found in quarries, waterfall areas, road cuts, landslide areas, and drainage basins. A Garmin GPS unit is used to determine the coordinates of the sample location.

The location of the granite is determined with the help of previous research where similar rock texture has been found (Liew 1983; Cobbing et al., 1992). The porphyritic melagranite is identified by using the previous Buloh Pelang granite research (Cobbing et al., 1992) macroscopic textural information as the standard. The mapped melagranite location is shown in Fig. 3.1. The core samples are collected from

Lenggong, Perak. The drilling locations are shown in Fig. 3.2. Field photos are shown from Fig. 3.3 to 3.5.

Consistency in sample collection is emphasized in order to acquire consistent range in petrography and bulk chemistry for possible future comparison works. Only fresh, non-weathered samples were taken, samples that demonstrate heavy weathering, noticeable alteration, heavy deformation/shearing and none of the primary granite textures are excluded from the study.

3.3 Geochemical analysis

For geochemical analysis, the core samples (~1 kg) and hand sample (~2 kg) are pulverized into smaller pieces and grinded to a fine powder using the mild steel swing mill. The pulverizing and grinding process in carried out at the Department of Geology, University of Malaya. Geochemical analysis (XRF and ICP-MS) for this study is done by service from Acme Analytical Laboratories.

3.3.1 X-ray fluorescence (XRF)

XRF spectrometer is an X-ray instrument used for routine, relatively non-destructive chemical analyses of rocks, minerals, sediments and fluids. This method is well suited for chemical analyzes of major elements in rocks. Two important steps have to be completed before the sample is ready for analysis. First, the sample has to be determined for loss on ignition (LOI). After then, the sample is fused with flux to form a fusion bead. The finished bead will then be ready to be analyzed by the XRF machine.

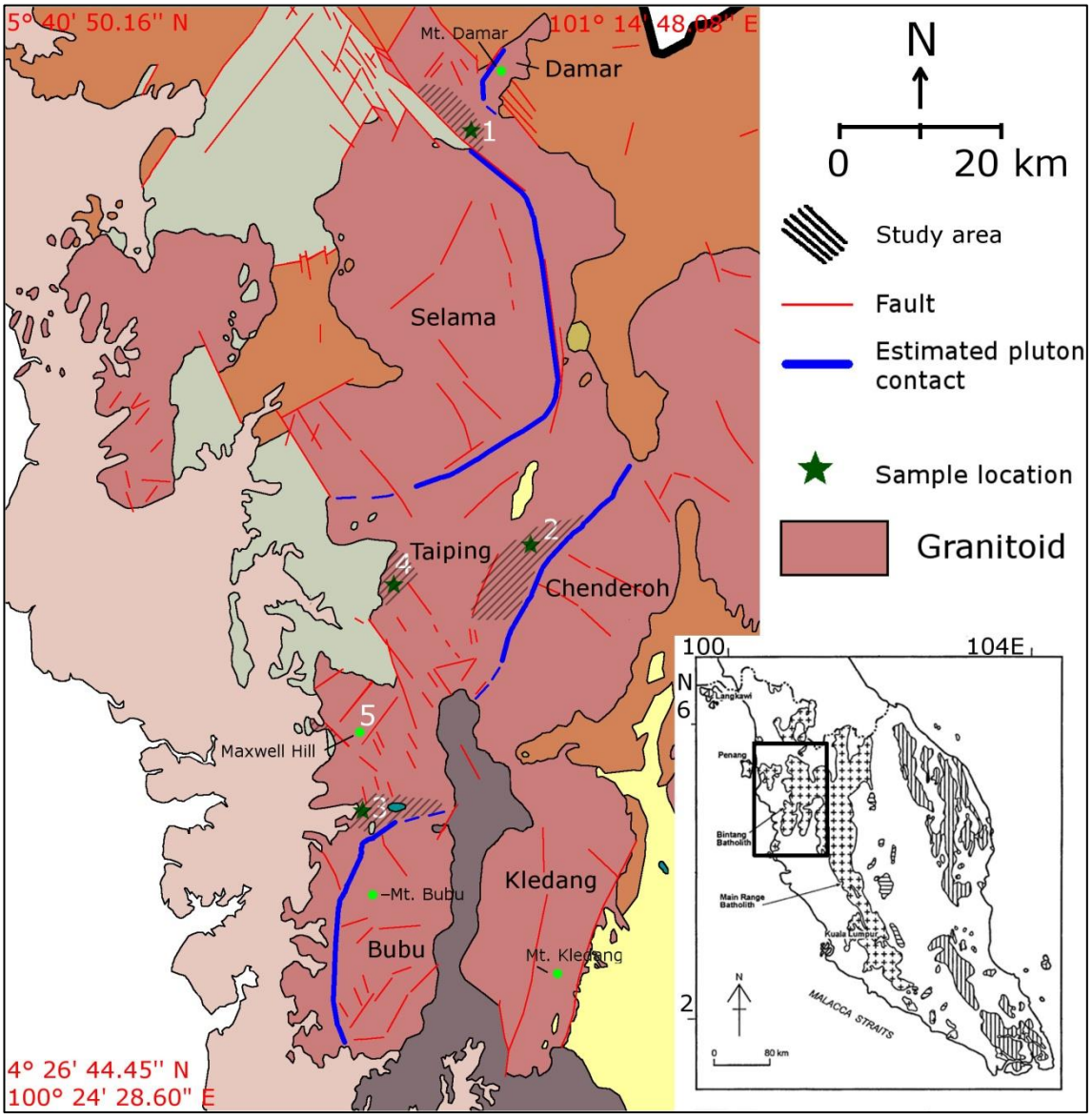

Fig. 3.1: Location of samples. Bottom right: Location of Bintang batholith in Peninsular Malaysia. The shaded areas indicate the extent of Taiping melagranite observed in this research. Key: 1, Baling-Gerik road; 2, Lenggong valley; 3, Bukit Berapit; 4, Batu Kurau; 5, One sample from Taiping is collected at the bottom of Maxwell Hill.

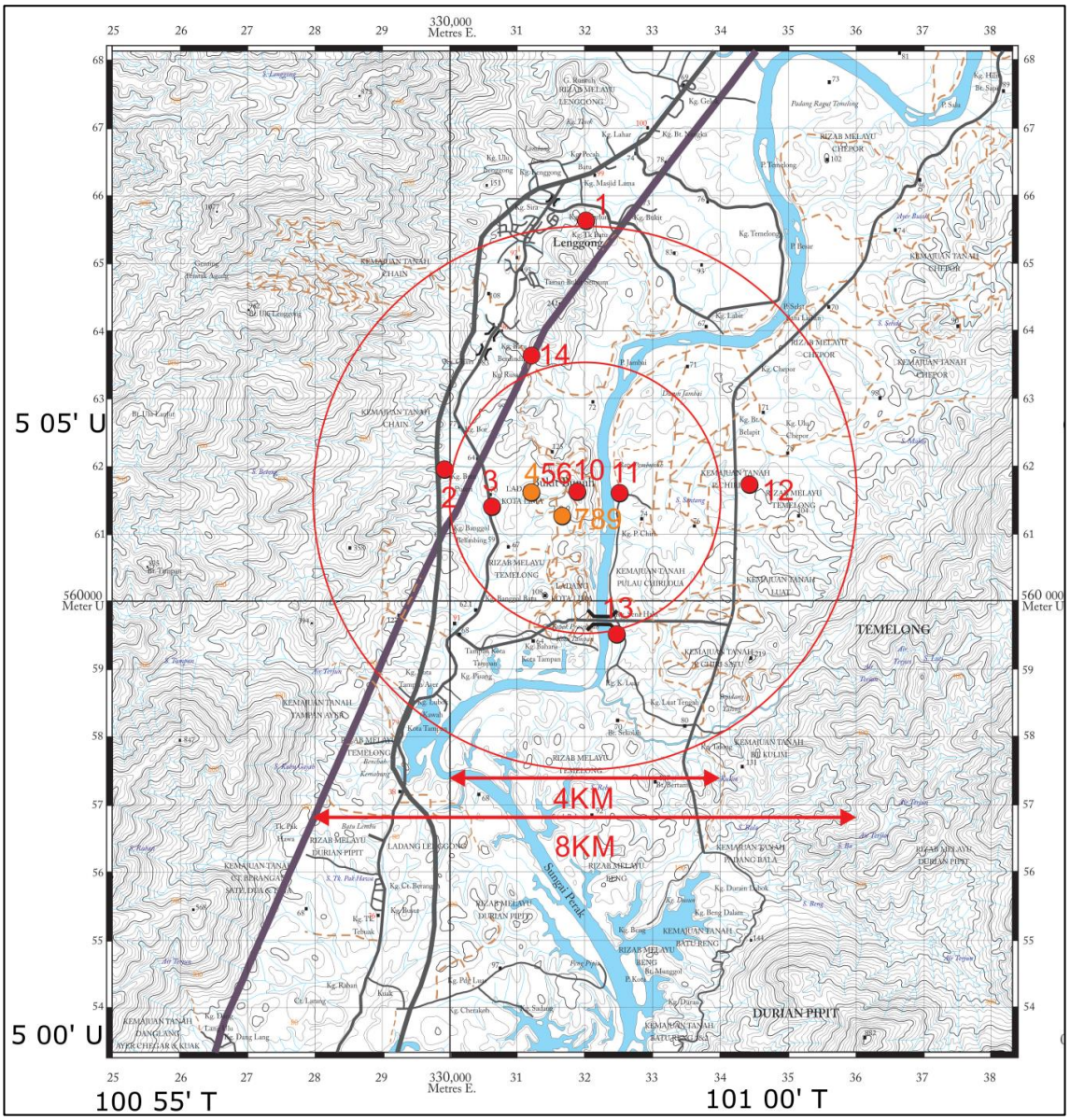

Fig. 3.2a: Borehole locations at Lenggong (Area 2, near Sungai Perak), Perak. Only samples from the yellow color location marker (4, 7, 8, and 9) are used. The circles in the map are for geophysical study (not related to this study) but their diameter can be used as scale.

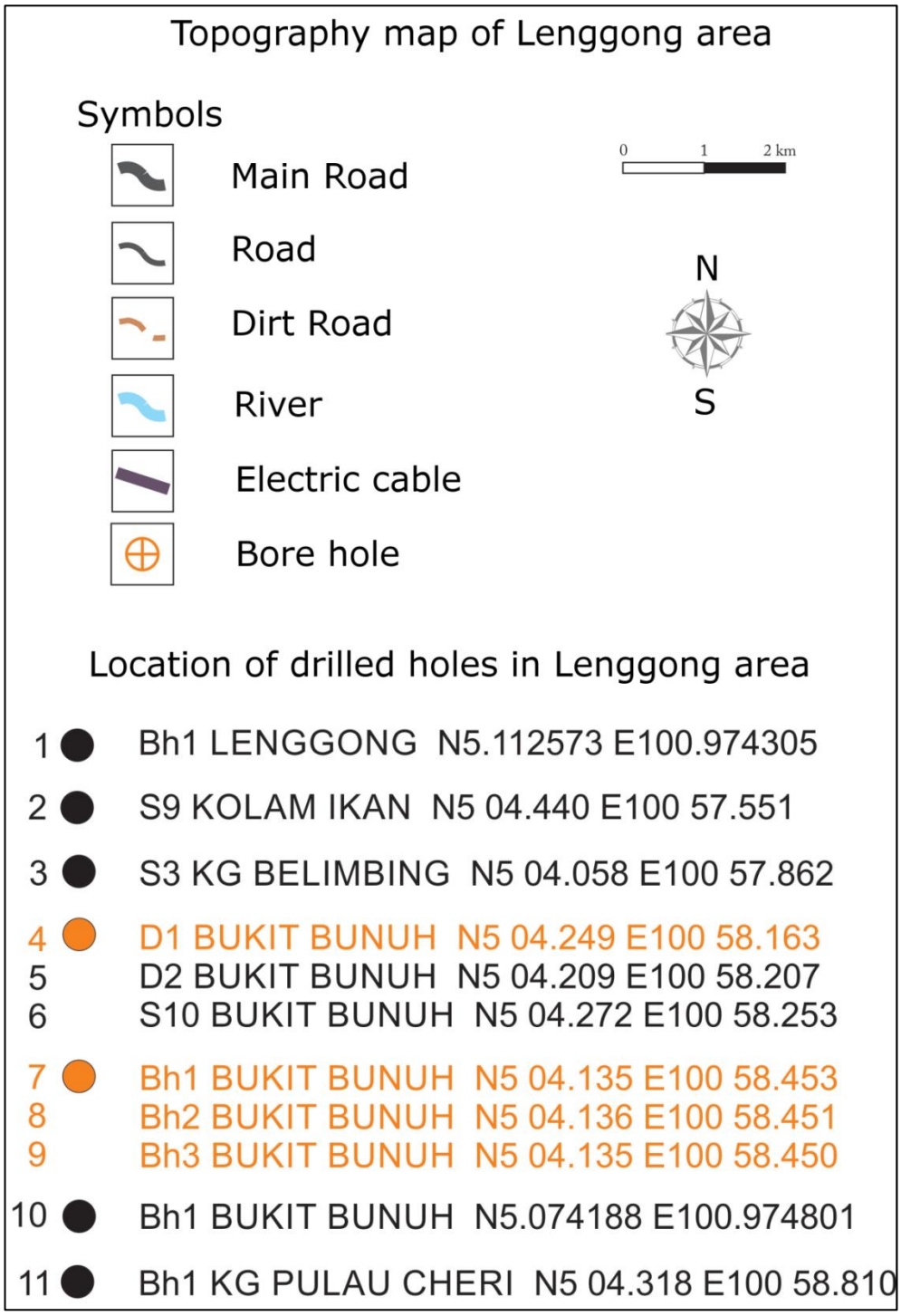

Fig. 3-2b: Map legend for the map in Fig. 3-2a. Yellow color font indicates the selected location markers (4, 7, 8 and 9)

Fig. 3.3: Top: Melagranite with a felsic mineral vein in it; location: Bukit Berapit. Bottom: The typical melagranite texture; location: Bukit Berapit. Hammer is provided as scale.

Fig. 3.4: Top: Melagranite boulder; location: Batu Kurau. Bottom: Melagranite boulder; location: Burmese pool, near Maxwell hill. Hammer is provided as scale.

Fig. 3.5: Top: Enclave on melagranite boulder; location: Bukit Berapit. Bottom: Enclave on Melagranite boulder; location: Bukit Berapit. Hammer is provided as scale.

The most typical way to determine LOI is explained here. To determine LOI of granite-like sample, about 1g of dry rock sample in powder form is put into a crucible and sintered at 1000ºC in an oven for 1 hour. The crucible is then cooled (about 10 minutes). The value of LOI (in weight %) can be determined from using the formula below:

$$\mathbf{LOI = 100\% \times ((a - b) / (a - c))}$$

a is the weight of the crucible with sample before sintering (in grams)

b is the weight of the crucible with sample after sintering (in grams)

c is the weight of the empty crucible (in grams)

Acme laboratory requires 12g of sample pulp for the fusion process

The common method to create fusion bead employs a lithium metaborate/tetraborate fusion. The sintered powder is mixed with flux (lithium metaborate, $LiBO_2$ is used in Acme laboratories, while the Department of Geology uses lithium tetraborate, $Li_2B_4O_7$, 8:1 ratio of flux to sample) and fused in a platinum crucible using an automated fusion machine, before the molten sample is casted into a glass bead. The glass bead is then analyzed by a XRF machine using acceptable values of standard samples for major elements. Fused glass beads are very durable and can survive for a long period if stored properly. Reference materials used for XRF analysis are STD SY-4(D) and STD OREAS72B (Table 3.1 and 3.2). All of the analyzed oxides show readings that are below detection limit when blanks are used.

Table 3.1: Reference materials for XRF (in wt. %)

Compound	STD SY-4(D)	Expected value	Accuracy (%)	STD OREAS72B	Expected value	Accuracy (%)
SiO_2	50.2	50.1	99.80	51.1	51.7	98.84
Al_2O_3	20.64	20.7	99.71	8.9	9.01	98.78
Fe_2O_3	6.15	6.26	98.24	9.73	9.85	98.78
CaO	7.95	7.98	99.62	3.92	3.96	98.99
MgO	0.52	0.54	96.30	16.15	16.24	99.45
Na_2O	7.07	7.09	99.72	1.31	1.34	97.76
K_2O	1.58	1.6	98.75	1.33	1.33	100.00
MnO	0.11	0.11	100.00	0.13	0.13	100.00
TiO_2	0.29	0.27	92.59	0.34	0.34	100.00
P_2O_5	0.13	0.13	100.00	0.05	0.06	83.33
Cr_2O_5	<0.001	0.003	-	0.149	0.148	99.32

Table 3.2: Detection limit for XRF (in wt. %)

Compound	Method detection limit (MDL)	Upper limit
SiO_2	0.1	100
Al_2O_3	0.01	100
Fe_2O_3	0.01	100
CaO	0.01	100
MgO	0.01	100
Na_2O	0.01	100
K_2O	0.01	100
MnO	0.01	100
TiO_2	0.01	100
P_2O_5	0.01	100
Cr_2O_5	0.001	100

3.3.2 Inductively coupled plasma-mass spectrometry (ICP-MS)

Acme laboratory requires 5g of sample pulp for this analysis (the pulp is separated from the prepared powder). There are a few ways to prepare samples for ICP-MS analysis: (1) aqua regia digestion, (2) acid digestion, (3) sodium peroxide fusion. The technique used by Acme Analytical Laboratories is a type of acid digestion; lithium tetraborate $Li_2B_4O_7$ fusion followed by diluted acid digestion. This decomposition technique is said to be able to report rare earths and refractory elements.

The bead preparation and fusion process is similar the one described for XRF analyses, except that a different flux is used instead. The resulting molten bead is rapidly digested in a weak nitric acid solution. It is only with this attack that major oxides including SiO2, REE and other high field strength elements are put into solution. Precious metals, base metals and their associated pathfinder elements are generated from an aqua regia digestion. Sample splits of 0.5g are leached in hot (95°C) Aqua Regia. Reference materials used for ICP-MS analysis are STD SO-18, STD DS9 and STD OREAS45EA (Table 3.3, 3.4 and 3.5). Most of the analyzed elements show readings that are below detection limit when blanks are used.

Table 3.3: Reference materials for ICP-MS (main, in ppm)

Element	STD SO-18	STD SO-18	Expected value	Expected value (2)	Accuracy (%)	Accuracy (2)(%)
Ba	546	536	470	478	86.08	89.18
Co	27.6	26.7	24.3	26.3	88.04	98.50
Cs	7.5	7.3	7.8	6.9	96.00	94.52
Ga	15.7	17	16.1	16.8	97.45	98.82
Hf	9.5	9.5	9.5	9.5	100.00	100.00
Nb	20.9	20	19.6	19.6	93.78	98.00
Rb	29.1	29.1	27.1	26.9	93.13	92.44
Sr	426.2	434.1	404	408.4	94.79	94.08
Ta	7.1	7.2	6.8	6.8	95.77	94.44
Th	10.5	10.4	10.5	10	100.00	96.15
U	16	15.7	16	16	100.00	98.09
V	210	204	192	193	91.43	94.61
Zr	307.1	305.4	295.3	292.4	96.16	95.74
Y	32.7	31.7	30.1	30.4	92.05	95.90
La	13.4	13.1	12.9	13.5	96.27	96.95
Ce	29.3	27.7	28.1	29	95.90	95.31
Pr	3.53	3.36	3.34	3.41	94.62	98.51
Nd	15.9	13.2	13	13.1	81.76	99.24
Sm	2.92	2.94	2.72	3.06	93.15	95.92
Eu	0.85	1.03	0.89	0.82	95.29	79.61
Gd	3.06	3.23	2.97	3.09	97.06	95.67
Tb	0.5	0.51	0.45	0.48	90.00	94.12
Dy	3.33	3.38	2.63	3	78.98	88.76
Ho	0.66	0.68	0.69	0.65	95.45	95.59
Er	1.79	1.88	1.8	1.84	99.44	97.87
Tm	0.28	0.28	0.24	0.26	85.71	92.86
Yb	1.78	1.83	1.66	1.66	93.26	90.71
Lu	0.3	0.28	0.27	0.27	90.00	96.43

Table 3.4: Reference materials for ICP-MS (other metals, in ppm)

Element	STD DS9	Expected value	Accuracy (%)	STD OREAS45EA	Expected value	Accuracy (%)
Cu	105.3	111.2	94.69	691.5	683.8	98.87
Pb	129.1	118.9	91.42	15.9	13.5	82.22
Zn	317	332	95.48	31	31	100.00
Ni	37.9	39.9	94.99	376.5	381.4	98.72

Table 3.5: Detection limit for ICP-MS (in ppm)

Element	Method detection limit (MDL)	Upper limit	Element	Method detection limit (MDL)	Upper limit
Ba	1	50000	Pr	0.02	10000
Co	0.2	10000	Nd	0.3	10000
Cs	0.1	10000	Sm	0.05	10000
Ga	0.5	10000	Eu	0.02	10000
Hf	0.1	10000	Gd	0.05	10000
Nb	0.1	50000	Tb	0.01	10000
Rb	0.1	10000	Dy	0.05	10000
Sr	0.5	50000	Ho	0.02	10000
Ta	0.1	50000	Er	0.03	10000
Th	0.2	10000	Tm	0.01	10000
U	0.1	10000	Yb	0.05	10000
V	8	10000	Lu	0.01	10000
Zr	0.1	50000	Cu	0.1	10000
Y	0.1	50000	Pb	0.1	10000
La	0.1	50000	Zn	1	10000
Ce	0.1	50000	Ni	0.1	10000

3.3.3 Geochronology

Geochronology analyses were carried out at the Pacific Centre of Isotopic and Geochemical Research (PCIGR) in University of British Columbia, Vancouver, Canada. Zircons were analyzed using laser ablation (LA) ICP-MS methods, employing methods as described by Tafti et al. (2009). Instruments employed for geochronology work comprises a New Wave UP-213 laser ablation system and a ThermoFinnigan Element2 single collector, double-focusing, magnetic sector ICP-MS.

Zircons greater than about 50 microns in diameter were picked from the heavy mineral separates and were mounted in an epoxy puck along with several grains of the 337.13 ± 0.13 Ma Plešovice zircon standard (Sláma et al., 2007), together with a Temora 2 reference zircon, and brought to a very high polish. The surface of the mount was washed for 10 minutes with dilute nitric acid and rinsed in ultraclean water prior to analysis. The highest quality portions of each grain, free of alteration, inclusions, or possible inherited cores, were selected for analysis.

Line scans rather than spot analyses were employed in order to minimize elemental fractionation during the analyses. A laser power level of 38% was used. A 30 micrometer spot size was used. Backgrounds were measured with the laser shutter closed for ten seconds, followed by data collection with the laser firing for approximately 35 seconds. The time-integrated signals were analysed using Iolite software (Patton et al, 2011), which automatically subtracts background measurements, propagates all analytical errors, and calculates isotopic ratios and ages. Corrections for mass and elemental fractionation were made by bracketing analyses of unknown grains with replicate analyses of the Plešovice zircon standard.

A typical analytical session at the PCIGR consists of four analyses of the Plešovice standard zircon, followed by two analyses of the Temora2 zircon standard (416.78 ± 0.33 Ma), five analyses of unknown zircons, two standard analyses, five unknown analyses, etc., and finally two Temora2 zircon standards and four Plešovice standard analyses. The Temora2 zircon standard was analysed as an unknown in order to monitor the reproducibility of the age determinations on a run-to-run basis. Final interpretation and plotting of the analytical results employed the ISOPLOT software of Ludwig (2003).

3.4 Chapter Summary

1. Samples for this study are collected from: (1) Baling-Gerik road, (2) Lenggong valley, (3) Bukit Berapit, (4) Batu Kurau, (5) Maxwell Hill.
2. Geochemical analyses are completed with the help from Acme Analytical Laboratories, Canada. Geochronology analyses were carried in Pacific Centre of Isotopic and Geochemical Research (PCIGR) in University of British Columbia, Vancouver, Canada.

CHAPTER 4: PETROGRAPHY

4.1 Introduction

This chapter will discuss the petrography features of the Taiping amphibole-bearing melagranite. Results from detailed petrographic examination are described here. A total of 21 thin sections were analyzed for rock forming minerals. Table 4.1 lists the mineral assemblages of each thin section and petrographic significant characteristics of specific thin sections.

4.2 Amphibole-bearing melagranite

Based on the mineral estimation on Table 4.2, the sample quartz and feldspar ratio is similar to granite rocks (20-60% quartz and 0.10-0.65 plagioclase/total feldspar ratio) based on QAP classification by Streckeisen (1976). However, the term *melagranite* (the prefix mela- means melanocratic) is used instead of granite, as the rocks are quite dark (high mafic content). The thin section photomicrograph for the melagranite is shown in Fig. 4.1, 4.2, 4.3 and 4.4.

The melagranite is characterized by large euhedral light grey feldspar phenocrysts and megacrysts (>5 cm) with medium to coarse grain dark color groundmass which provide a rather strong color contrast effect. The distribution of large porphyry and megacrysts is erratic. They could often be found aligned (possible syn-magmatic flow as the crystal are not fractured or deformed), pointing towards a direction (estimated as N-W). The matrix grain size remains fairly constant and is also sometimes found weakly foliated in the N-W direction.

Table 4.1: Thin section description

Sample ID	Rock type	Petrographic description
BH1-3B	Melagranite (phenocryst)	• Large, euhedral K-feldspar phenocryst • Quartz, biotite, apatite, chlorite and opaque minerals are present as inclusions • Some part of the phenocryst are microcline
BH1-5A	Melagranite	• Mineral present: plagioclase, K-feldspar, quartz, amphibole, pyroxene, biotite, titanite, zircon, apatite • Pyroxene is rare. Amphibole is more common
BH1-9B	Melagranite	• Mineral present: plagioclase, K-feldspar, pyroxene, amphibole, biotite, quartz, titanite, zircon, apatite • Large elongated orthopyroxene (2 mm) • Microcline is present but rare
BH2-2B	Melagranite	• Mineral present: plagioclase, K-feldspar, biotite orthopyroxene, amphibole, quartz, titanite, zircon, apatite • Zircon crystal are fairly large (0.3 mm)
BH2-3B	Melagranite	• Mineral present: quartz, plagioclase, K-feldspar, biotite, pyroxene, titanite, zircon, apatite • Higher quantity of biotite (for mafic mineral) •
BH2-7A	Melagranite	• Mineral present: quartz, plagioclase, K-feldspar, pyroxene, amphibole, biotite, titanite, zircon, apatite • Pyroxene are slightly larger than usual
	Enclaves	• Mineral present: pyroxene, biotite, plagioclase, K-feldspar, quartz, amphibole, titanite, zircon, apatite • More orthopyroxene than clinopyroxene • Exsolution texture in orthopyroxene • Felsic minerals (plagioclase, K-feldspar, quartz) grains are larger
BH3-3B	Melagranite	• Mineral present: quartz, plagioclase, K-feldspar, amphibole, biotite, titanite, zircon, apatite • Amphibole present as small grains that fills the K-feldspar phenocryst cracks
BH3-7B	Melagranite	• Mineral present: quartz, plagioclase, K-feldspar, biotite amphibole, pyroxene, titanite, zircon, apatite, calcite • Calcite vein within K-feldspar phenocryst

Sample ID	Rock type	Petrographic description
DH1-10A	Melagranite (phenocryst)	• Large, euhedral K-feldspar phenocryst • Quartz, biotite, apatite, chlorite and opaque minerals are present as inclusions • Small amount of myrmekite is present • Biotite lining around K-feldspar phenocryst • Tourmaline within one of the K-feldspar porphyry
DH1-18A	Melagranite	• Mineral present: quartz, plagioclase, K-feldspar, pyroxene, amphibole, biotite, titanite, zircon, apatite, chlorite, allanite • K-feldspar: perthite/microcline
	Melagranite (phenocryst)	• Large, euhedral K-feldspar phenocryst • The phenocryst is not uniform. Perthitic texture are present in some part of the crystal • Quartz, biotite, plagioclase, zircon, apatite and opaque minerals are present as inclusions
DH1-14A	Melagranite	• Mineral present: plagioclase, biotite, quartz, K-feldspar, amphibole, pyroxene, titanite, zircon, apatite, chlorite • Plagioclase phenocryst is present
	Enclaves	• Mineral present: plagioclase, biotite, K-feldspar, quartz amphibole, pyroxene, titanite, zircon, apatite, chlorite • Higher quantity of biotite (for mafic mineral) • Pyroxene are small and rare • Quartz-chlorite vein cutting through the enclave
BK-1	Melagranite	• Mineral present: plagioclase, K-feldspar, quartz clinopyroxene, amphibole, biotite, titanite, zircon, apatite, chlorite, sericite, calcite • Patchy texture in plagioclase grains
BB-A, BB-B	Melagranite	• Mineral present: plagioclase, K-feldspar, biotite, quartz clinopyroxene, amphibole, titanite, zircon, apatite, allanite • Perthite phenocryst found
BB-2A, BB-2B	Melagranite	• Mineral present: plagioclase, K-feldspar, biotite, quartz, amphibole, clinopyroxene, titanite, zircon, apatite, allanite • Amphibole cluster (clot?) is present

Sample ID	Rock type	Petrographic description
T	Melagranite	• Mineral present: quartz, plagioclase, K-feldspar, amphibole, biotite, titanite, zircon, apatite, pyroxene, allanite • Quartz phenocryst is present • Concentric and patchy zoning in plagioclase
BB-E	Enclaves	• Mineral present: pyroxene, plagioclase, K-feldspar, biotite, amphibole, titanite, zircon, apatite • Higher pyroxene content • Feldspar phenocryst is present • Euhedral titanite are present at rim
GE1, GE2	Enclaves	• Mineral present: plagioclase, biotite, K-feldspar, pyroxene, amphibole, titanite, zircon, apatite, rutile • Higher plagioclase content • Pyroxene form clots within the enclaves

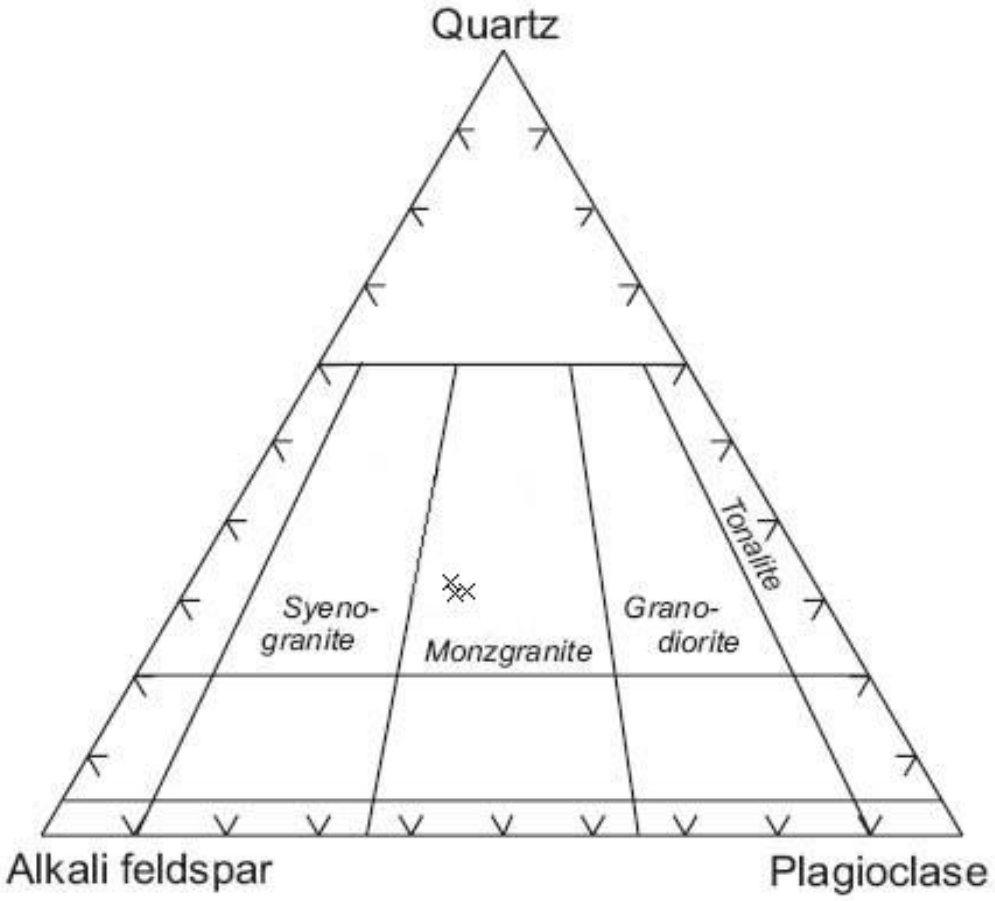

Fig. 4.1: QAP diagram, Streckeisen (1974). Data from point counting (Table 4.2) are plotted here.

Table 4.2: Melagranite mineral estimation

Minerals	Percentage	Description
Biotite	~25%	Well defined grain with clear cleavage. Sometimes loose and open clusters may occur within the quartz-feldspar groundmass. They are also found interstitially around the K-feldspar megacryst.
K-feldspar phenocrysts/ megacrysts	18-20%	Euhedral tabular grey crystals scattered around the granitoid. Observation suggests the tabular crystals are homogeneous and have a solid appearance. Random minor inclusions of biotite, plagioclase or quartz could sometimes be found.
Quartz	21-22%	Mostly grey in color and translucent. On the thin section, it mainly comprised of globular and irregular cluster. Usually anhedral.
Plagioclase	~20%	White color, generally near euhedral crystals. Anhedral crystals occur within groundmass.
K-feldspar	8-10%	Grey anhedral and interstitial within the quartz-feldspar groundmass
Pyroxene	1-2%	Mostly anhedral. Grains with good cleavage often go unnoticed as they are so rare. Clinopyroxene is usually more common than orthopyroxene. Orthopyroxene are larger than clinopyroxene.
Amphibole	~4%	Appear in tiny, anhedral grains. Cleavage is not easily noticed. Most show golden yellow color in crossed nichols light.

Mineral	Count 1	Count 2	Count 3
Biotite	246	247	249
K-feldspar phenocrysts/ megacrysts	182	180	200
Quartz	222	223	216
Plagioclase	198	199	200
K-feldspar	100	91	80
Pyroxene	10	20	11
Amphibole	42	40	44
Total	1000	1000	1000

* Estimations of mineral abundance are obtained using point counting method. A Swift model E point counter fitted with an automated stage was used.

Quartz, plagioclase and alkali feldspar are the common felsic minerals. Mafic minerals are chiefly represented by biotite and amphibole. Pyroxenes (both clino- and ortho-) occur in trace amount. Accessory minerals are zircon, apatite, titanite, allanite rutile and tourmaline (rutile is quite rare but tourmaline is rarer). Small amount of secondary chlorite, calcite, sericite has also been found, suggesting minimal chemical alteration (probably from post magmatic hydrothermal activity).

K-feldspar is the most abundant mineral in the melagranite, if the porphyry and megacryst are included. K-feldspar porphyry and megacryst usually have a grayish appearance. Minor perthite and microcline do occur in parts of the K-feldspar crystal. Some of them might show Carlsbad twining (uncommon). Zoned K-feldspars are quite rare. These large K-feldspars may contain various inclusions such as quartz, biotite, plagioclase, apatite, chlorite, amphibole, tourmaline, zircon, rutile and opaque minerals.

In the matrix, however, it is quartz or plagioclase that usually dominates. K-feldspar is smaller and present in anhedral phase. Plagioclase, subhedral but rarely euhedral, often shows diffuse lamellae and sharply defined albite twin. Patchy texture (where several plagioclases grew and merge to form a single larger grain) is common among plagioclase. However, concentric zoning is rarely observed. Quartz could occur as a single grain or in a cluster. They are mostly anhedral and are randomly distributed.

Biotite is strongly pleochroic from light brown to dark red. Most biotite in the melagranite is euhedral in shape and has a clear cleavage. Smaller subhedral biotite grain occurs within the quartz-feldspar groundmass. Some might show very minor straining/foliation. Biotite is also found arranged around the K-feldspar phenocrysts or megacrysts. They are sometimes associated with amphibole and pyroxene, forming small mafic clots. Tiny biotite grains surrounding the amphibole and pyroxene suggest some of them are contributed from alteration on the rim of the crystal. Minor chlorite is sometimes found in between biotite cleavages.

Amphibole usually exhibits weak green pleochroism and appears as clusters of fine granules. Due to this condition, it is difficult to notice the cleavage in most grains. Only in a few cases, the amphibole characteristic cleavage can be identified. Amphibole is usually identified from the relief difference between quartz, feldspar and biotite. Besides that, amphibole also shows bright yellow under crossed nicols light. Most observed amphibole show pyroxene cores in the middle of the cluster, which suggest they are being formed by replacement of pyroxene (possible showing reaction rims from reaction with hydrous residual melt) (Fig. 4.4 b, c, d, e).

Pyroxene has wide range of sizes and is typically subhedral. Good cleavages are typically absent; they are usually identified by their high relief and interference color. Orthopyroxene (Fig. 4.3 e and f) are typically brown or colorless in plane polarized light. Large orthopyroxene (~2.0 mm) are rare and often enclosed other minerals such as plagioclase and opaque minerals. Clinopyroxene are typically colorless in plane polarized light and may sometimes show weak green pleochroism. Clinopyroxene (Fig. 4.3 c) are usually easily distinguished by their second order bright blue color under crossed nicols light.

Zircon is the most common accessory mineral in the granitoid. Most of them are found inside the pleochroic halos of biotites. Others are found scattered among the other minerals. Zircon size is usually within 0.1 to 0.2 mm. However, zircons as large as 0.4 mm can be found (Fig. 4.5 e). Such stubby and equant forms of zircon are common in deep seated, slowly cooled intrusion (Corfu et al. 2003). Apatite is abundant and can be easily noticed in acicular form within feldspar or in hexagonal shape within biotite in plane polarized light. Titanite (Fig. 4.5 b, c, d) is common as shapeless, strained grains; though near perfect grains can be found. Allanite is very rare (Fig. 4.4 f) but tourmaline is much rarer. Only one small tourmaline grain was found, embedded within one of the K-feldspar phenocrysts.

4.3 Mafic microgranular enclaves

The mafic microgranular enclave's size could vary from small to large (5 cm to 30 cm). The enclaves are widespread within the rock body. They are easily distinguished, as they are fine grained and dark colored compared to the host rock. Their shape is either ovoid or angular-irregular. The enclaves are typically found aligned with the large K-feldspar porphyry or megacryst. Macroscopic observation suggests feldspar phenocrysts are sometimes found in the enclaves (possible magma mixing?).

The contact between the enclaves and host rock vary between sharp to gradual (Fig. 4.6 a and b). Contacts may look smooth on macroscopic observation, but under microscopic observation, they look jagged, with many slightly coarser biotite clots protruding into the host. The enclave shows an intergranular bulk rock texture. The mineral assemblage in enclaves typically consists of biotite, pyroxene, amphibole, quartz, feldspar. Titanite, zircon and apatite may also occur in the enclaves. The thin section photomicrograph for the melagranite is shown in Fig. 4.5 and 4.6.

Quartz and K-feldspar are regarded as minor/accessory minerals (both are less than 5%) within the enclaves. They (and plagioclase) often appear as anhedral to subhedral phenocryst. Plagioclase, the more common felsic minerals, also occurs as small anhedral to subhedral grains and show simple twins or Carlsbad twining. Plagioclase is about ~30% in most enclaves except for a few from the Baling-Gerik area. Those enclaves have slightly higher plagioclase content (~40%).

Biotite is very common (30 to 40%) in the enclaves. Their presence is the main reason for the enclave dark color. They are subhedral within the enclaves and only euhedral near the rim. Very small biotite inclusions can be found inside plagioclase and pyroxene grain. Amphibole (~5%) is usually associated with pyroxene. They are in

small subhedral to anhedral grains and often do not show clear cleavage. I suggest they are probably altered from nearby clinopyroxene.

Pyroxene (~15%) in the enclaves are mostly unaltered (to amphibole) compared to the ones in the granite. Clinopyroxene (some display simple and lamellar twin, which suggest possible augite) is often more common than orthopyroxene in the enclaves. Exsolution texture, which is usually associated with slow cooling in large mafic intrusion (Gill, 2010), can sometimes be found in pyroxene. These textures are not very common, but they do occur. Pyroxene, amphibole and biotite are often found together forming larger mafic clots.

Titanite is the most common accessory in the enclaves. Euhderal titanite is most often found near the rim of the enclaves. Smaller, anhedral, fractured titanite fragments are found deeper within the enclaves. Zircon is also widespread in the enclaves. They are smaller than their counterparts in the granite and are identifiable by their high relief. Apatite occurs as both acicular and hexagonal crystal in the enclaves. Rutile, a rare accessory mineral, is brown colored, anhedral, shows extreme positive relief and birefringence. Quartz-chlorite veins can be seen cutting through one of the enclaves. Secondary alteration of biotite into chlorite is observed in the veins.

4.4 Chapter summary

1. Amphibole-bearing melagranite main mineral assemblage is: K-feldspar + quartz + plagioclase + biotite + amphibole ± orthopyroxene ± clinopyroxene. Acessory minerals are: zircon, apatite, titanite and allanite.
2. Mafic microgranular enclave main mineral assemblage is: Biotite + pyroxene + amphibole + quartz + feldspar. Titanite, zircon, apatite and rutile appear as accessory minerals.
3. The contact between the melagranite and enclaves is sharp to gradual. No chill margin is observed in the contact.
4. Minor post-magmatic alteration is observed in the rocks. Elements (especially LILE) which are mobile during alteration will be interpreted with caution.

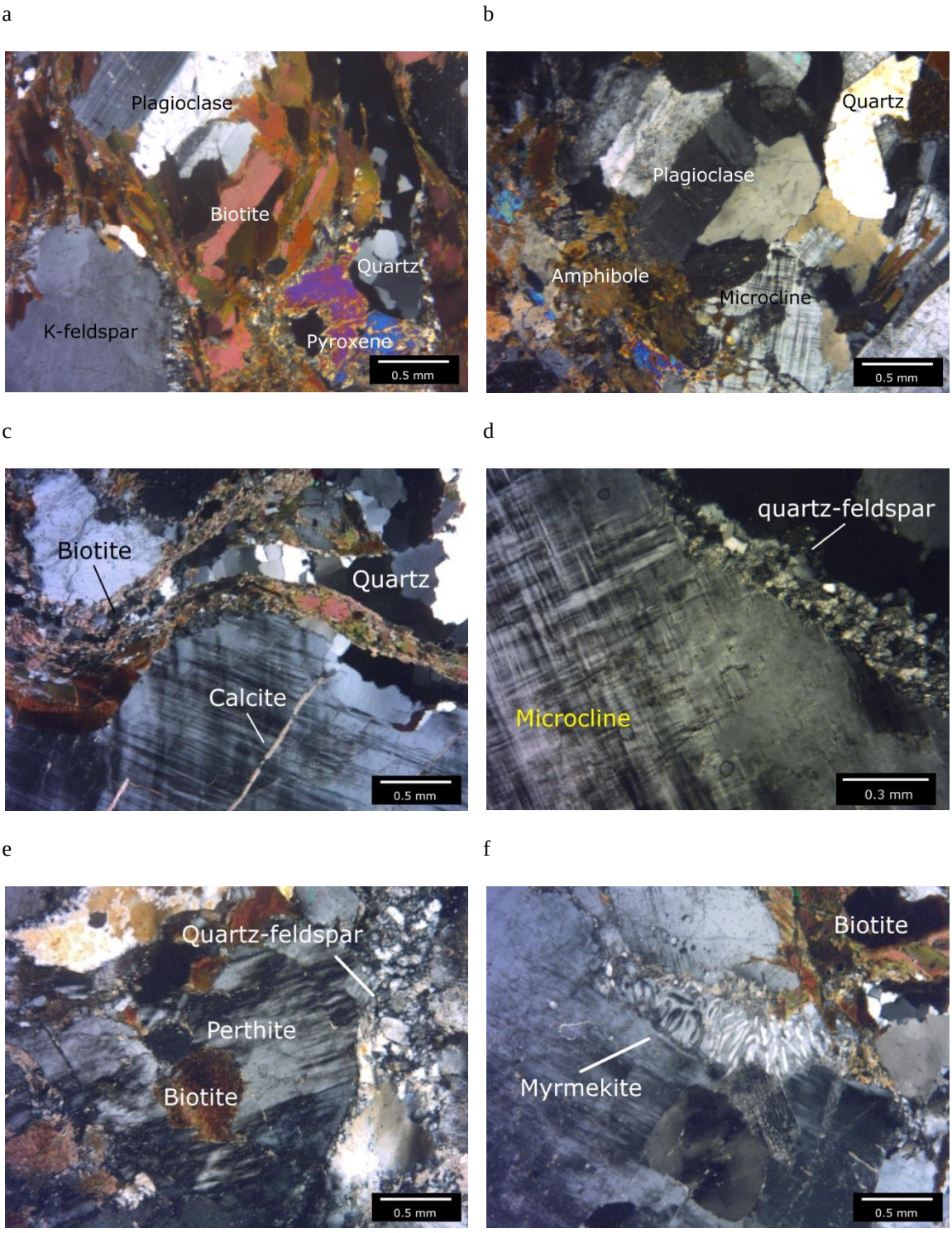

Fig. 4.2: Thin section photomicrograph of melagranite (a) typical Taiping melagranite mineral assemblage, (b) another view of Taiping melagranite mineral assemblage, (c) strained biotite grains around the feldspar, (d) Tiny quartz-feldspar grains around large K-feldspar phenocryst, (e) biotite inclusion within the K-feldspar (pethitic texture) grain. (f) myrmekite within large K-feldspar phenocryst. Scale bar is shown on the bottom right of the picture.

a

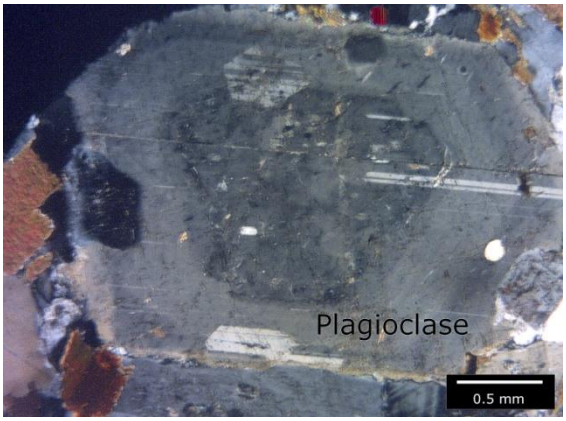

b

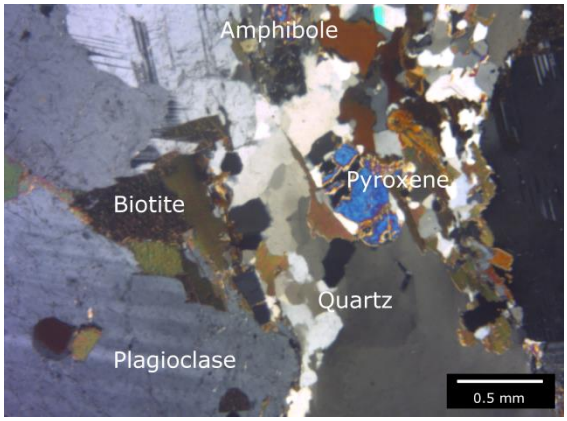

c

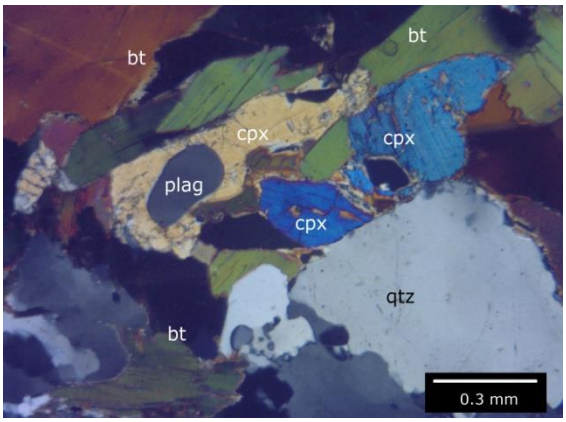

d

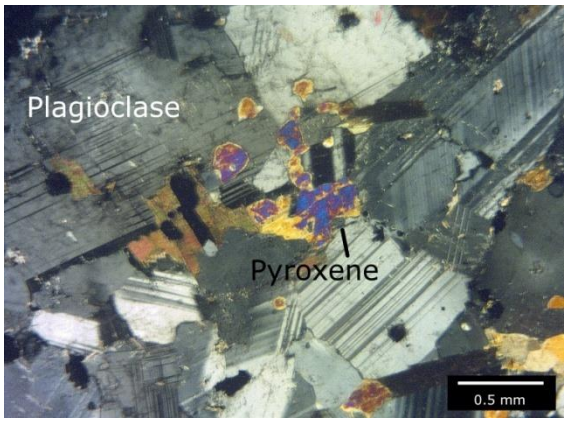

e

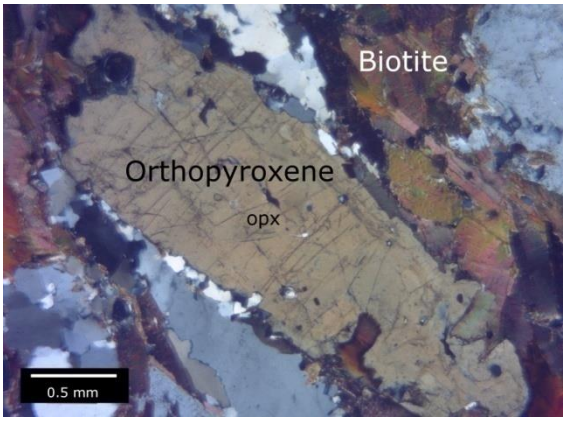

f

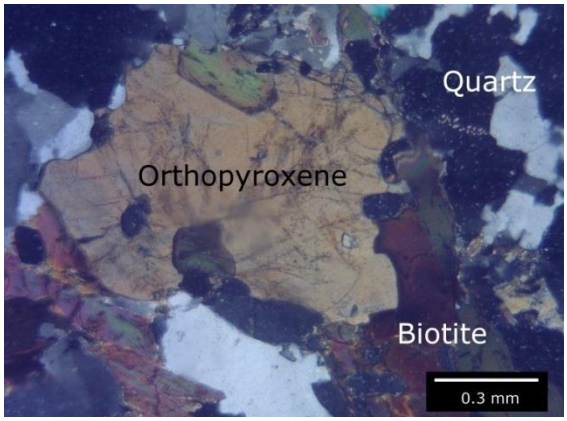

Fig. 4.3: Thin section photomicrograph of melagranite (a) concentric zoning within plagioclase grain, (b) tiny clinopyroxene grain within a group of biotite, (c) pyroxene showing tiny exsolution texture within a group of biotite, (d) tiny pyroxene grain within a group of plagioclase, (e) large orthopyroxene grain, (f) orthopyroxene grain similar to (e), but smaller. Scale bar is shown on the bottom right of the picture.

a

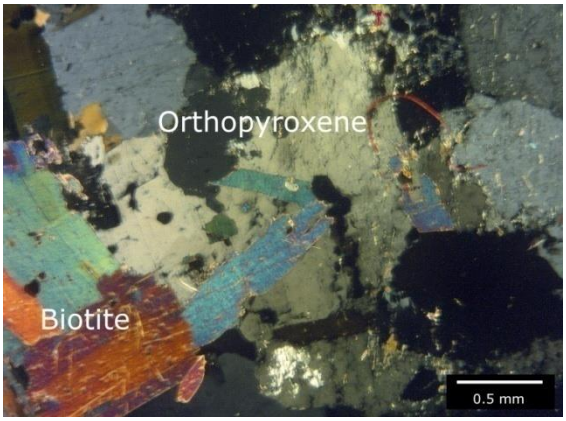

b

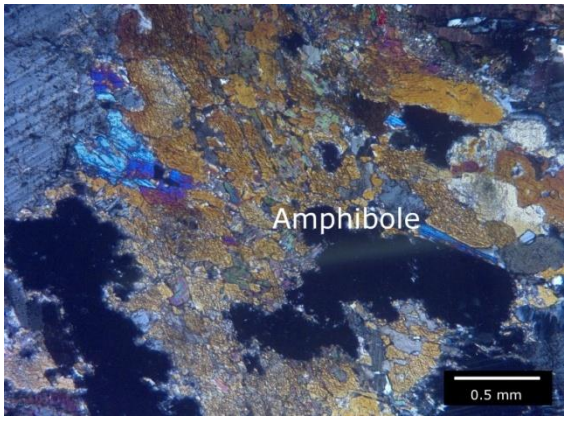

c

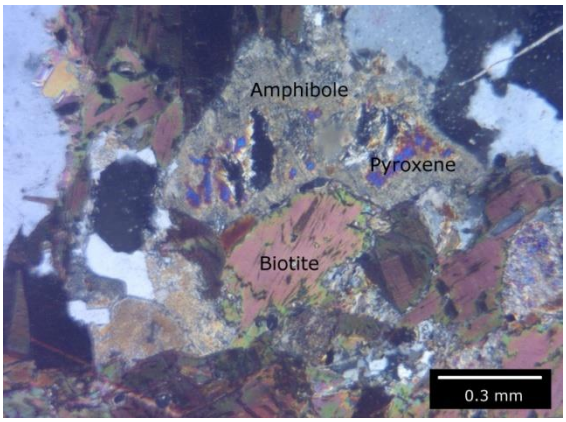

d

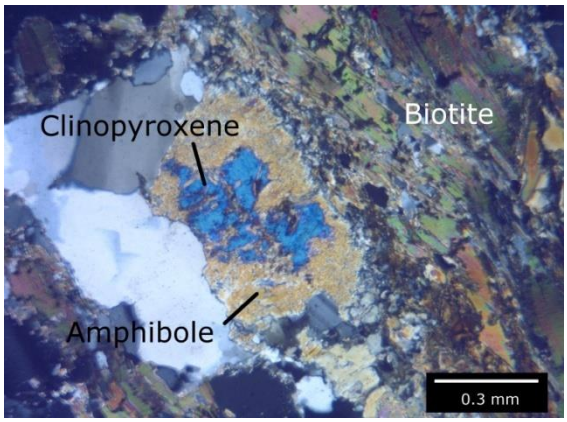

e

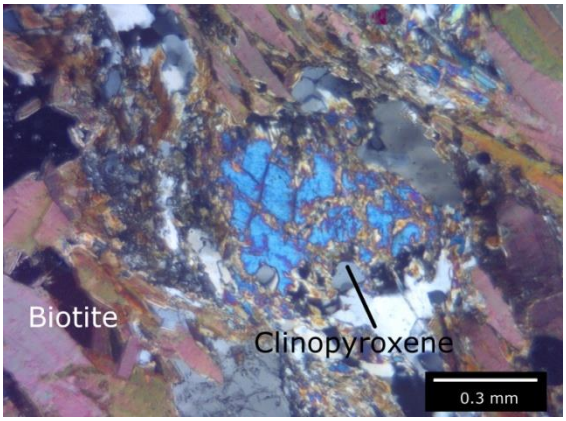

f

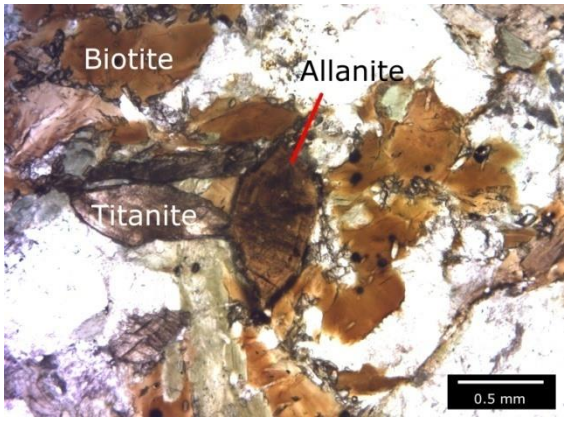

Fig. 4.4: Thin section photomicrograph of melagranite (a) grey orthopyroxene within a group of biotite, (b) large amphibole grains which show clear cleavage, (c) a group of tiny amphibole grains with pyroxene inclusion within a group of biotite, (d) a group of tiny amphibole grains with pyroxene inclusion within a group of biotite, (e) a group of tiny amphibole grains with pyroxene inclusion within a group of biotite. The amphibole cleavage is noticeable, (f) allanite and titanite within a group of biotite. Scale bar is shown on the bottom right of the picture.

a

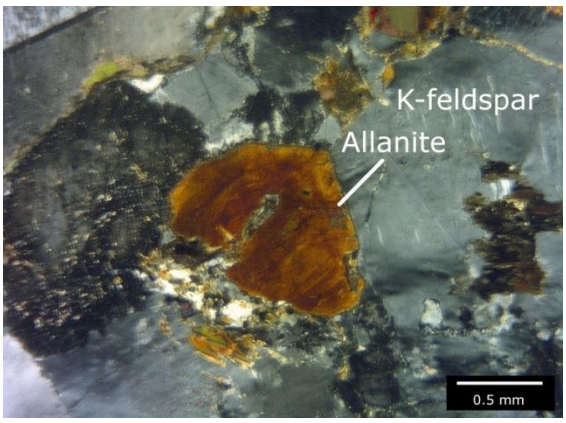

b

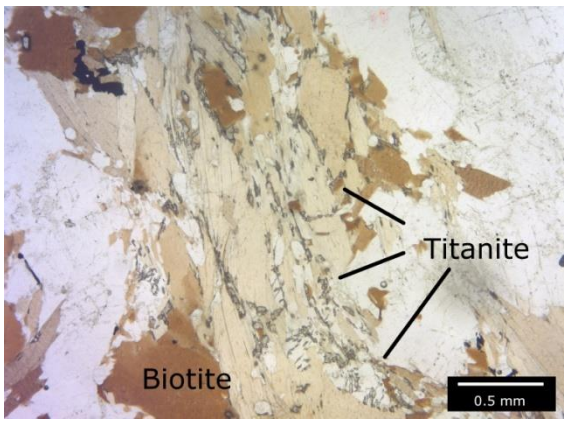

c

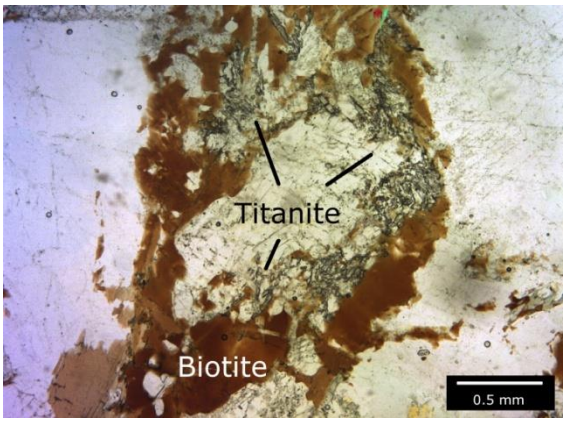

d

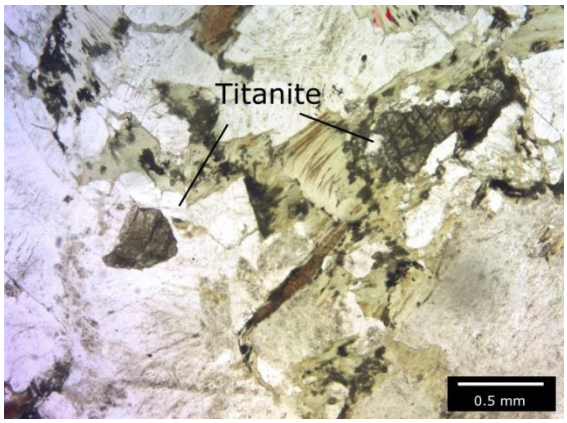

e

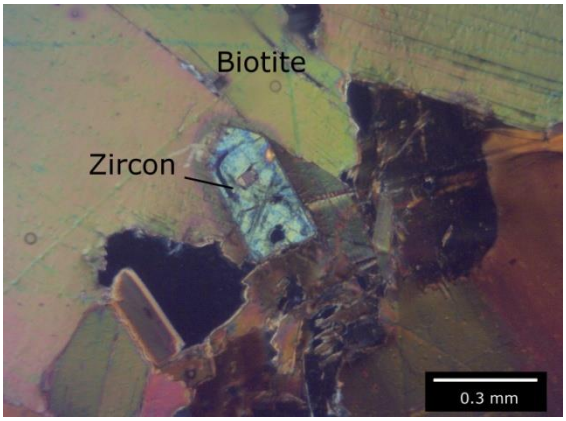

f

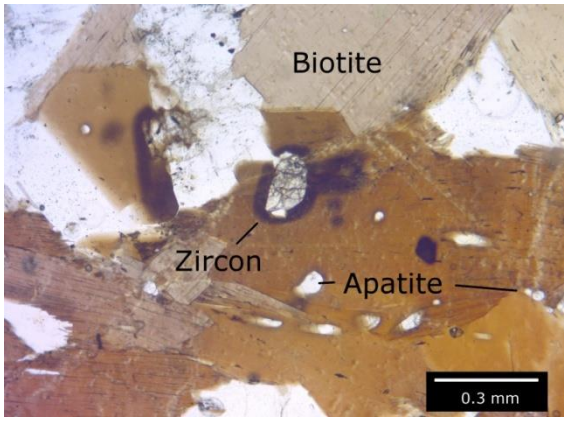

Fig. 4.5: Thin section photomicrograph of melagranite (a) allanite in cross nichols light, (b) tiny titanite grain within a group of biotite, (c) tiny titanite grain within a group of biotite, (d) near euhedral, fragmented titanite in a heavily chloritized biotite, (e) large zircon grain, (f) zircon and apatite accessory within biotite group. Scale bar is shown on the bottom right of the picture.

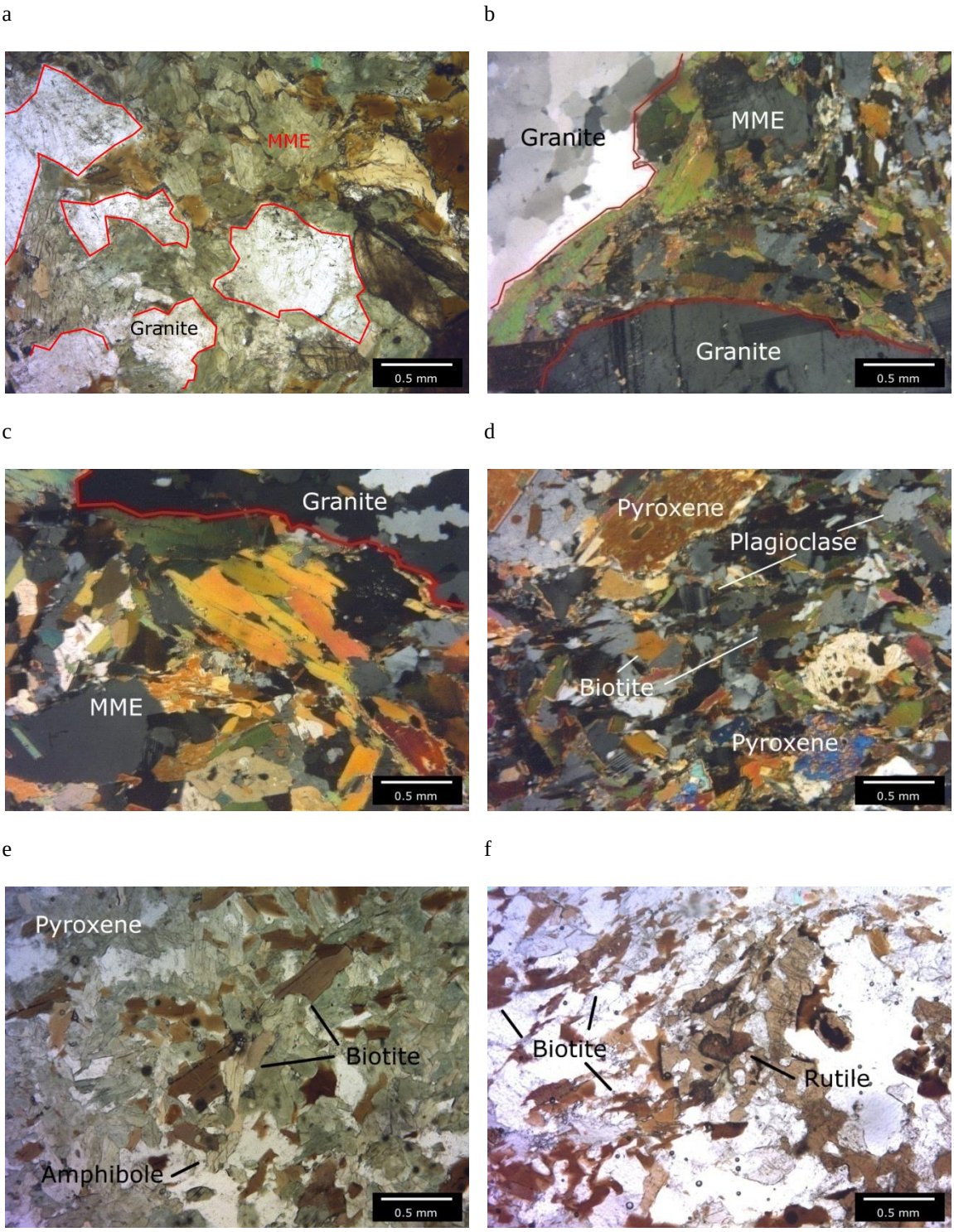

Fig. 4.6: Thin section photomicrograph of MME (a) contact (red line) between MME and granite, (b) contact (red line) between MME and granite, (c) contact (red line) between MME and granite, (d) typical mineral assemblage within MME, (e) typical mineral assemblage within MME in plane polarized light, (f) rutile fragment within a group of biotite and pyroxene. Scale bar is shown on the bottom right of the picture.

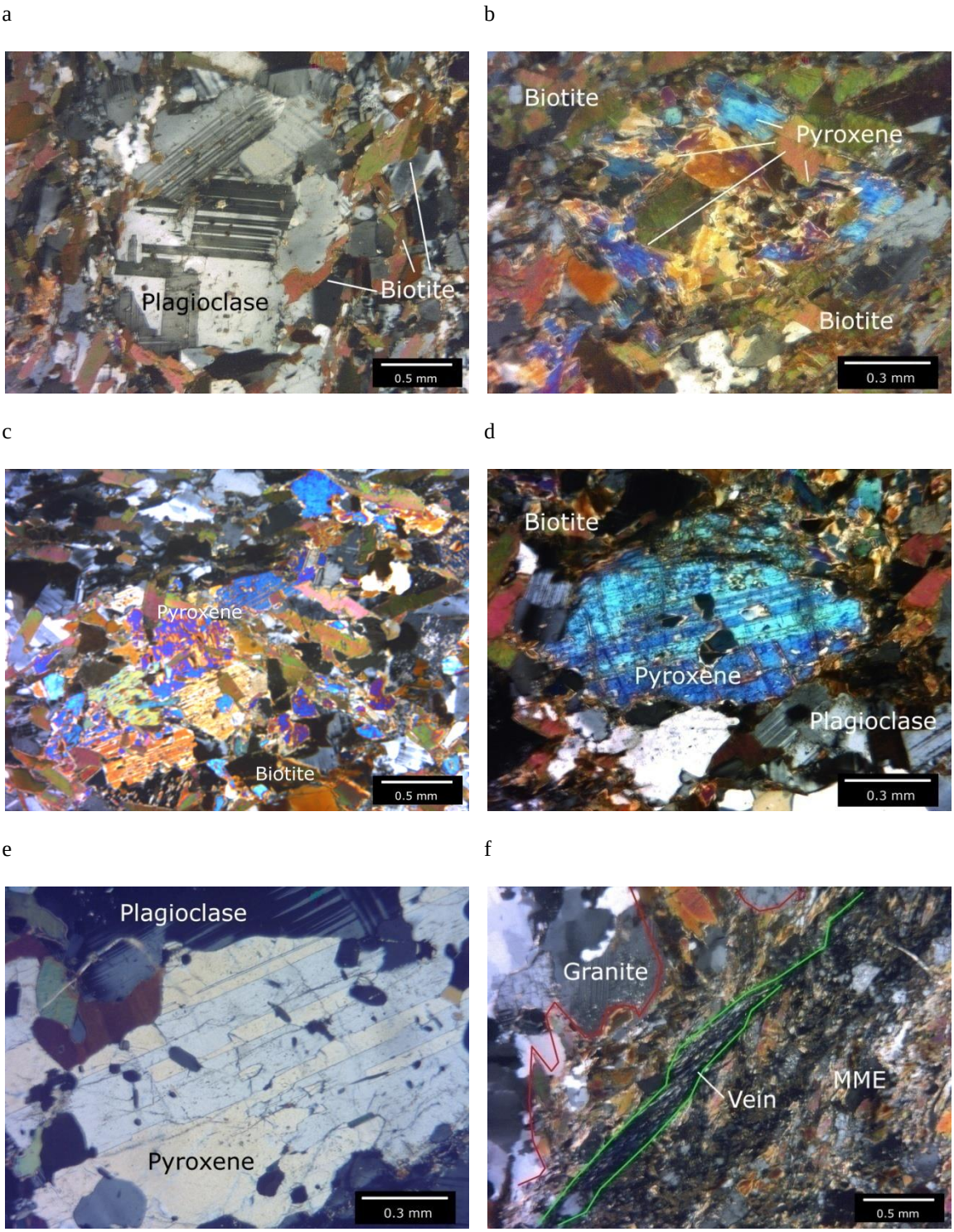

Fig. 4.7: Thin section photomicrograph of MME (a) patchy texture in plagioclase phenocryst, (b) pyroxene within a group of biotite, (c) pyroxene with patchy texture and tiny biotite inclusion within a group biotite, (d) pyroxene with multiple mineral inclusion showing exsolution texture, (e) pyroxene with well developed exsolution texture, (f) quartz-chlorite vein within one of the MME, red line mark the granite-MME contact. Scale bar is shown on the bottom right of the picture.

CHAPTER 5: GEOCHEMISTRY

5.1 Introduction

Samples are sent to Acme Analytical Laboratories, Canada for X-ray fluorescence (XRF) spectrometer and inductively coupled plasma mass spectrometry (ICP-MS) analysis. The major elements are in oxide form and expressed as weight percentage (wt. %). Trace elements are expressed in parts per million (ppm). All data are tabulated in Appendix 1 (ultrapotassic samples label are in bold and italic).

5.2 Amphibole-bearing melagranite

Taiping amphibole-bearing melagranite are metaluminous to weakly peraluminous (A/CNK = 0.65 – 1.06) with SiO_2 range from 68.3 to 58.4 wt. %. While petrographic results might suggest possible similarity to granite, these rocks bear no geochemical similarities to typical granite. Table 5.1 shows the average and standard deviation of the melagranite major elements compared with average of standard diorite, monzonite, granodiorite and granite (Le Maitre, 1976).

5.2.1 Harker, rare earth elements (REE) and multi-elements variation diagram

Major element Harker variation diagrams are shown in Fig. 5.1 and selected trace Harker variation diagrams are shown in Fig. 5.2. Negative trend are shown in the SiO_2 vs. FeOt, CaO, MgO, TiO_2 and P_2O_5 plot. No clear trend can be observed in SiO_2 vs. Na_2O and SiO_2 vs. K_2O plots. The scatter on the alkalis is due to their mobility during post magmatic processes (through hydrothermal fluids) (Rollinson 1993).

Table 5.1: Comparison with Le Maitre (1976) averages

Major elements	Le Maitre (1976) average				Amph-bearing melagranite	
	Diorite	Monzonite	Granodiorite	Granite	Average	σ
SiO2	57.48	62.00	66.09	71.30	63.85	2.61
Al2O3	16.67	15.65	15.73	14.32	14.34	0.94
FeO	4.92	3.08	2.73	1.64	4.19	0.81
Fe2O3	2.50	1.92	1.38	1.21	0.52	0.10
CaO	6.58	4.17	3.83	1.84	3.26	0.80
MgO	3.71	2.02	1.74	0.71	3.56	1.14
Na2O	3.54	3.73	3.75	3.68	2.04	0.31
K2O	1.76	4.06	2.73	4.00	5.07	1.23
MnO	0.12	0.10	0.08	0.05	0.06	0.02
TiO2	0.95	0.78	0.54	0.31	0.91	0.17
P2O5	0.29	0.25	0.18	0.12	0.36	0.09

LILE (large-ion lithophile elements; selected: Ba, Rb, Sr, Cs) show poor linear correlations (strong scatter) while most HFSE (high field strength elements; selected: Zr, Nb, Y, Ga) barely register a negative trend. Stronger scattering in LILE can be explained by their higher mobility compared to HFSE during post magmatic alteration processes (Rollinson 1993).

Chondrite normalized REE plots are historically based on volatile-free chondrite (vfCI), such as from Boynton (1984) (Korotev, 2009). Compared to the carbonaceous chondrite (CI), vfCI normalizing values are higher. The chondrite normalized rare earth element (REE) variation diagram after Boynton (1984) (Fig. 5.3) shows the REE patterns for Taiping melagranite. REE patterns for the majority of the suite are slightly light REE (LREE) enriched with Ce_N/Yb_N = 47.5 – 2.2. They also show moderate negative Eu-anomalies (Eu/Eu* = 0.1 – 1.0)

The primitive mantle normalized multi-element variation diagram (Fig 5.4) after Mcdonough and Sun (1995) shows absence of Pb-anomaly in all three patterns, which suggest a stronger continental contribution and a weaker arc signature (Sun and Mcdonough, 1989). The contribution of subduction related materials are also confirmed by the T-N-T (Ta, Nb and Ti) depletion (Sun and Mcdonough, 1989).

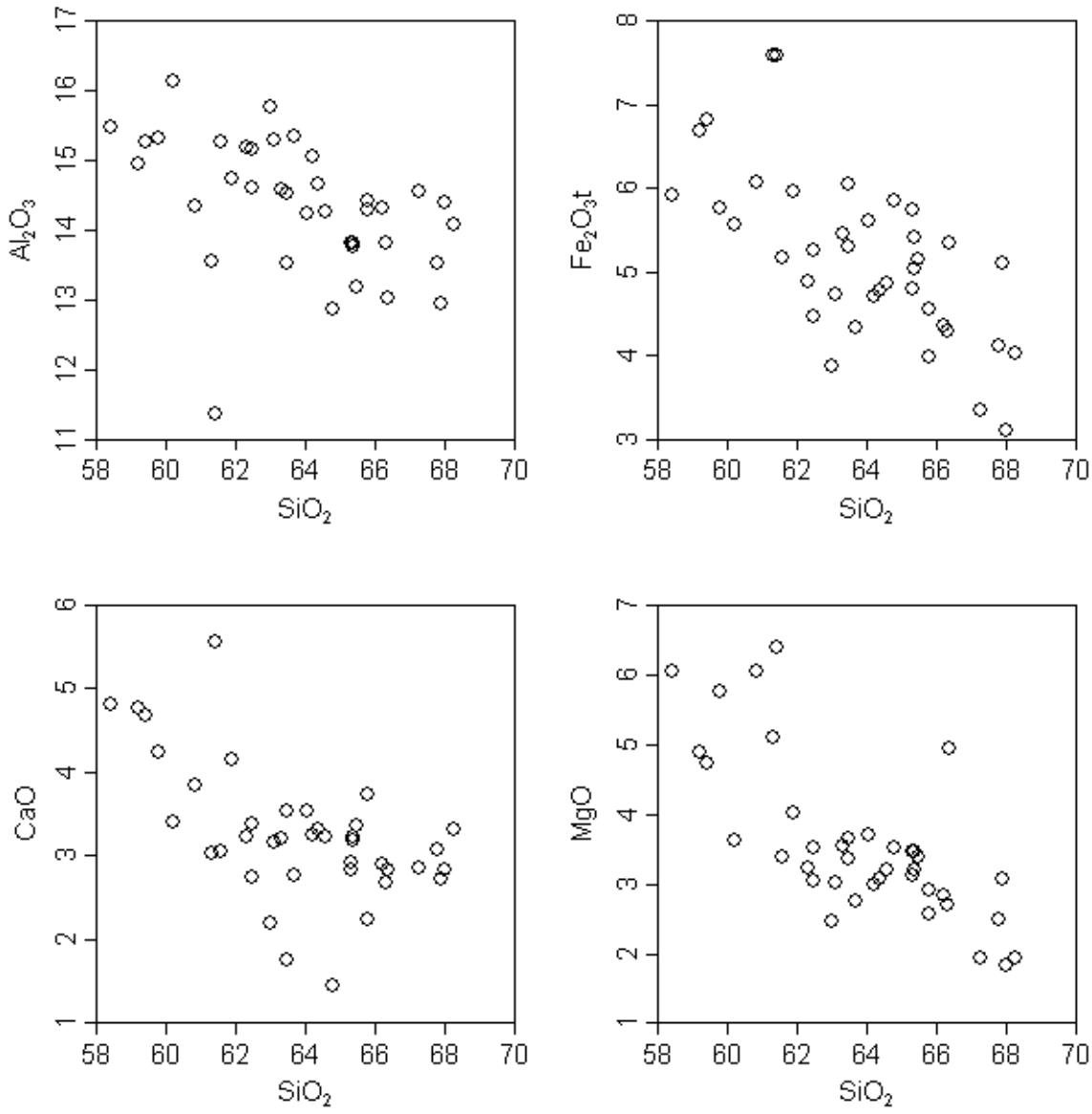

Fig. 5.1a: Major element Harker diagram for Al_2O_3, FeOt, CaO and MgO

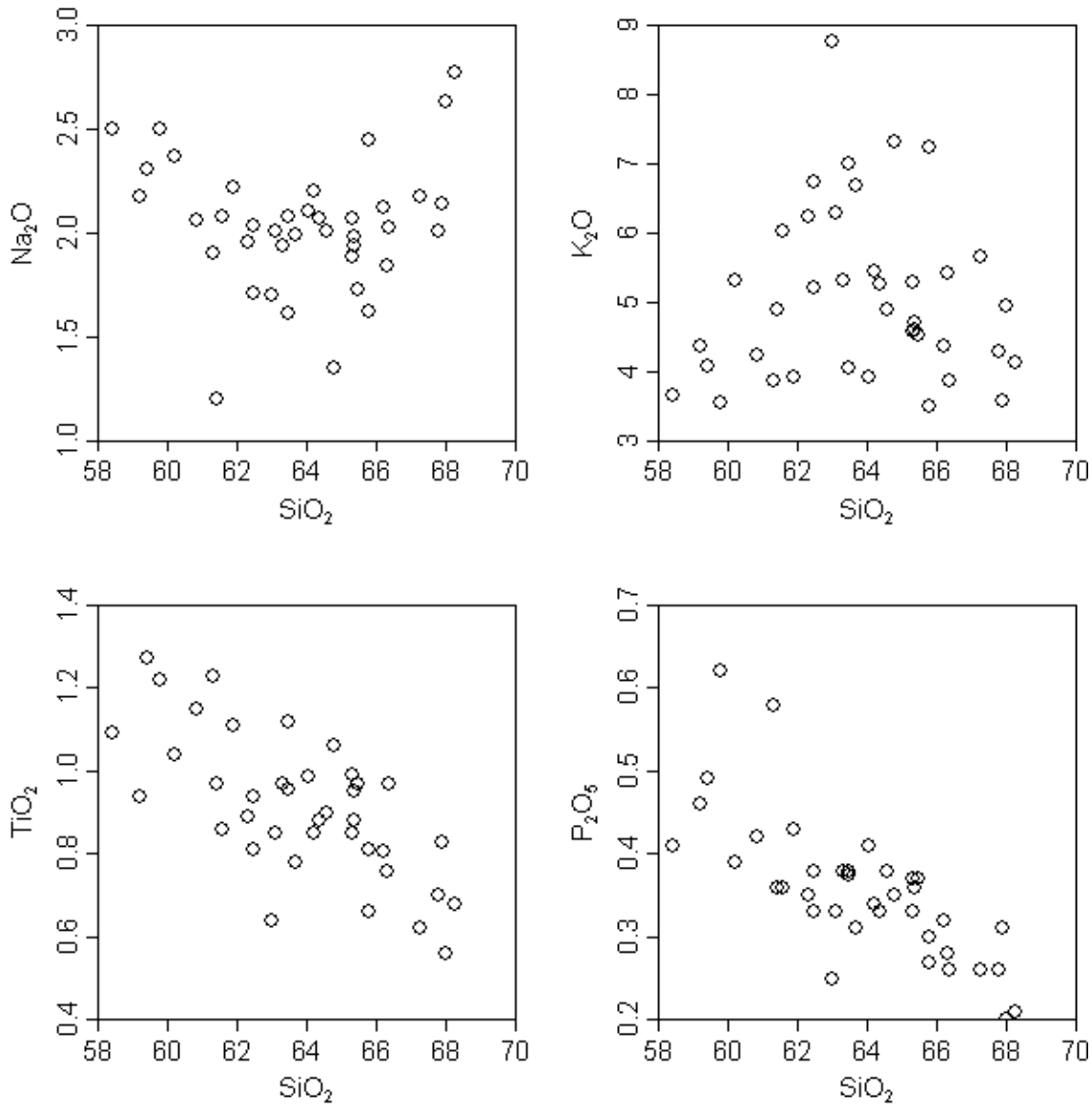

Fig. 5.1b: Major element Harker diagram for Na_2O, K_2O, TiO_2 and P_2O_5

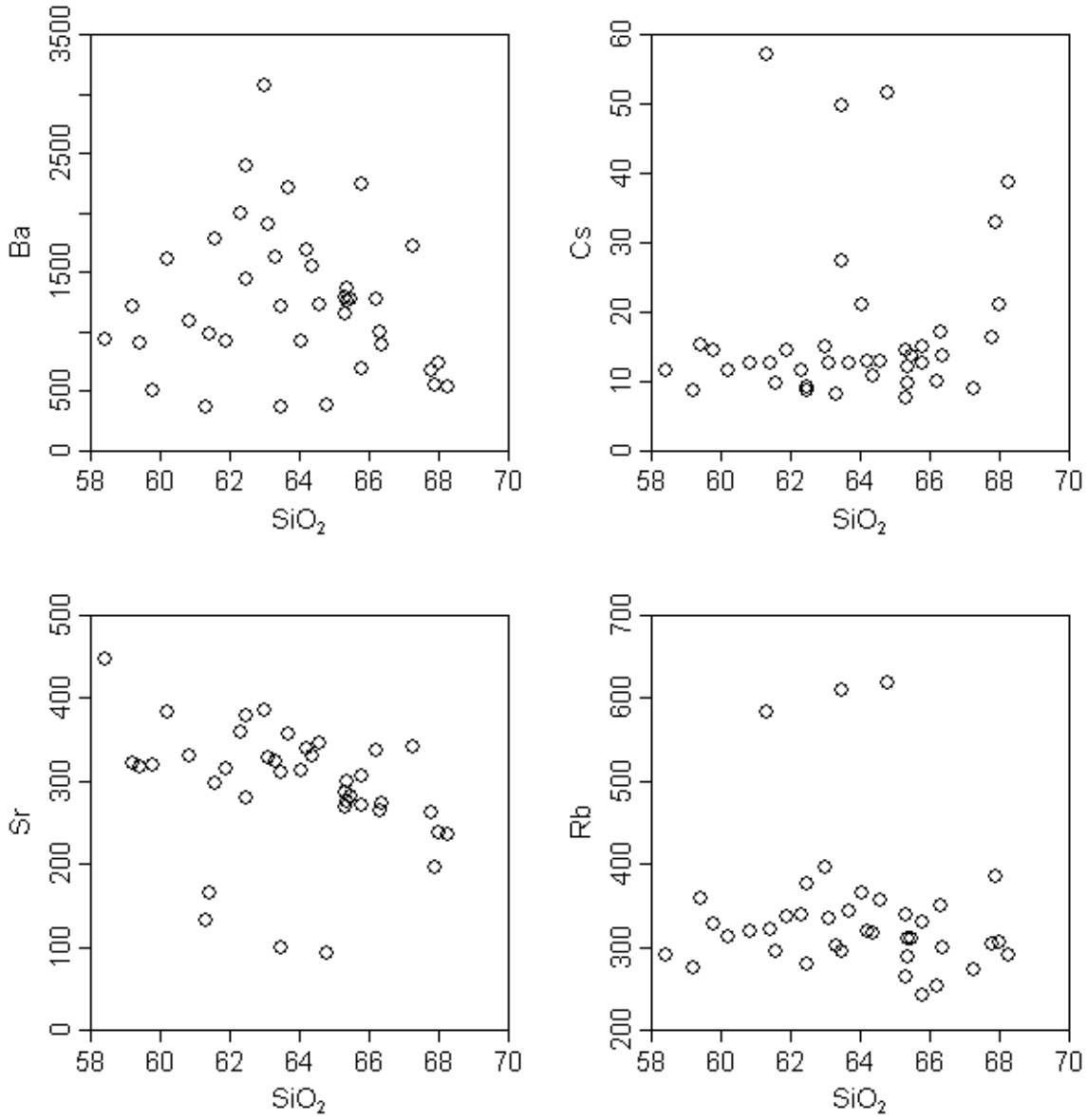

Fig. 5.2a: Trace element Harker diagram for Ba, Sr, Rb and Cs (LILE)

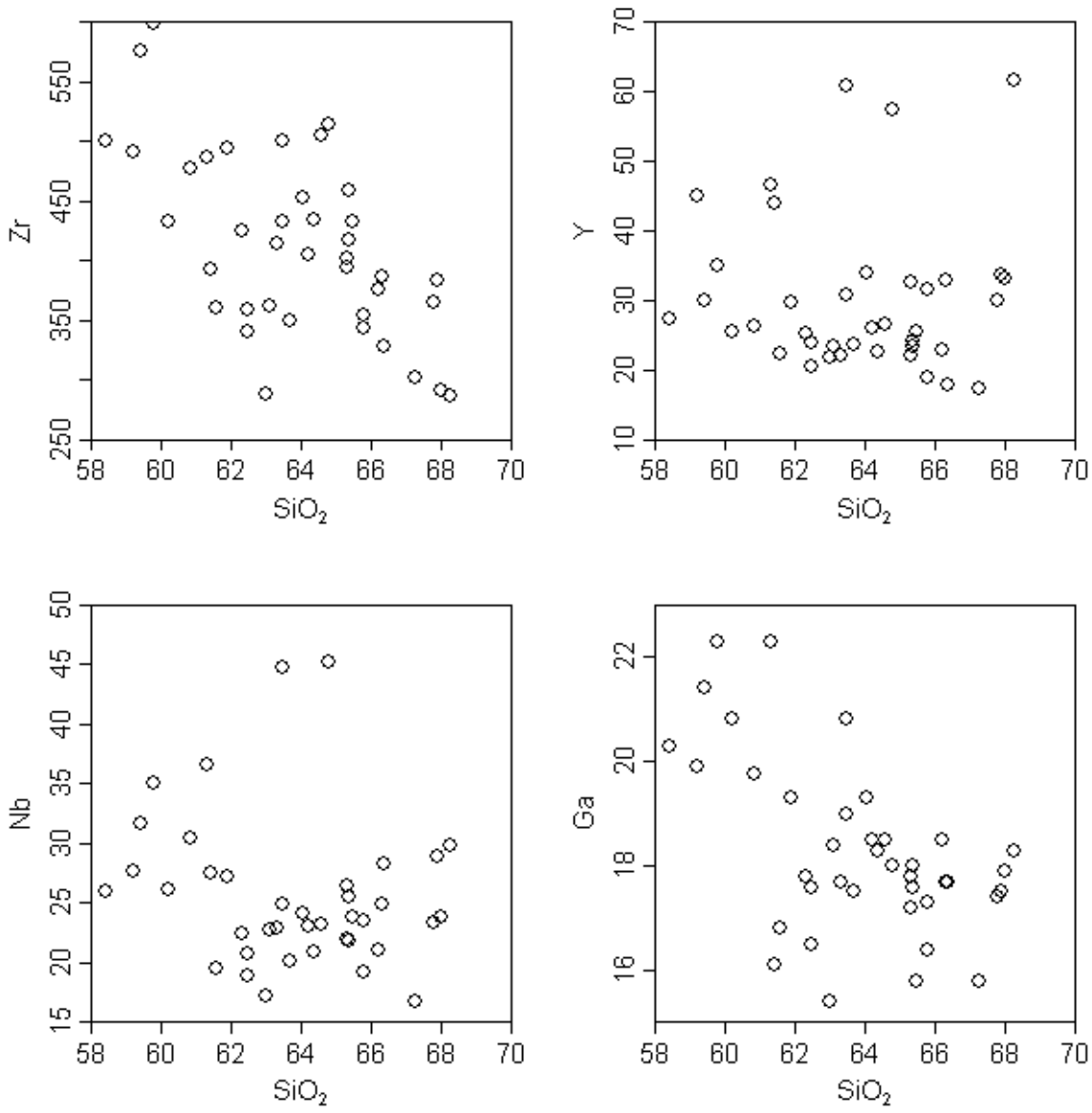

Fig. 5.2b: Trace element Harker diagram for Zr, Nb, Y and Ga (HFSE)

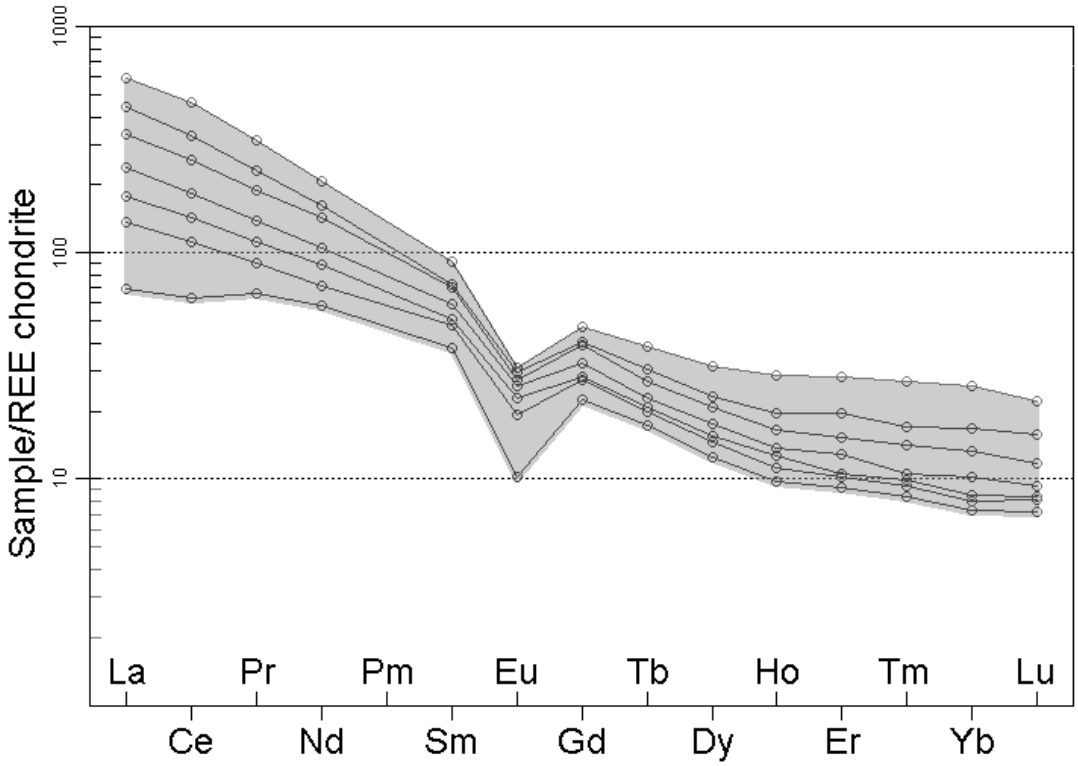

Fig. 5.3: Melagranite Boynton (1984) Chondrite normalized REE plot

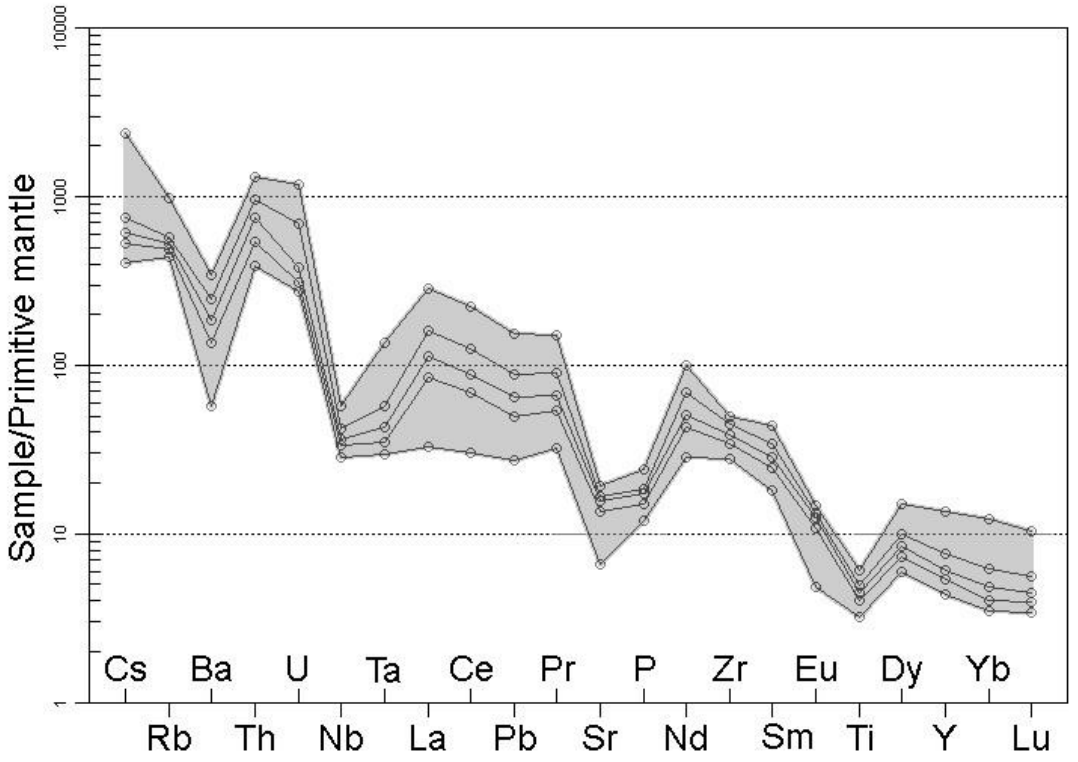

Fig. 5.4: Melagranite Mcdonough and Sun (1995) Primitive mantle normalized multi element diagram

5.2.2 Ultrapotassic characteristics

The ultrapotassic melagranites are screened out from the non-ultrapotassic ones using the definition of Foley et al. (1987), where rocks with K_2O > 3 wt. %, K_2O/Na_2O > 2 and MgO > 3 wt. % are considered ultrapotassic. 21 samples (total samples: 39) are ultrapotassic. Ultrapotassic samples are identified and indicated in Appendix 1 (bold and italic). Utrapotassic samples have a high magnesium number (54.2 – 66.4) and high K_2O (3.86 to 7.31 wt. %).

As the samples show very high potassium content, most of them plot within the shoshonite series on SiO_2 vs. K_2O plot by Peccerillo and Taylor (1976) (Fig. 5-1). In the shoshonite-appinites-durbachite K vs. Rb discrimination diagram (Fig. 5-2) by Bowes and Kosler (1993), most samples fall within the durbachite field, indicating that the samples are related to the durbachite series. The diagram also suggests that the samples are a more evolved product of the shoshonitic magma series.

The durbachite series relationship is further discussed here. The melagranite shares several geochemical similarities with the durbachite series, a type of ultrapotassic rock which originated from Central Europe:

1. The Mg number (54.2 – 66.4) and Cr content (233 – 568 ppm) of the ultrapotassic rocks is comparable to intermediate durbachite (Certovo Bremeno suite) of Janousek et al. (2000) (Mg number: 58.23 – 69.9; Cr: 122 – 498 ppm).
2. Their CaO/MgO ratio falls between 0.41 and 1.09, comparable to the durbachite where the ratio is usually less than 1 (Kusiak et al., 2010).
3. Their high Th/U ratio (2.38 to 12.8) and Rb/Sr ratio (0.82 to 6.64) are comparable to durbachite, where the Th/U ratio is usually up to 12-13 and the Rb/Sr ratio ranges from 0.7 to 1.2 (Scarrow et al., 2009).

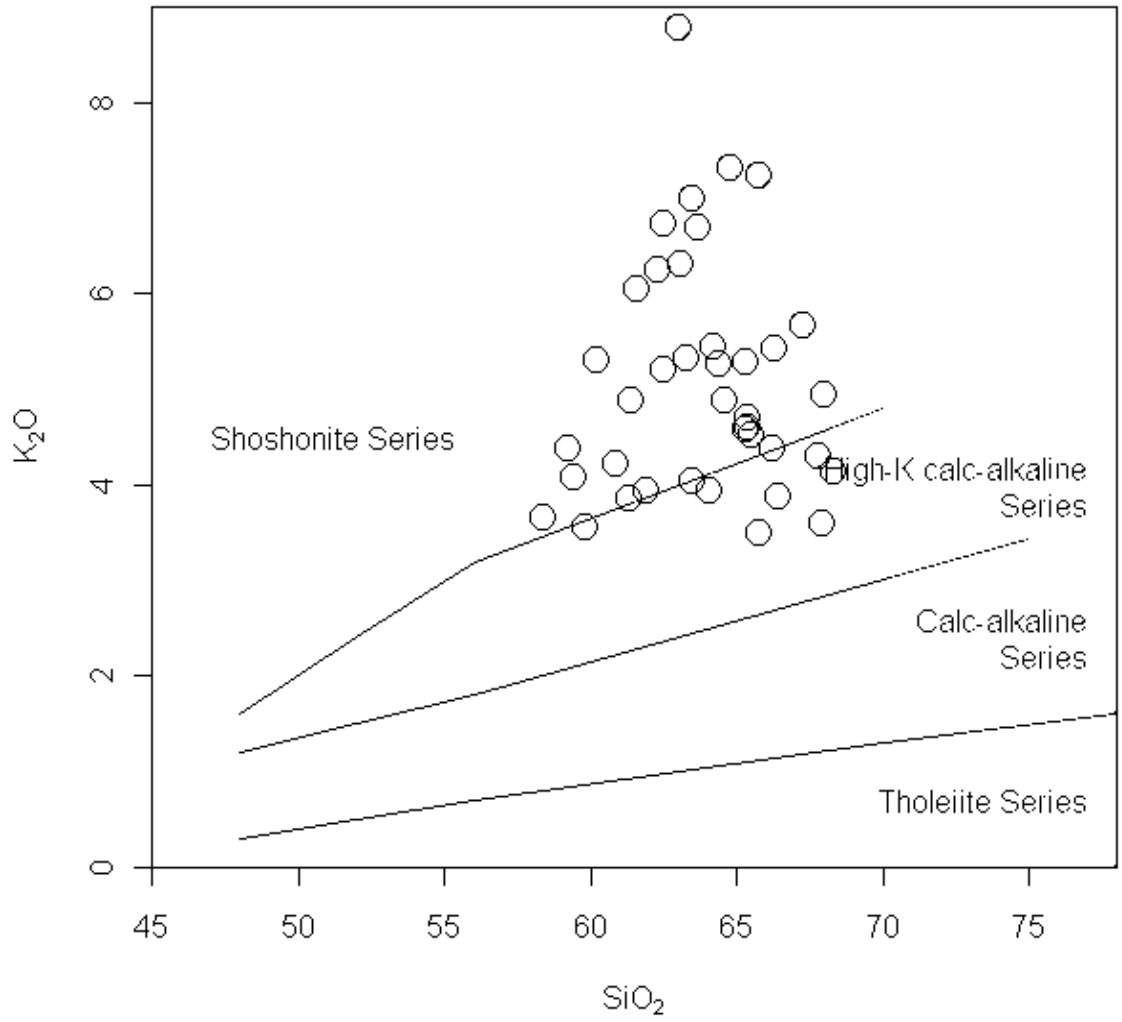

Fig. 5.5: Peccerillo and Taylor (1976) SiO_2 vs. K_2O plot. Most samples falls within the shoshonite series

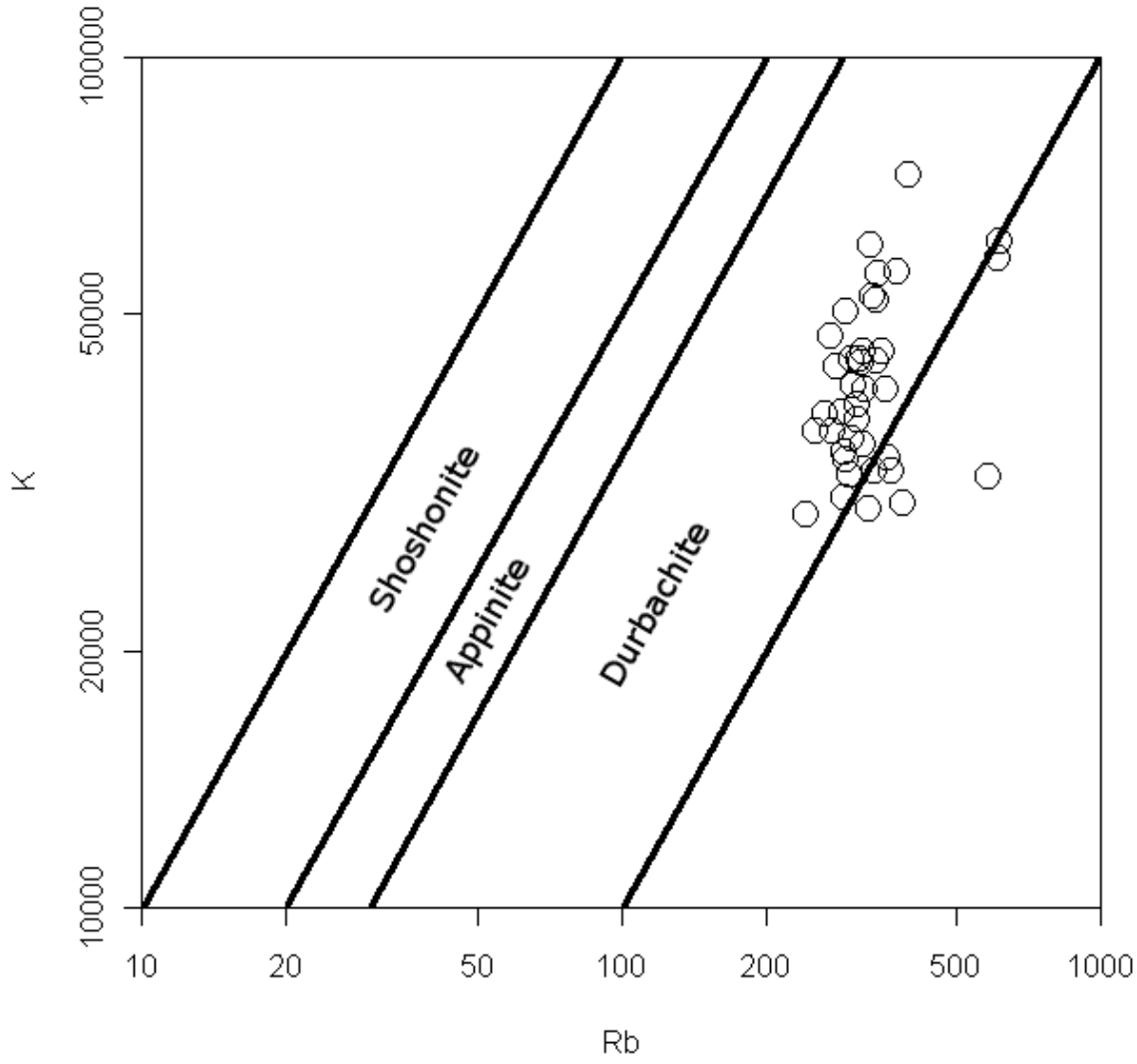

Fig. 5.6: Bowes and Kosler (1993) Shoshonite-appinites-durbachite K vs. Rb discrimination diagram. Most ultrapotassic samples falls within the durbachite field

Such geochemical characteristics are also present in other ultrapotassic rock type, e.g., lamproites, kamafugites, plagioleucitites (Foley, 1992; Bowes and Kosler, 1993). It is the geochemical plus the petrographic features that make the ultrapotassic melagranite comparable to the durbachite group. Therefore, the ultrapotassic melagranite are grouped here to form a new group, Taiping "durbachite".

Taiping "durbachite" is further compared with the European durbachite suite (Bowes and Kosler, 1993; Janousek et al., 2000; Kotkova et al., 2010) chondrite normalized rare earth elements diagrams (Fig. 5.7 upper). In general, the patterns are quite similar. Taiping "durbachite" do have a larger LREE range and a slightly more negative Eu-anomaly compared to the typical durbachite. The difference in Eu-anomaly indicates a slightly stronger plagioclase fractionation (Weill and Drake, 1973). Still Taiping "durbachite" show typical durbachite features (Janousek et al., 1997; Holub, 1997): high ΣREE, high LREE/HREE ratios (reflected in its steep pattern), elevated LREE content and weak/ moderate Eu-anomaly (Eu/Eu*).

Taiping "durbachite" primitive mantle normalized trace elements pattern (Fig. 5.7 lower) is also comparable to the European durbachite suite (Janousek et al., 2000; Kotkova et al., 2010). The patterns show elevation in some LILE such as Cs, Rb, Ba and HFSE such as Th, U, Zr but show clear Ta-Nb-Ti (TNT) negative anomaly relative to the adjacent elements. Significant features are: (1) moderately enriched LREE patterns, (2) flat HREE patterns, (3) weak Eu depletion, (4) negative Ba, Nb, Ta, Sr and Ti anomalies, (5) positive Cs, Rb, Th, U, Nd, Zr, Sm anomalies. Absence of positive Pb anomaly in Taiping "durbachite" suggests a possible weaker arc signature (Sun and Mcdonough, 1989).

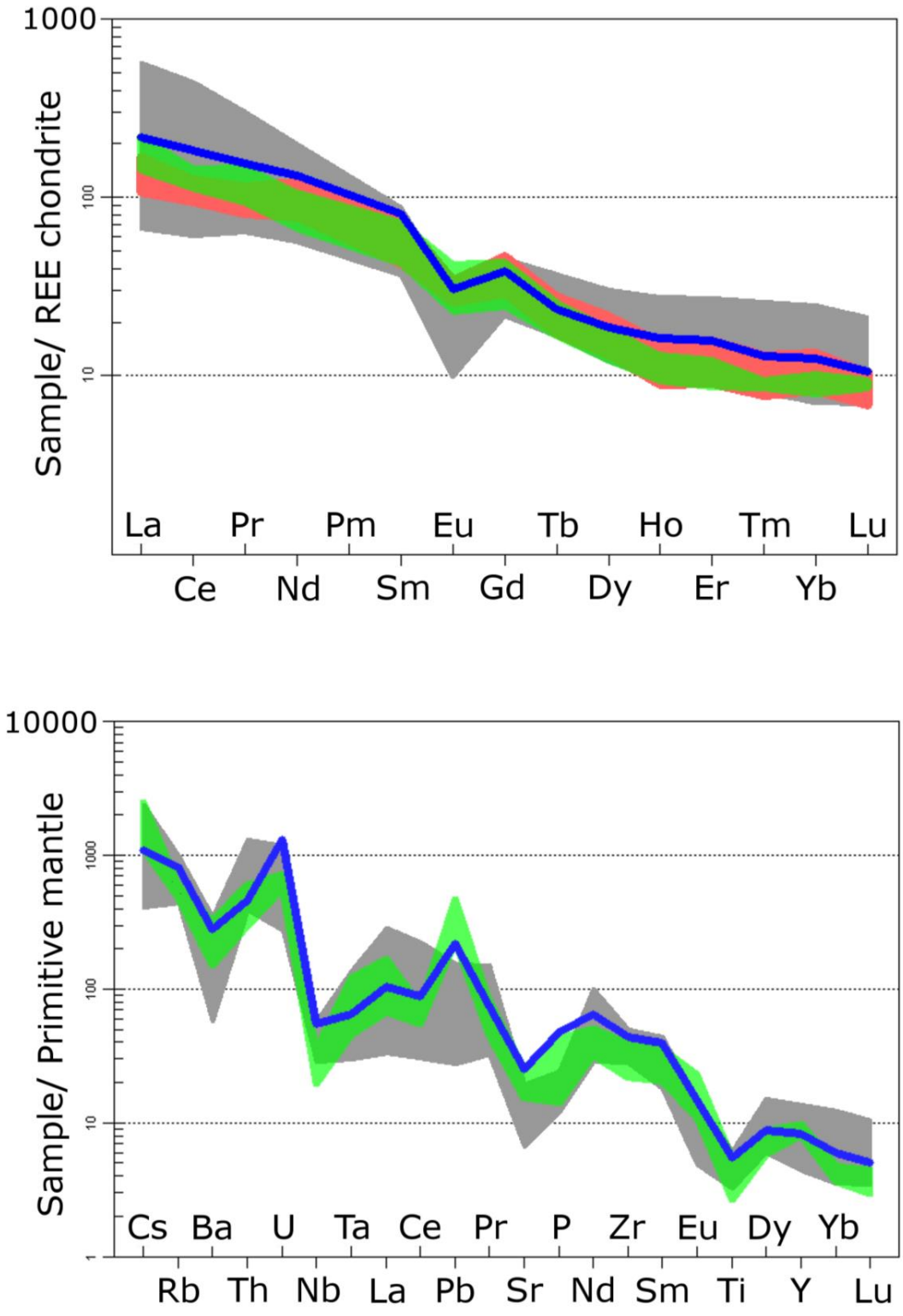

Fig. 5.7: Durbachite series comparison. Top: Boynton (1984) Chondrite normalized REE plot. Bottom: Mcdonough and Sun (1995) Primitive mantle normalized multi element diagram. Grey: Taiping "durbachite"; Blue: Trebic mafic durbachite (1 sample, melagranite) from Kotkova et al. (2010); Green: Certovo Bremeno suite from Janousek et al. (2000); Red: Bowes and Kosler (1993) durbachite.

5.2.3 Variation within melagranite

The pattern of all available non-ultrapotassic samples show near similar pattern to the Taiping ultrapotassic durbachite sample in both chondrite-normalized REE diagram and primitive mantle normalized trace element diagram (where a wider range of trace element is included). Careful observation of geochemical data and geochemical variation diagram such as AFM diagrams (below, Fig. 5.11) for the melagranite also did not show any particular trend, suggesting that there are no considerable differences between both types of samples.

The minor variation in the ultrapotassic indicator element (K, Na and Mg) in these samples could be caused by the erratic distribution peritectic minerals (Clemens and Stevens, 2012). Peritectic minerals are mineral crystals that form from peritectic reaction during partial melting of the protolith (Clemens and Stevens, 2012). Granitic melts are usually accompanied by these peritectic minerals (in varying degrees) as it moves away from the source region. Minerals such as pyroxene, plagioclase and K-feldspar could be the peritectic minerals for our rock and its distribution may affect the element K, Na and Mg in samples.

A large sample size is required to improve the ultrapotassic geochemistry detection and geochemical understanding of Taiping amphibole-bearing melagranite. Besides erratic distribution of peritectic minerals creating geochemical variation within the melagranite, minor post-magmatic alteration (hydrothermal activity perhaps?) may also cause element mobility (especially in the alkalis, K and Na), creating irregularities in sample geochemistry.

5.3 Comparison with typical Main Range type granite

Previous workers (Cobbing et al., 1992) have suggested that the Taiping amphibole-bearing melagranite is relatively un-evolved or primitive (primitive in the sense of being closer to the original melt from the source) in character compared to the typical Main Range granite (Liew, 1983; Cobbing et al., 1992). Primitiveness of igneous rocks is commonly measured using igneous differentiation and magma evolution indices such as Larsen differentiation index (DI) (Larsen, 1938) (for formula, see note on page 116) and Kuno solidification index (SI) (Kuno, 1959) (for formula, see note on page 116). It also could be observed through major element MgO and TiO_2 and transitional metals level.

The melagranite DI is 7.3 to 22.0, much lower (a lower value indicates more primitive) than the Main Range granite index range, 17.9 to 31.7. The SI for the melagranite is higher (a higher value indicates more primitive) for the melagranite (14.9 – 34.4), compared to the Main Range granite (0.1 – 17.0). The melagranite primitive character is also shown by a slightly higher MgO/TiO_2 ratio (Fig. 5-8), and higher levels transitional metals (such as V and Ni) (Fig. 5.8, Fig. 5.9 and Fig. 5.10).

5.3.1 AFM diagram

The AFM diagram (Fig. 5.11) is a popular triangular variation diagram where the A, F, M stands for alkalis ($Na_2O + K_2O$), Fe oxides (total Fe) and MgO. It is most commonly used to distinguish between tholeiitic and calc-alkaline differentiation trends but it also could be used to identify rock series (Rollinson 1993).

Taiping melagranites fall on the low FeO/MgO side of the calc-alkaline series. Compared to the typical Main Range granite (data from Liew, 1983; Cobbing et al., 1992, all Bintang batholith member are excluded), the amphibole-bearing melagranites

show clear deviation from the Main Range trend. Such characteristic has been previously described in Cobbing et al. (1992).

Although the AFM diagram could not provide any quantitative petrogenetic information (Rollinson 1993), clear separate trends on the AFM diagram does suggest a qualitative petrogenetic difference between Taiping pluton amphibole-bearing granite and Main Range province granite. This is supported by the petrographic evidence; Taiping amphibole bearing melagranite contain amphibole and pyroxene, which are typically absent within the granites of Main Range granite province.

5.3.2 Rb/Sr vs. TTDI (Cobbing et al., 1992)

This variation diagram (Fig. 5.12) is introduced by Cobbing et al. (1992) for the granitoid of Main Range and Eastern provinces. A line separating the two provinces has been empirically drawn by the author. For the same Thornton-Tuttle differentiation index (TTDI) value (for formula, see note on page 116), Eastern province granite typically show a lower Rb/Sr value compared to the Main Range granite. Majority of the Taiping amphibole-bearing melagranite falls in the Main Range area, close to the division line. Besides some outliers, most samples are more primitive (low TTDI) and show a low Rb/Sr value compared to the Main Range granite.

5.3.3 Variation diagram pattern comparison with Main Range type granite

The melagranite REE and multi element variation diagram patterns are compared with Main Range type granite, Langkawi island granite, from Kyaw Kyaw Nyein (2014) (Fig. 5.10 and 5.11). On the REE variation diagram, the Langkawi granite has stronger negative Eu-anomalies and shows less steep pattern than the Taiping melagranite. LREE enrichment is much more pronounced on the Taiping melagranite.

The Taiping melagranite shows higher values for most elements compared to the Langkawi granite on the primitive mantle normalized multi element variation diagram. The Langkawi granite show stronger Ba, Nb, Sr, Eu and Ti anomalies compared to the Taiping melagranite. T-N-T anomaly is not observed in Langkawi granite; Langkawi granite has a positive Ta-anomaly. Analysis of these variation diagrams pattern suggest that both granites might not share a similar origin, as they are very different in terms of geochemistry.

5.4 Apatite saturation temperature

The saturation level of P_2O_5 is calculated using the following formula by Harrison and Watson (1984) for metaluminous rock (A/CNK < 1):

$$\ln(D_p) = \frac{8400 + 26400(SiO_2 - 0.5)}{T} - 3.1 - 12.4(SiO_2 - 0.5)$$

$$P_2O_5 concentration = \frac{42}{D_p}$$

Where: T = absolute temperature (in K); D_p = distribution coefficient for phosphorus between apatite and melt; SiO_2 = weight fraction of silica in the melt (wt. %). We will be using the saturation temperature as the minimum temperature of the melagranite melt, which will be used to interpret the pseudosection from Perple_X (see Fig. 6.3).

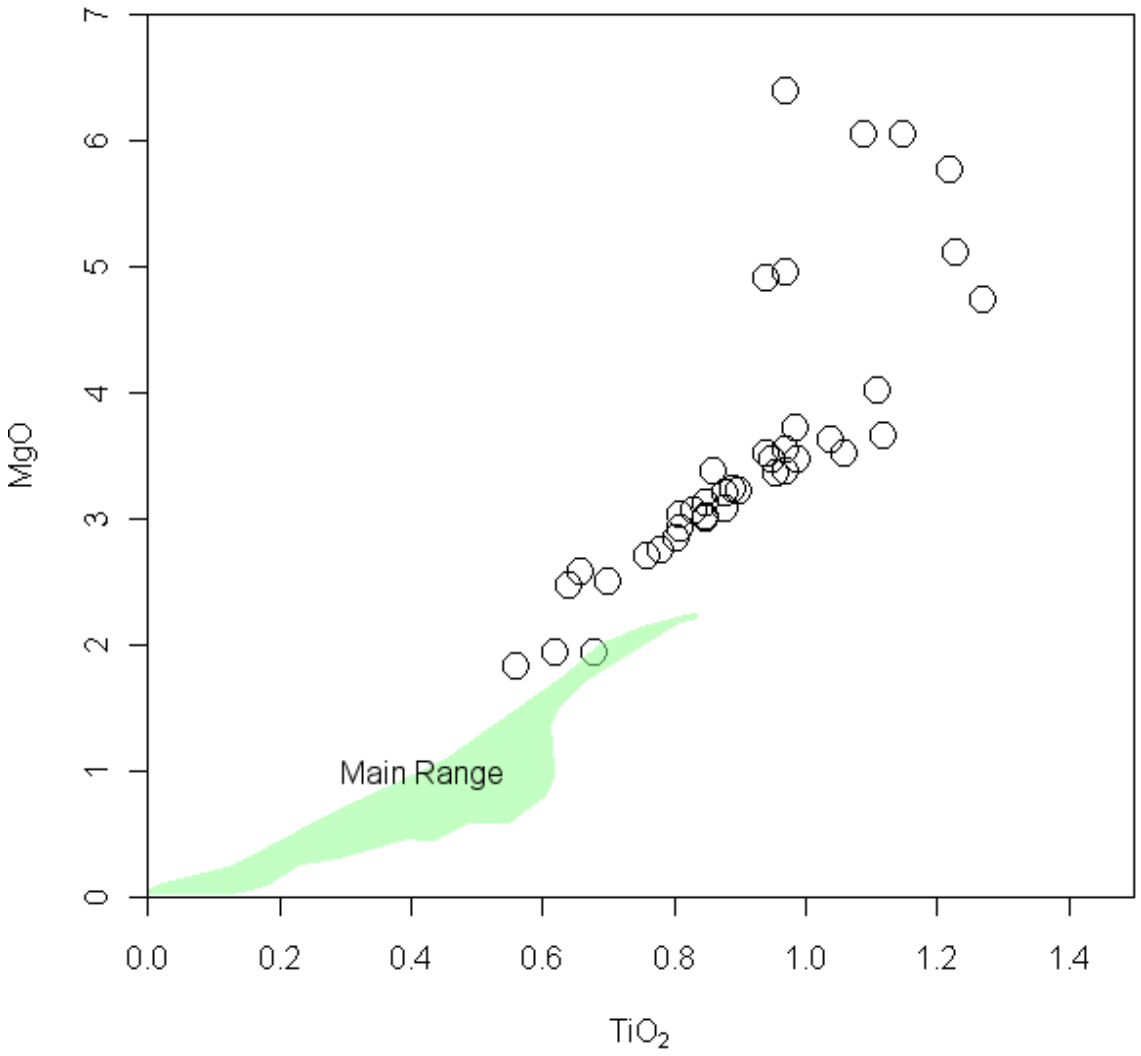

Fig. 5.8: MgO vs. TiO2. Circles: Taiping melagranite; Green area: Main Range granites, data from Liew (1983) and Cobbing et al. (1992).

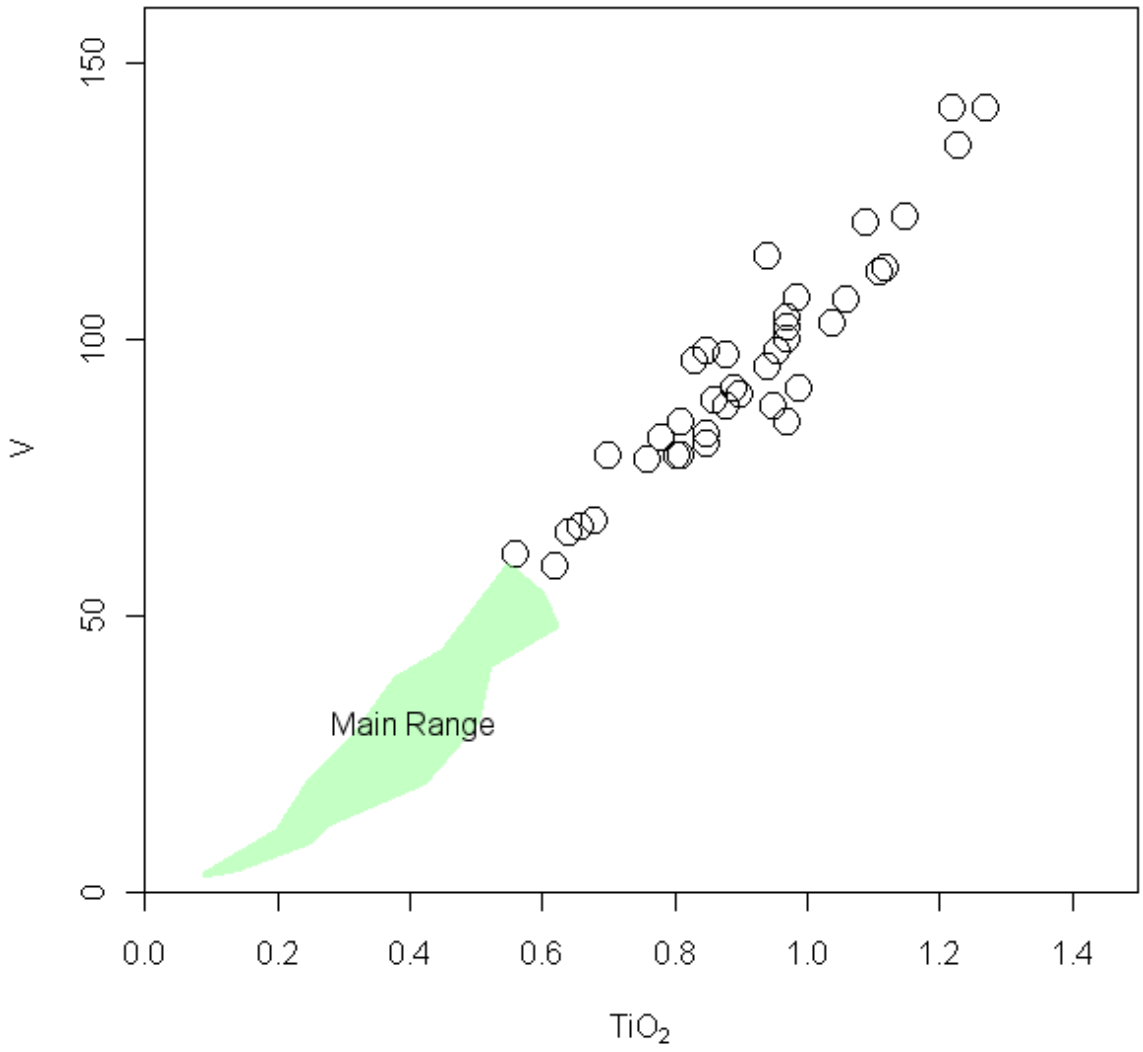

Fig. 5.9: V vs. TiO2. Circles: Taiping melagranite; Green area: Main Range granites, data from Liew (1983) and Cobbing et al. (1992).

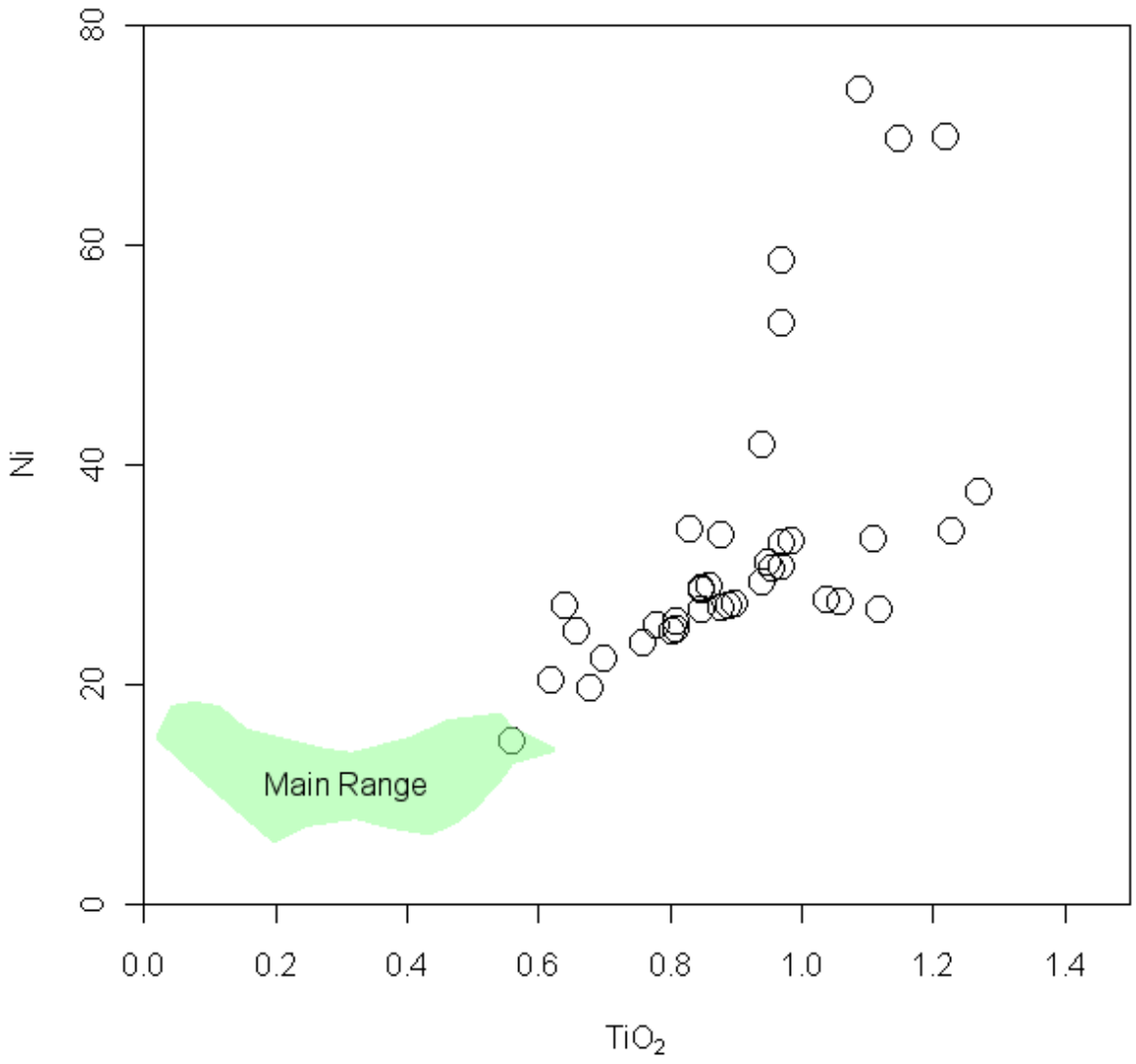

Fig. 5.10: Ni vs. TiO2. Circles: Taiping melagranite; Green area: Main Range granites, data from Liew (1983) and Cobbing et al. (1992).

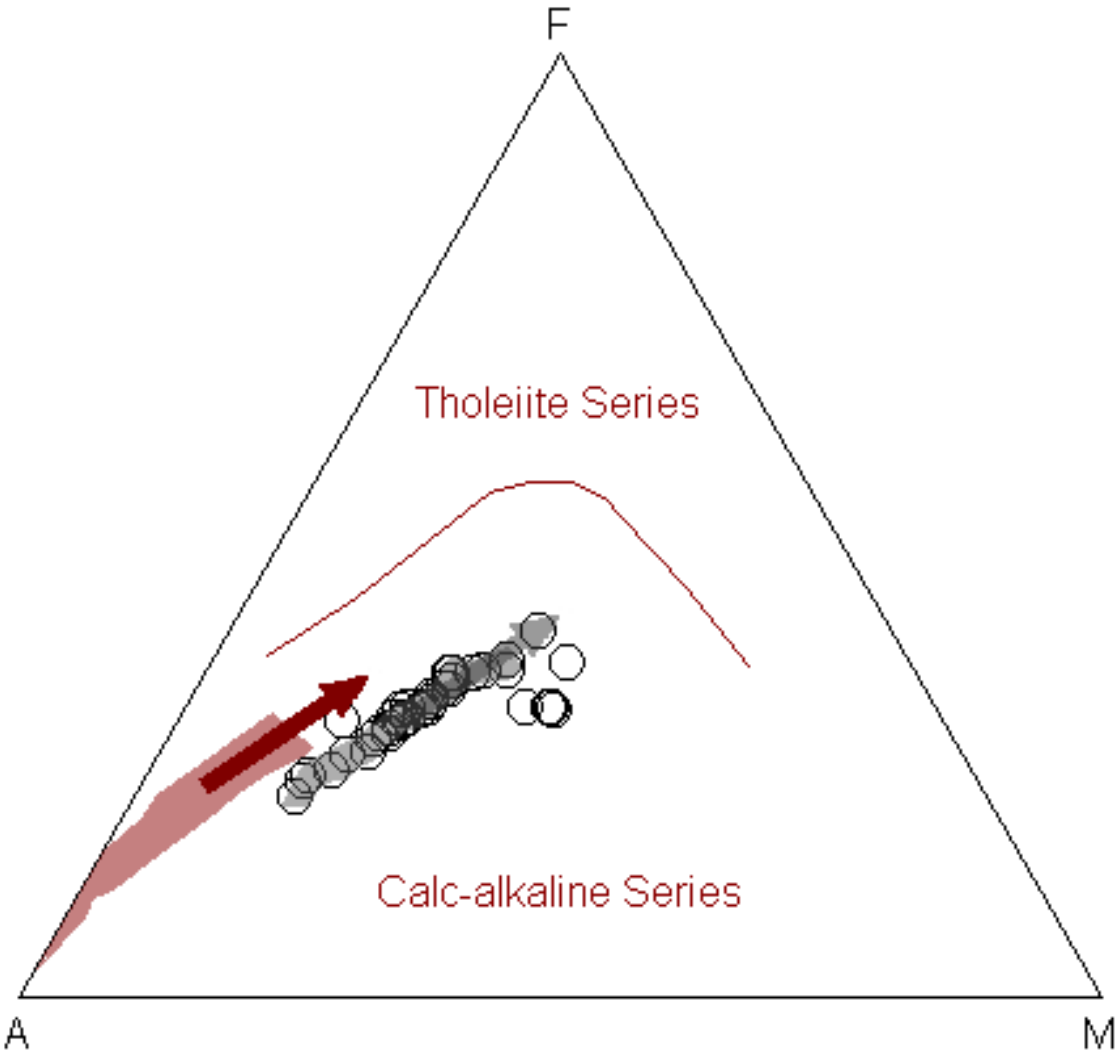

Fig. 5.11: Irvine and Baragar (1971) AFM diagram. Red: Main Range granite province trend (Liew, 1983; Cobbing et al., 1992). Grey: Taiping melagranite.

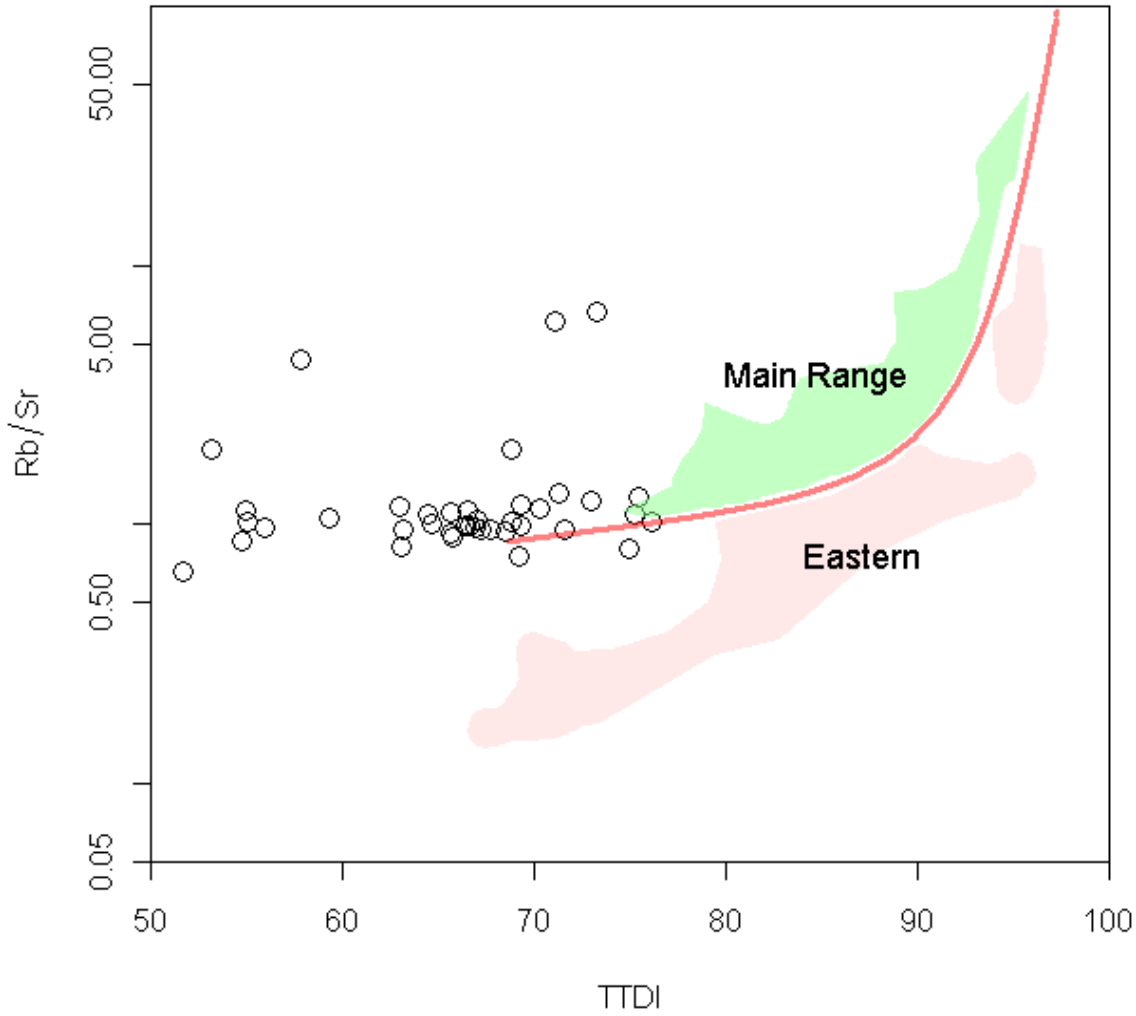

Fig. 5.12: Cobbing et al. (1992) Rb/Sr vs. TTDI. Red line: empirical division line between the two granite provinces. Main Range and Eastern data are from Cobbing et al. (1992).

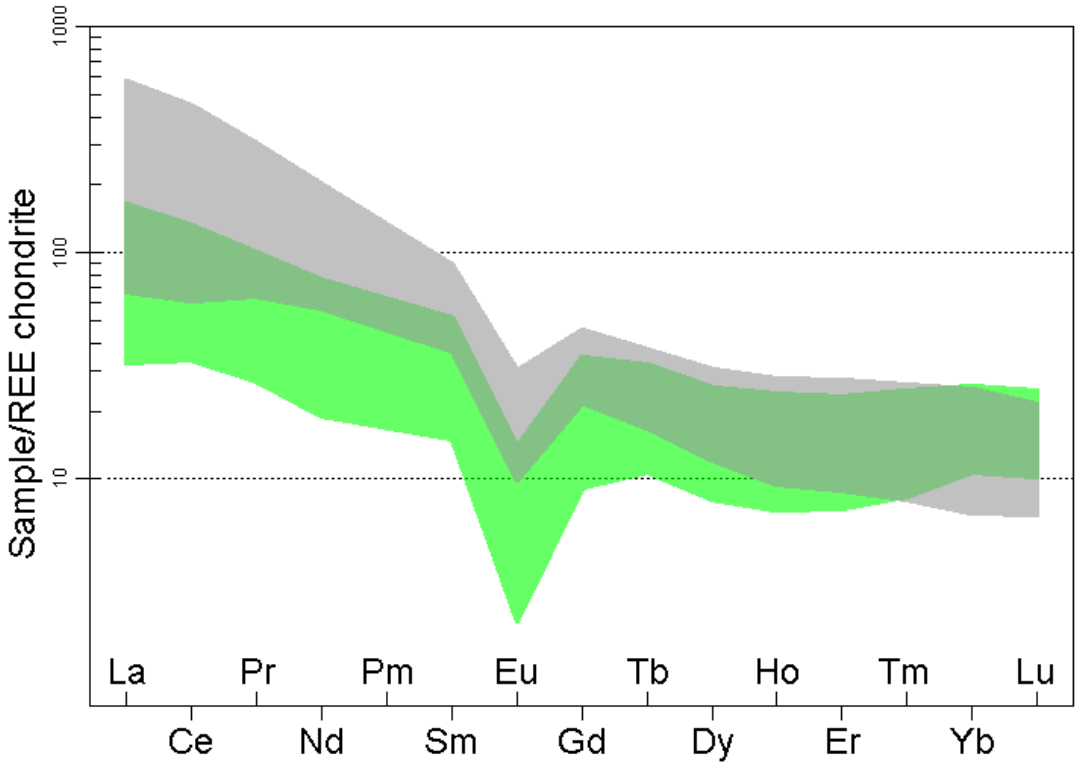

Fig. 5.13: Boynton (1984) Chondrite normalized REE plot. Grey: Taiping melagranite, Green: Langkawi granite (Main Range type) (Kyaw Kyaw Nyein, 2014).

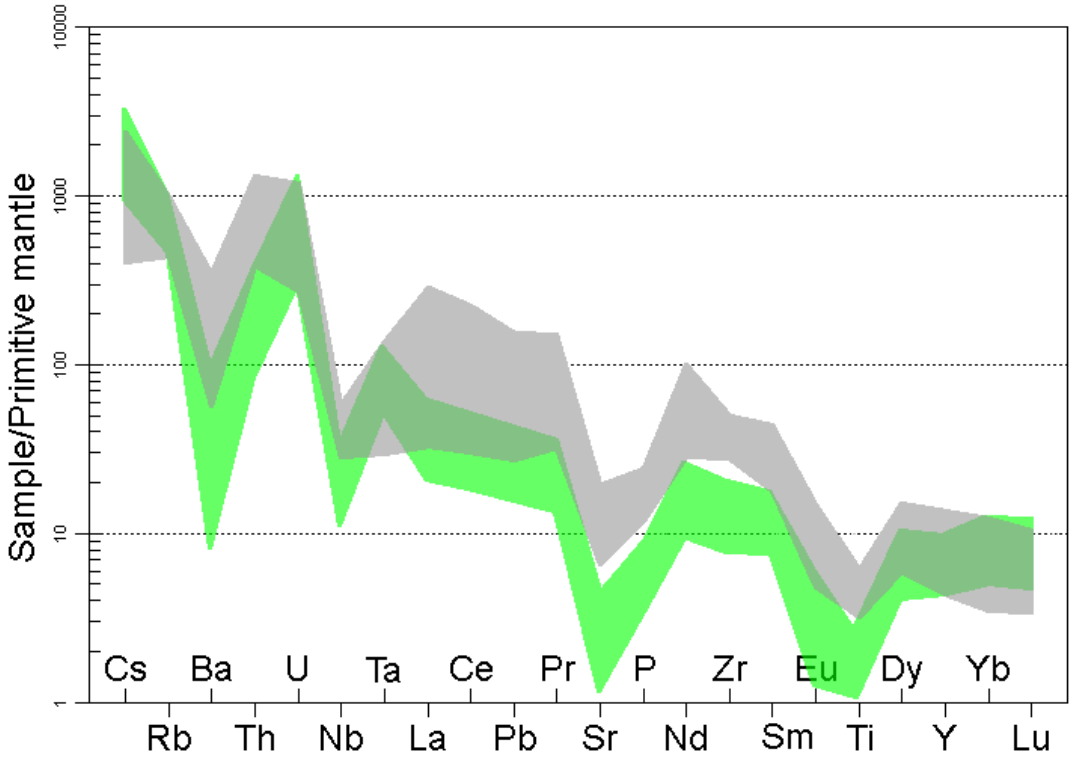

Fig. 5.14: Mcdonough and Sun (1995) Primitive mantle normalized multi element diagram. Grey: Taiping melagranite, Green: Langkawi granite (Main Range type) (Kyaw Kyaw Nyein, 2014).

For peraluminous rocks (where A/CNK > 1), the P_2O_5 concentration is corrected for higher phosphorus solubility in the peraluminous melts ($P_2O_5^{pera}$) using the following equations by Bea et al. (1992):

$$P_2O_5^{pera} = P_2O_5 concentration \cdot e^{\frac{6429(ACNK-1)}{T-273.15}}$$

The Bea et al. (1992) correction is preferred over Pichavant et al. (1992) correction because the latter gave lower temperatures and wider temperature ranges (higher uncertainty). The temperatures of metaluminous rocks are calculated solving Harrison and Watson (1984) equations above for T (in K):

$$T(K) = \frac{8400 + 26400(SiO_2 - 0.5)}{\ln\left(\frac{42}{P_2O_5}\right) + 3.1 + 12.4(SiO_2 - 0.5)}$$

The corrected expression for peraluminous rock (Bea et al., 1992), however, needs to be solved for T (in K) by iterations:

$$P_2O_5^{pera} = 42 \cdot e^{\frac{6429(ACNK-1)}{T-273.15} - \frac{8400+26400(SiO_2-0.5)}{T} + 3.1 + 12.4(SiO_2-0.5)}$$

This numerical model appears to be valid from 45% to 75% SiO_2, 0% to 10% water and for the range of pressures expected in the crust (Harrison and Watson, 1984). The calculated apatite saturation temperatures will not be reliable for felsic and strongly peraluminous melts (Janousek, 2006). The apatite saturation temperature ranges from 928.8 °C to 1014.8 °C. The calculated temperatures are shown in Appendix 2.

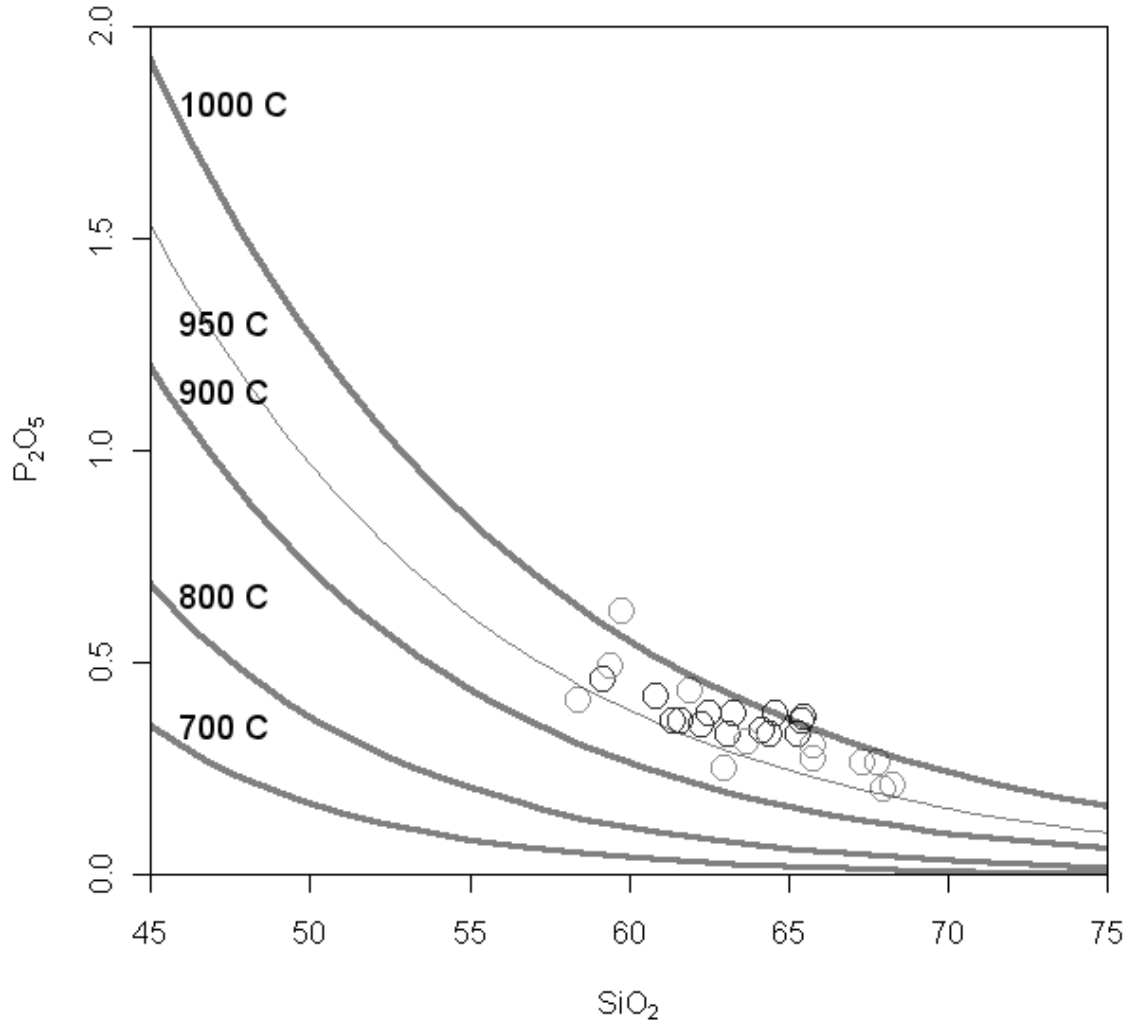

Fig. 5.15: Harrison and Watson (1984) phosphorus saturation level (P_2O_5 wt. %) as a function of SiO_2 (wt. %) and temperature (°C). Due to modeling restriction, only metaluminous sample are plotted here.

Interpreting mineral saturation temperature can be tricky, due to crystal accumulation and inheritance (Miller et al., 2003) and disequilibrium crystallization, particularly of apatite (Bacon, 1989). However, a case can be made for apatite saturation in the melt as the melagranite characteristics appear to fall within the model limitation. From the results, the minimum temperature for apatite stability is ~920°C. This temperature is significantly higher than temperature of granitoid melt generated by melting of sedimentary source (experimentally, ≤ 700°C) (Liew and McCulloch, 1985).

5.5 Chapter summary

1. Some of the Taiping melagranite sample show ultrapotassic character and their geochemical variation diagram pattern are comparable to Central European durbachite suite.
2. Taiping amphibole-bearing melagranite is relatively un-evolved or primitive in character compared to the typical Main Range granite. Their geochemical variation diagram pattern are not comparable to typical Main Range type granite (Langkawi granite)
3. Apatite saturation temperature for the Taiping amphibole-bearing melagranite ranges from 928.8 °C to 1014.8 °C. This temperature is significantly higher than temperature of granitoid melt generated by sedimentary source.

CHAPTER 6: DISCUSSION

6.1 Introduction

The final chapter is focused on the answering the objectives mentioned in the first chapter. Discussions will be based on field observation, petrographic data and geochemical data. Additional data may be introduced when necessary.

6.2 Implication to Main Range granite province I-S classification

Taiping amphibole-bearing melagranite do not show typical S-type minerals (such as muscovite, biotite and sillimanite) or geochemical features (peraluminous with high SiO_2) besides being rich in potassium and poor in sodium (Chappell and White, 1974). They do, however, contain several I-type characteristics, such as being metaluminous and containing amphibole and pyroxene (Chappell and White, 1974).

The Main Range granite province is previously believed to be S-type (Liew, 1983). Only recently, the province's granites are suggested to have both I and S-type characteristics (Ghani, 2000; Ghani et al., 2013). The discovery of the Taiping melagranite with a near absence of S-type characteristics supports the ideas presented in Ghani et al. (2013) that the Main Range granite province is not an exclusively S-type granite province and its batholiths can be quite complex in terms of petrography and geochemistry.

It is not possible to use the I-S classification on Taiping melagranite as it does not show a clear I- or S-type character. When using Chappell and White (1974) K_2O vs. Na_2O discrimination diagram (Fig. 6.1), it plots within S-type. However, on Chappell and White (1992) ACF diagram (Fig. 6.2), it plots within I-type. Since melagranite

belongs to the ultrapotassic group, and possess an odd petrography and geochemistry, the I-S classification could not accurately account for the petrogenesis of Taiping amphibole-bearing melagranite. Besides that, the classification did not cover the source rock for ultrapotassic granitoid

6.3 Possible source

Following Janousek et al. (2007), the source of such rocks will be discussed in the following lines. Although high Cr and Ni as well as high Mg clearly point to derivation from a mantle source, elevated concentrations of U, Th, LREE and LILE, pronounced depletion in Nb and Ta as well as high K_2O/Na_2O and Rb/Sr ratios apparently contradict this origin (Janousek et al., 1997). They could not be explained by partial melting of known crustal lithologies or crustal contamination of more depleted basic magmas (Janousek et al., 1997).

Previous workers (Janousek et al., 1997; Holub, 1997; Janousek and Holub, 2007; von Raumer et al., 2013) have suggested that durbachite petrogenesis requires a crustal component with a sub-continental lithospheric mantle source with a complex history of depletion (indicated by low Na, Ca, Sr, Ca/Mg and relatively high Si) (Holub, 1997) and re-enrichment by hydrous, K-rich, LILE- and LREE-bearing fluids. The mixing of these two distinct magma (ultrapotassic, derived from enriched mantle domains and acid, crustal derived) would form durbachite-type magmatic rock (Janousek et al., 2003; Kotkova et al., 2010; Parat et al., 2010).

The geochemical similarity of the Taiping durbachite-type rocks with rocks from Central Europe suggests comparable sources and formation processes; through melting of anomalous lithospheric mantle sources, metasomatized and contaminated by mature crustal material. Phlogopite harzburgite/ phlogopite-clinopyroxene-bearing

metasomatized peridotite has been suggested as a possible source for Central Europe durbachite as it is strongly enriched in K, Rb, Cs, Th, U and some other incompatible elements (Holub, 2001; Parat et al., 2010).

6.4 Perple_X modeling

From the foregoing petrographic study, it is shown that the Taiping amphibole-bearing melagranite main mineral assemblage is quartz + K-feldspar + plagioclase + biotite + amphibole + pyroxene (clinopyroxene dominated). For modeling purposes, the parental melt is assumed to be granitic and the rest of the mineral assemblage is best reproduced by the addition of peritectic K-feldspar, plagioclase, biotite and pyroxene.

The two protoliths used in this modeling are greywacke (to represent the crustal component) and minette (to represent the crustal contaminated partial melt from the enriched mantle component; the enclaves within the granite are not used as they represent an end-member of a mixing process) (Parat et al., 2010). Fig. 6.3 presents a pseudosection calculated using the Perple_X Software (Connolly, 1990, 2005, 2009; Connolly and Petrini, 2002) with an updated (2002, unpublished) Holland and Powell (1998) thermodynamic dataset. The figure show an estimate of melting relations in a compositional range extending from an average greywacke to lamproites composition at the pressure of 0.8 GPa. The 0.8 GPa is the estimated pressure at the depth of 30 km, assuming the crust thickness of Peninsular Malaysia is 30-35 km (Wu et al., 2004).

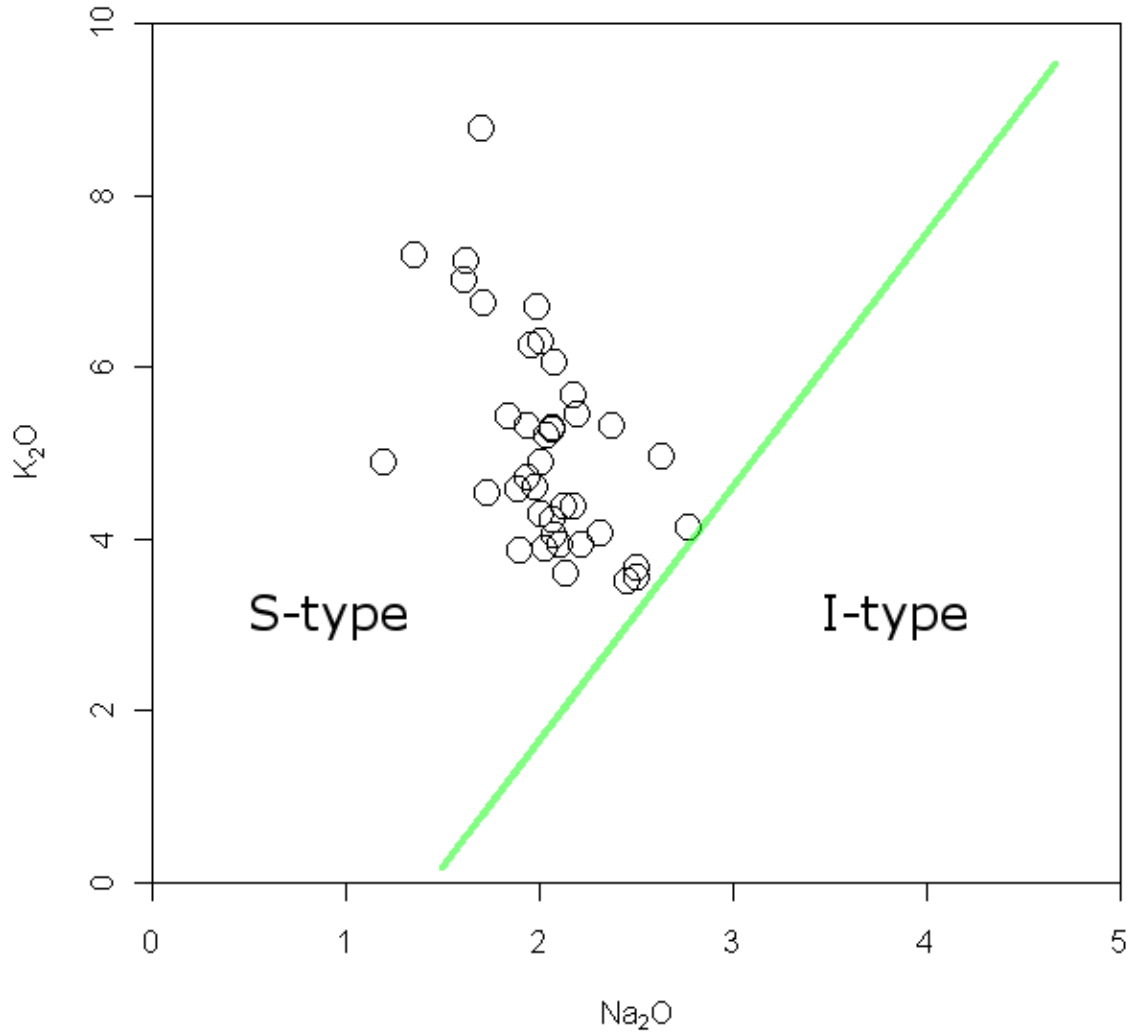

Fig. 6.1: Chappell and White (1974) K_2O vs. Na_2O discrimination diagram. The line shown on the plots joins the points 2 wt. % K_2O, 2.2 wt. % Na_2O and 5% K_2O, 3.2% Na_2O, which was given by Chappell and White (1974) as a boundary between the two types. Due to its high potassium content, the Taiping melagranite samples fall within S-type field.

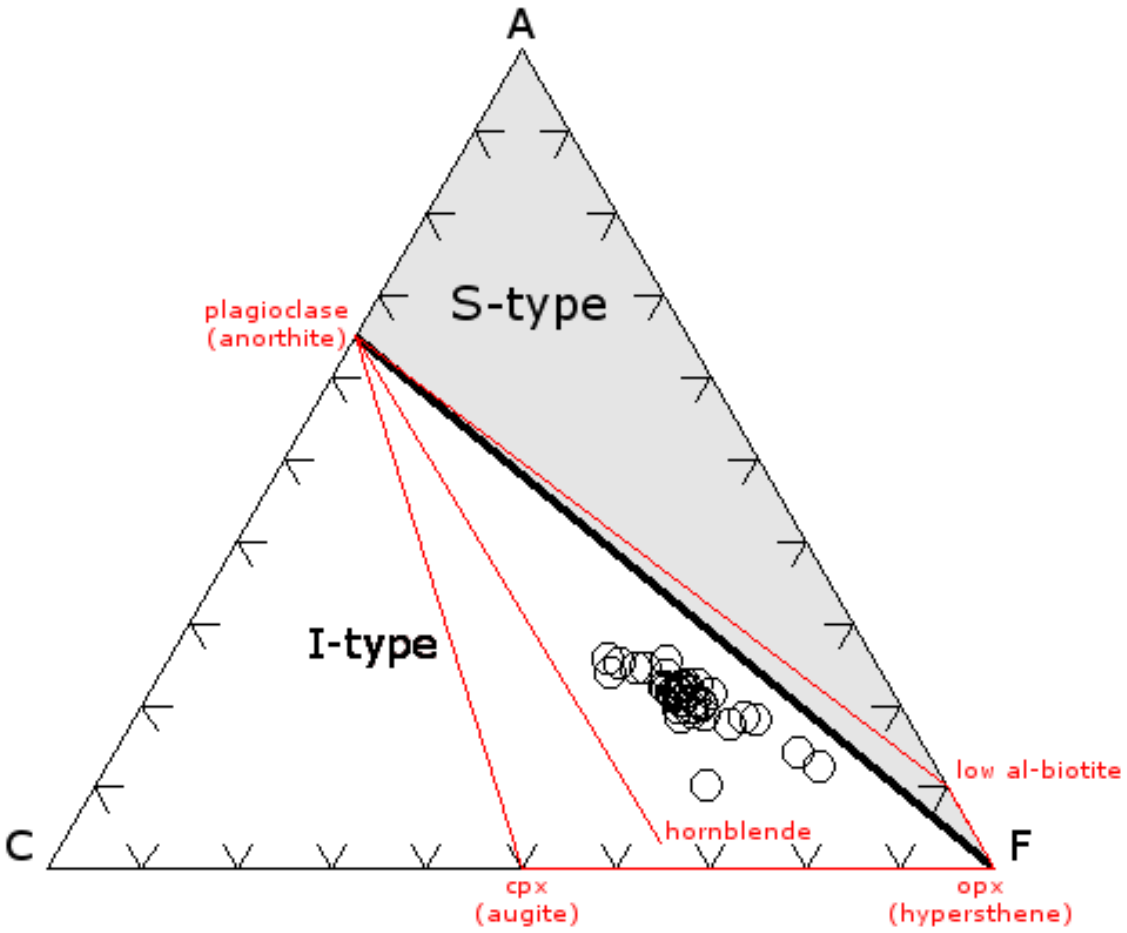

Fig. 6.2: Chappell and White (1992) ACF diagram, where A = Al – Na – K, C = Ca, F = Mg + Fe (in molecular). Quartz, K-feldspar and albite are included in all of the mineral assemblage. Taiping melagranite samples fall within I-type field. This is odd, considering that most LFB granites have no problem falling back into the same field determined in Chappell and White (1974) K_2O vs. Na_2O discrimination diagram.

The melt or *melt (HP)* (in the model) by Holland and Powell (2001) and White et al. (2001) in this pseudosection is a granitic, Na-Mg-Al-Si-K-Ca-Fe hydrous silicate melt. Note that the calculated solidus (red line) suggests that a source with higher minette component will undergo fluid absent melting before the greywacke rich source. At around 970 °C (using the melt temperature inferred from apatite saturation temperature), source with 75% greywacke and 25% minette could generate a granitic melt with entrained peritectic minerals (clinopyroxene, orthopyroxene, plagioclase, biotite, sanidine and ilmenite) which are close to our granitoid mineral assemblage.

6.4.1 Fate of the peritectic crystals

Decompression during the ascent of granitic melts can results in superheating and crystallization which raises $a H_2O$ and $a K_2O$ (alkalis dissolved by hydrous volatile fluids), causing early anhydrous, ferromagnesian minerals (such as pyroxene) to be replaced by hornblende and biotite (Clemens et al., 2011; Clemens and Stevens, 2012). This could explain the scarcity of pyroxene within the melagranite and the presence of amphibole or biotite with pyroxene cores. These small peritectic crystals are readily re-equilibrated with the magma during ascent and emplacement. In the end, only traces of the original entrained peritectic crystals are likely to survive in granitic magma (Clemens et al., 2011, Clemens and Stevens, 2012). Common pyroxene peritectic reactions are:

1. Orthopyroxene + melt ↔ biotite + quartz (Chappell and Wyborn, 2012)
2. Clinopyroxene + orthopyroxene + melt ↔ amphibole + plagioclase (Johannes and Koepke, 2001)

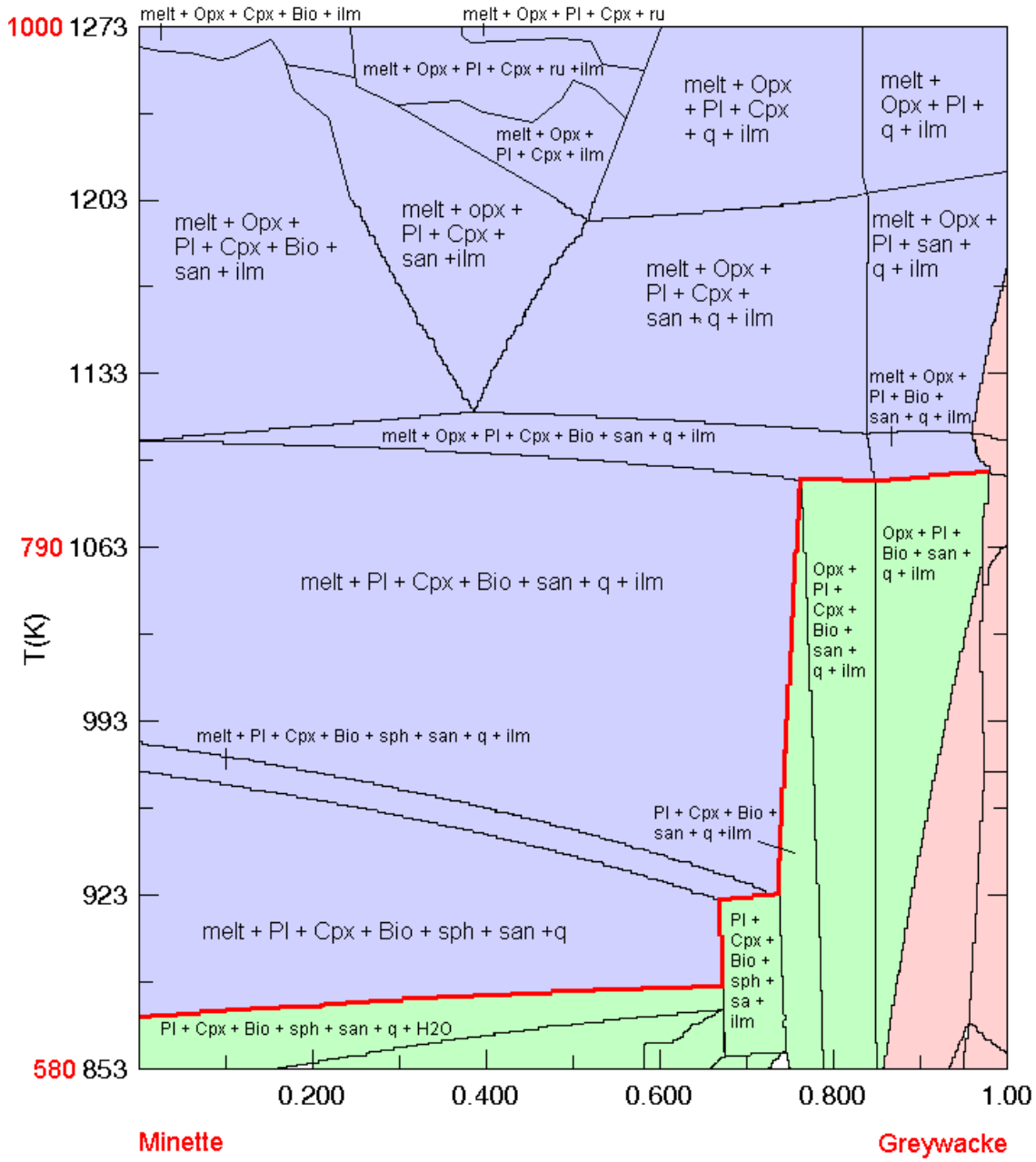

Fig. 6.3: Temperature-composition pseudosection at 0.8 GPa, depicting the partial melting behavior of rock that range in composition from minette to greywacke. The compositions of both rocks are given in wt. % in Appendix 4. Clemens et al. (2011) suggested that the temperatures of biotite disappearance are probably underestimated by the software compared to melting experiment.

6.5 Possible tectonic setting

Durbachite series rocks require an enriched sub-continental lithospheric mantle source. Such enrichment process is hypothesized to come from subduction. The high LILE/HFSE ratios of European durbachite and Taiping amphibole-bearing melagranite support their parental magmas derivation from partial melting of subduction modified lithospheric mantle sources (Holub, 2001), where the source is modified through influx of hydrous fluids from a subducted slab (Janousek et al., 1997; von Raumer et al., 2013). Enrichment/modification of mantle source may also occur under maturing arc, due to decreased heat flow and continuing mantle degassing and metasomatism, unrelated to the subducted slab (Wheller, 1986; Foley et al., 1987).

Harris et al. (1986) tectonic discrimination diagram (Fig. 6.4) suggests the Taiping melagranite falls within Group 1 (contribution from subduction). It is, however, important to note that durbachite series rocks are complex and may not have generated from subduction directly. Subduction contribution could be inherited later from the source, e.g. underplated source. It is unnecessary for the subduction stage needs to be active during the durbachite magma generation/emplacement; it could pre-date durbachite emplacement age significantly (Janousek et al., 1997; Ferre and Leake, 2001). Source partial melting could be triggered as the heat flow under the source is restored (Holub, 2001). Such assumptions explain how "subduction geochemical signature" is produced in different setting and in a different time.

For European durbachite rocks, partial melting of the source begins with the increase of thermal input by asthenospheric lithospheric mantle upwelling from tectonothermal events, such as: (1) lithospheric delamination, (2) slab break-off/ slab retreat/ slab window, (3) mantle plume (Janousek et al., 1997; Holub, 2001; von Raumer et al., 2013). The Variscan Europe durbachite plutons intruded well after peak

of compression and metamorphism at the beginning of rapid post-collisional exhumation (Janousek and Holub, 2007; Stampfli et al., 2013). However, due to difference in geological time and setting, the case could be slightly different for Taiping amphibole-bearing melagranite.

Taiping melagranite is situated on the Sibumasu plate, which hosts the entire Main Range granite province and is bounded by the Bentong-Raub line to the east. The U-Pb zircon geochronology work on Main Range granite province is still going on. The hitherto obtained age data of the Main Range granite range from 198 to 219 Ma (Searle et al., 2012; Ghani et al, 2013; Oliver et al., 2013). Detrital zircons suggest granites from Main Range granite age ranges from 209 to 220 Ma (Oliver et al., 2013).

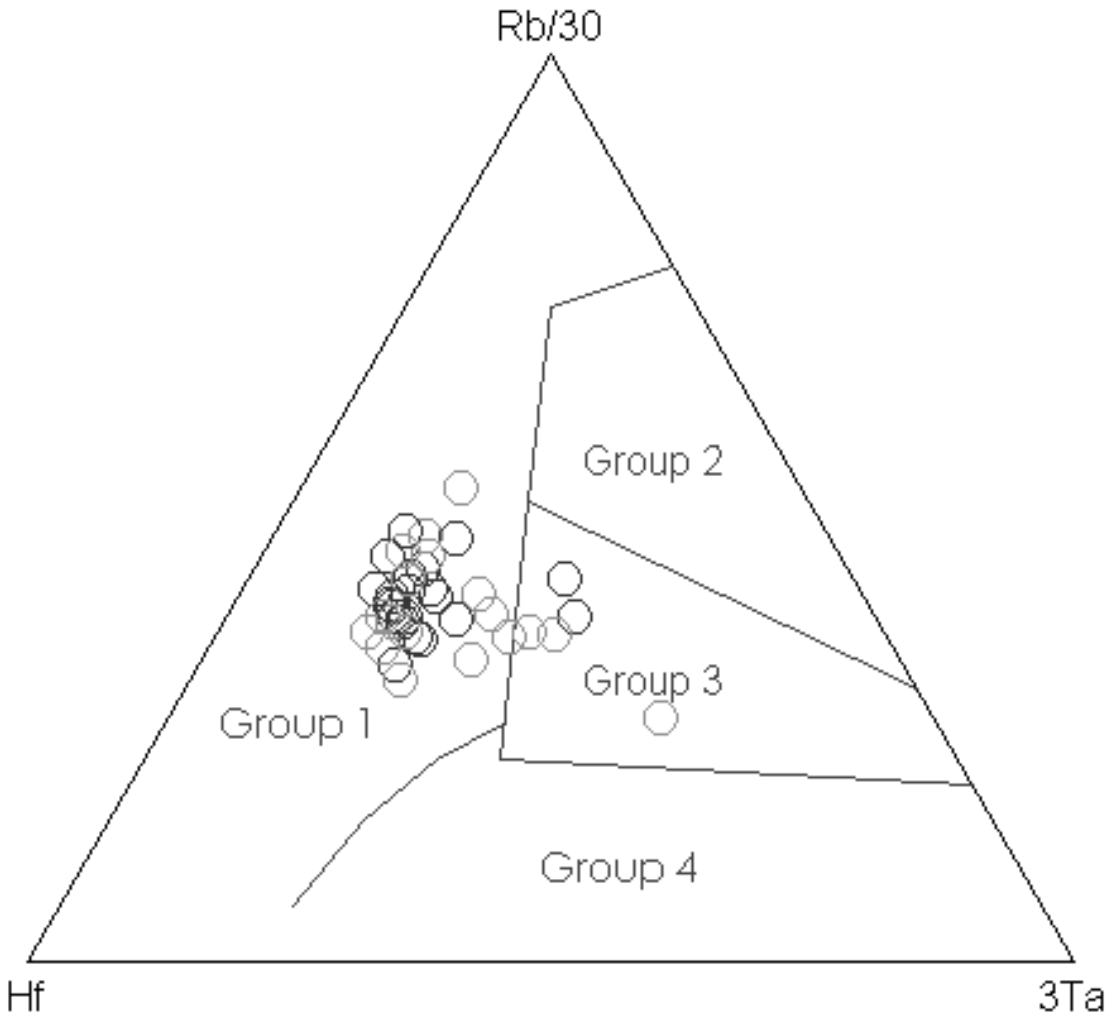

Fig. 6.4: Harris et al. (1986) tectonic discrimination diagram (trace elements are in ppm). Group 1: Pre-collision calc alkaline intrusions mostly derived from mantle modified by a subduction component; Group 2: Syn-collision peraluminous intrusions which may be derived from the hydrated bases of continental thrust sheets; Group 3: Late or post-collision calc-alkaline intrusions which may be derived from a mantle source but undergo extensive crustal contamination; Group 4: Post-collision alkaline intrusions which may be derived from mantle lithosphere beneath the collision zones.

6.5.1 Geochronology of Taiping melagranite

One sample (BB-1) was sent to Pacific Centre of Isotopic and Geochemical Research (PCIGR) lab in University of British Columbia, Vancouver, Canada for laser ablation (LA) ICP-MS analysis. Zircon crystals collected from sample BB-1 typically have euhedral, elongated shape with sharp facets and pointed tips on one side. Selected cathodoluminesence image of zircon grain are shown in Fig. 6.5.

About 20 zircons have been collected from BB-1 sample for geochronology analysis. Th/U ratios for BB-1 range from 0.11 to 0.93. All of the analyses are concordant, and the $^{206}Pb/^{238}U$ ages for BB-1 scatter between 213.3 ± 5 and 223.5 ± 7.6 Ma, giving a weighted mean age of 218.0 ± 1.3 Ma (one age 229.4 ± 6.7 Ma is discarded). Data table are shown in Appendix 3 while the plots are shown in Fig. 6.6.

6.5.2 Current accepted model for Peninsular Malaysia tectonics

The popular model suggested by, e.g. Metcalfe (2011), Sevastjanova et al. (2011), Searle et al. (2012) and Oliver et al. (2013) explain that the Main Range granite province is emplaced during the collision between Sibumasu and Indochina around Late Triassic, where the Paleo-Tethys Ocean from Sibumasu side subducted under Indochina plate before the collision. The Paleo-Tethys closure age is interpreted as early Triassic (Metcalfe, 2013) and 219 Ma is generally accepted as beginning of crustal thickening and partial melting (Oliver et al., 2013).

This places the Taiping melagranite (218.0 ± 1.3 Ma) early with respect to the collision event. As the setting for Taiping melagranite is early collision, its magmatism trigger is assumed to be different from post-collisional Central Europe durbachite (Janousek and Holub, 2007; Stampfli et al., 2013; von Raumer et al., 2013). Lithospheric delamination is expected late in the collision when crustal thickness is

higher and slab break-off usually occurs during post-collision. These two mechanisms are clearly in conflict with the Taiping melagranite setting.

Here, two possible triggers are offered for the Taiping amphibole-bearing granitoid: mantle plume (von Raumer et al., 2013) and extension during early collision (Sacks and Secor, 1990) (Fig. 6.7, Fig. 6.8). It is worth remarking that there could be other possible triggers but these two triggers are simpler and fit easily into the current setting. Our suggestions are based on the current understanding Main Range granite province tectonic history. Mantle plume would have reheated the source, which could results in stretching of the crust, allowing the durbachitic rocks to be emplaced.

It is also possible for minor extension episode to occur during the early collision on the Sibumasu side. Slab pull created by subduction of a higher density oceanic lithosphere could results in extensional deformation within the subducted slab below the area of the slab bend (Sacks and Secor, 1990). Enriched source will then be heated by the upwelling of asthenospheric mantle from lithosphere necking, generating the necessary ultrapotassic magma. Such extension episode will be short lived if both plates continue to converge, as the compressive tectonic regime will be re-established (Sacks and Secor, 1990).

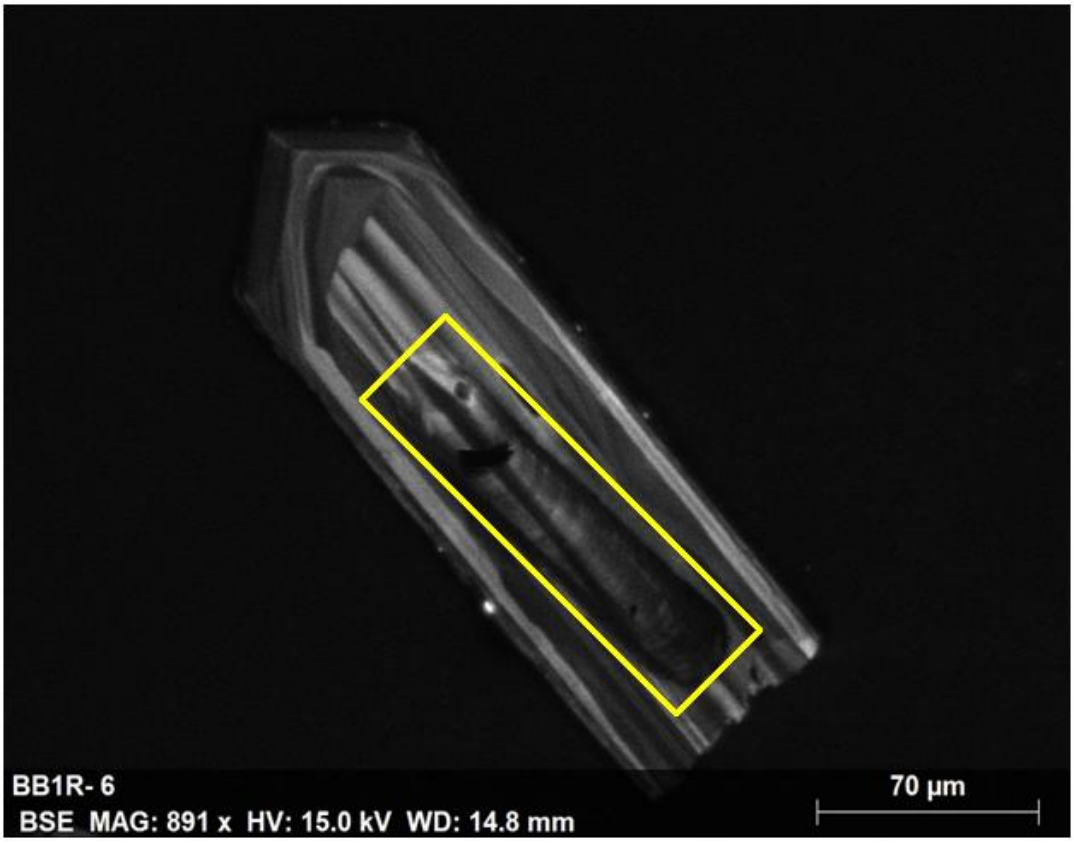

Fig. 6.5: Cathodoluminescence (CL) image of a representative zircon from the dated sample. Yellow box shows the line scan on the zircon.

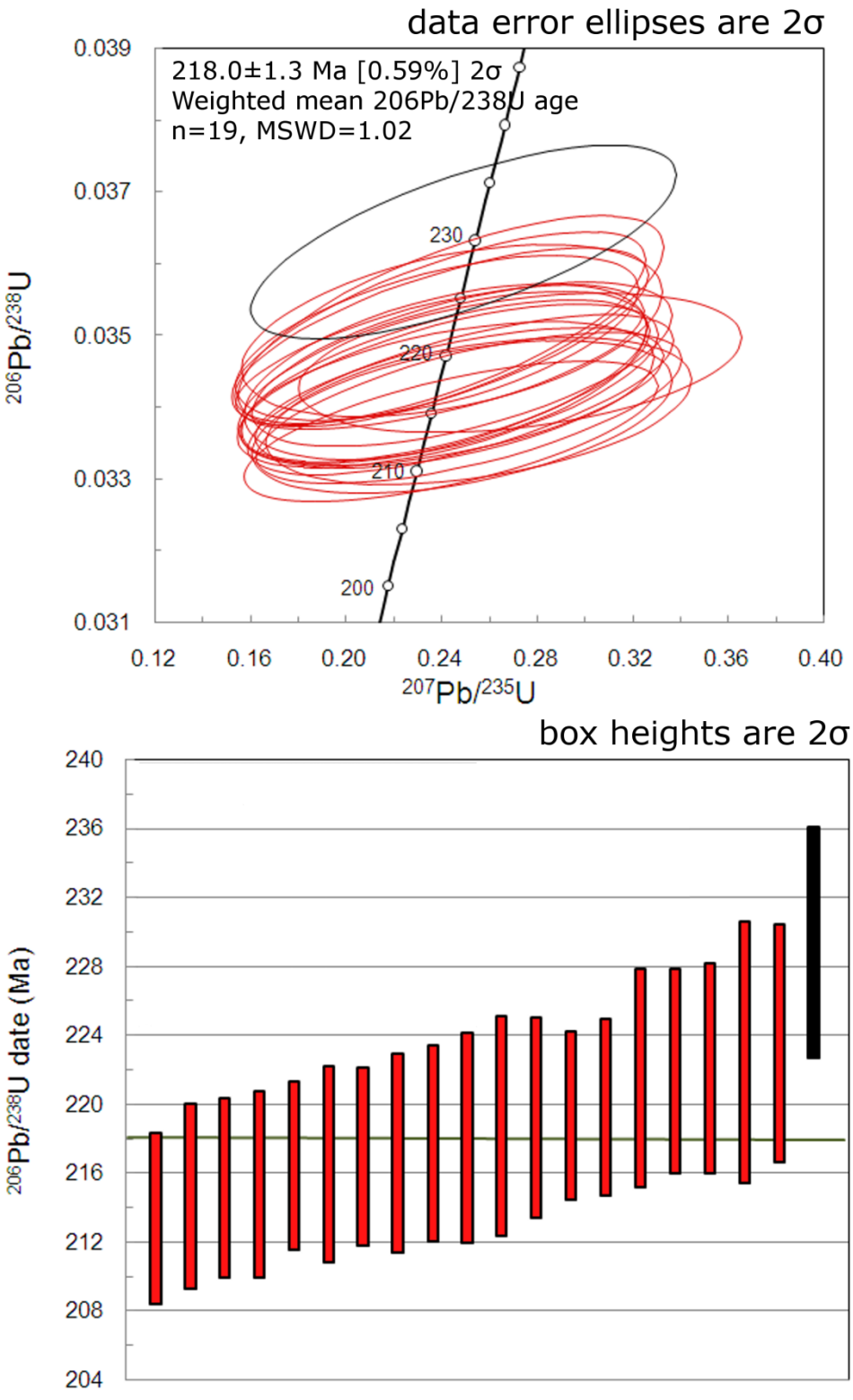

Fig. 6.6: Top: Concordia diagram with the results of zircon dating. Bottom: Weighted average plot with the results of zircon dating. Black: omitted.

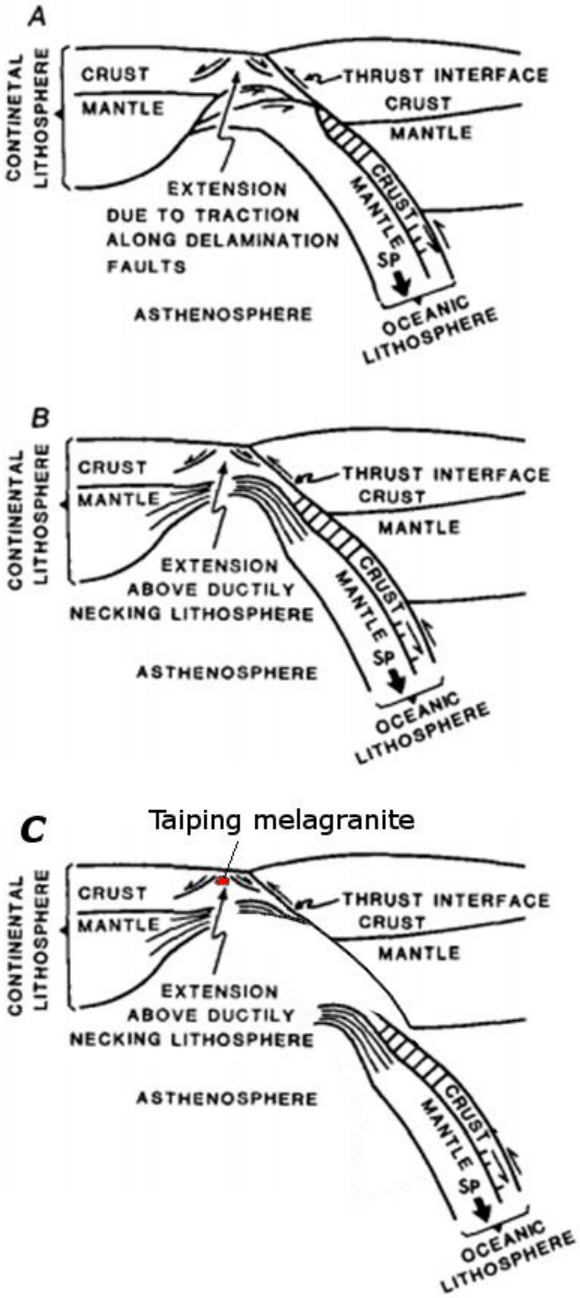

Fig. 6.7: Sacks and Secor (1990) model sketch. The above is reminiscent of a slab break off process. This is one of the models that provide explanation to the puzzling emplacement of Taiping melagranite. During the beginning of continental collision, the weight down going oceanic slab may lead to an extensional shearing in the descending plate. Slab pull (SP) will later causes detachment of subducted slab. Continued convergence may collapse the remaining crust back onto the edge of the left plate (not shown here). A: Simple shear model; B: Pure shear model. Figure adapted from Sacks and Secor (1990). This model is applied in Fig. 6.8 scenario 2.

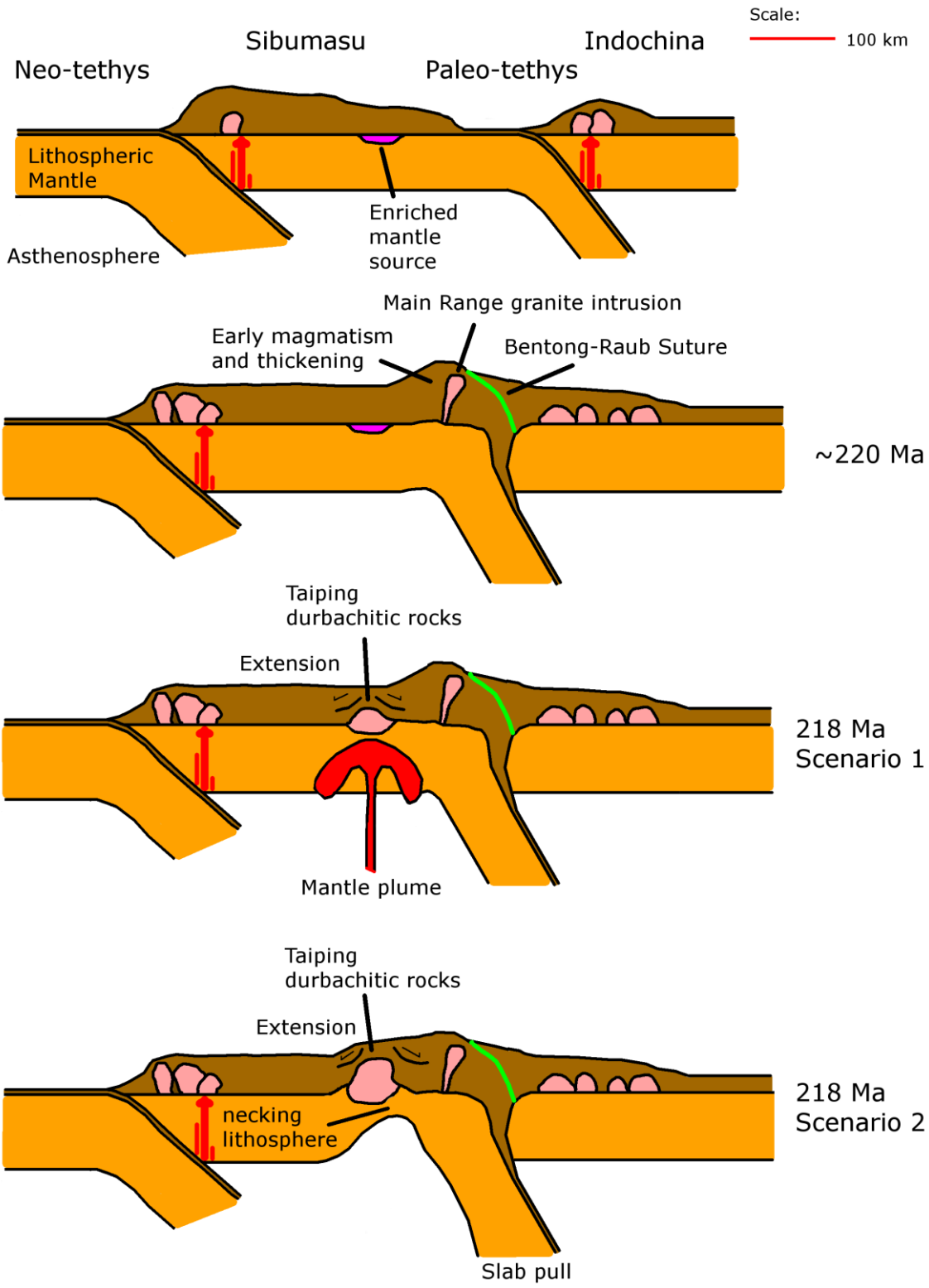

Fig. 6.8: Tectonic sketch of Taiping amphibole-bearing melagranite emplacement illustrated with four sections (after Searle et al., 2012; Metcalfe, 2013): (a) tectonic setting at ~250 Ma, (b) early collision at 220 Ma, (c) Scenario 1 (mantle plume); (d) Scenario 2 (after Sacks and Secor, 1990).

6.6 Conclusion

6.6.1 Physical characteristics and petrography

The amphibole-bearing melagranite can be described as K-Mg rich, megacrystic to porphyritic, coarse grained melagranite. Petrographic examination shows the rocks contain granite felsic mineral proportion with high amount of biotite, amphiboles with pyroxene relics and traces of pyroxene. The amphibole-bearing melagranite main mineral assemblage is: K-feldspar + quartz + plagioclase + biotite + amphibole ± orthopyroxene ± clinopyroxene. Acessory minerals in the melagranite are: zircon, apatite, titanite and allanite. Mafic microgranular enclave main mineral assemblage is: Biotite + pyroxene + amphibole + quartz + feldspar. Titanite, zircon, apatite and rutile appear as accessory minerals in the enclaves. From our data and discussion, we suggest the microgranular enclaves are minor hybridized magmas which accompanied the granitoid magma to its emplacement site.

6.6.2 Geochemistry

The geochemistry Taiping amphibole-bearing melagranite is unique, different from the typical granite. Some of Taiping melagranite samples are ultrapotassic according to Foley et al. (1987) and it is comparable to the Central European durbachite suite. Most samples are intermediate in SiO_2 composition and show high Mg and Cr. They are also high in certain incompatible elements (Ba, Zr, Rb, Th) and LREE. Microgranular enclaves are more mafic than the host rocks and some show slightly higher sodium and aluminum content. The melagranite (both ultrapotassic and non ultrapotassic) and enclaves do not show significant difference on geochemical variation diagrams. When compared to the typical Main Range granite, Taiping amphibole-bearing melagranite is relatively un-evolved or primitive in character

6.6.3 Final conclusion

Concluding, we present new petrographic and geochemical data, suggesting the existence of durbachite type magmatic rocks of Triassic age in the Taiping pluton of Peninsular Malaysia, comparable in their genetic evolution to those observed in the Central European Variscan domain. Their specific genetic evolution still needs more detailed research, but there are some reasons, which would point to an evolution very similar to the plate-tectonic evolution in Central Europe (lithospheric delamination, e.g. Stampfli et al., 2013; von Raumer et al., 2013).

References

Bacon, C. R. (1989). Crystallization of accessory phases in magmas by local saturation adjacent to phenocrysts. *Geochimica et Cosmochimica Acta, 53*(5), 1055-1066.

Bea, F., Fershtater, G., & Corretgé, L. G. (1992). The geochemistry of phosphorus in granite rocks and the effect of aluminium. *Lithos, 29*(1), 43-56.

Bowes, D. R., & Kosler, J. (1993). Geochemical Comparison of the Subvolcanic Appinite Suite of the British Caledonides and the Durbachite Suite of the Central-European Hercynides - Evidence for Associated Shoshonitic and Granitic Magmatism. *Mineralogy and Petrology, 48*(1), 47-63.

Boynton, W. V. (1984). Cosmochemistry of the rare earth elements: meteoric studies. *Rare earth element geochemistry*, 63-114.

Buehler (2004). Preparation of petrographic thin sections. *E-notes: Sum of our experience, 1*(3), 1-3.

Burton, C. K. (1986). The Baling group/Bannang Sata group of the Malay/Thai Peninsula. *Journal of Southeast Asian earth sciences*, *1*(2), 93-106.

Burton, C. K. (1973). Mesozoic. In D. J. Gobbett & C. S. Hutchison (Eds.), *Geology of the Malay Peninsula* (pp. 97-141). New York: Wiley-Interscience.

Chappell, B. W., & White, A. J. R. (1974). Two contrasting granite types. *Pacific Geology, 8*, 173–174.

Chappell, B. W., & White, A. J. R. (1992). I-Type and S-Type Granites in the Lachlan Fold Belt. *Transactions of the Royal Society of Edinburgh-Earth Sciences, 83*, 1-26.

Chappell, B. W., & White, A. J. R. (2001). Two contrasting granite types: 25 years later. *Australian Journal of Earth Sciences, 48*(4), 489-499.

Chappell, B. W., & Wyborn, D. (2012). Origin of enclaves in S-type granites of the Lachlan Fold Belt. *Lithos, 154*, 235-247.

Clemens, J. D., Stevens, G., & Farina, F. (2011). The enigmatic sources of I-type granites: The peritectic connexion. *Lithos, 126*(3-4), 174-181.

Clemens, J. D., & Stevens, G. (2012). What controls chemical variation in granitic magmas?. *Lithos, 134*, 317-329.

Cobbing, E.J., & Mallick, D.I.J. (1987). *South East Asia granite project: Field report for Peninsula Malaysia*. Keyworth: British Geological Survey.

Cobbing, E.J., Pitfield, P.E.J., Darbyshire, D.P.F., Mallick, D.I.J. (1992). *The granites of the South–East Asian tin belt*. Keyworth: British Geological Survey.

Connolly, J.A.D. (1990). Multivariable phase diagrams: an algorithm based on generalized thermodynamics. *American Journal of Science, 290*, 666–718.

Connolly, J.A.*D*. (2005). Computation of phase equilibria by linear programming: a tool for geodynamic modeling and its application to subduction zone decarbonation. *Earth and Planetary Sciences Letters, 236*, 534–541.

Connolly, J.A.D., Petrini, K. (2002). An automated strategy for calculation of phase diagram sections and retrieval of rock properties as a function of physical conditions. *Journal of Metamorphic Geology 20*, 697–708.

Connolly, J. A. D. (2009). The geodynamic equation of state: what and how. *Geochemistry, Geophysics, Geosystems*, *10*(10), 1-19.

Corfu, F., Hanchar, J. M., Hoskin, P. W., & Kinny, P. (2003). Atlas of zircon textures. *Reviews in mineralogy and geochemistry*, *53*(1), 469-500.

Didier, J. and Barbarin, B. (1991). The different type of enclaves in granites: Nomenclature. In J. Didier and B. Barbarin (1991) (Eds.), *Enclaves in Granite Petrology* (pp. 19-23). Amsterdam: Elsevier.

Erkül, S. T., & Erkül, F. (2012). Magma interaction processes in syn-extensional granitoids: the Tertiary Menderes Metamorphic Core Complex, western Turkey. *Lithos*, *142*, 16-33.

Farina, F., Stevens, G., Dini, A., & Rocchi, S. (2012). Peritectic phase entrainment and magma mixing in the late Miocene Elba Island laccolith–pluton–dyke complex (Italy). *Lithos*, *153*, 243-260.

Ferre, E. C., & Leake, B. E. (2001). Geodynamic significance of early orogenic high-K crustal and mantle melts: example of the Corsica Batholith. *Lithos, 59*(1-2), 47-67.

Foley, S. F., Venturelli, G., Green, D. H., & Toscani, L. (1987). The Ultrapotassic Rocks - Characteristics, Classification, and Constraints for Petrogenetic Models. *Earth-Science Reviews, 24*(2), 81-134.

Foley, S. (1992). Petrological characterization of the source components of potassic magmas: geochemical and experimental constraints. *Lithos, 28*(3), 187-204.

Ghani, A. A. (2000). The Western Belt granite of Peninsular Malaysia: some emergent problems on granite classification and its implication. *Geosciences Journal, 4*(4), 283-293.

Ghani, A. A. (2009). Plutonism. In C. S. Hutchison & D. N. K. Tan (Eds.), *Geology of Peninsular Malaysia* (pp. 211-231). Kuala Lumpur: The University of Malaya and Geological Society of Malaysia.

Ghani, A. A., Searle, M., Robb, L., & Chung, S.-L. (2013). Transitional I S type characteristic in the Main Range Granite, Peninsular Malaysia. *Journal of Asian Earth Sciences, 76*, 225-240.

Gill, R. (2010). *Igneous rocks and processes: a practical guide*. Hoboken: Wiley-Blackwell.

Harris, N. B., Pearce, J. A., & Tindle, A. G. (1986). Geochemical characteristics of collision-zone magmatism. *Geological Society, London, Special Publications, 19*(1), 67-81.

Harrison, T. M., & Watson, E. B. (1984). The behavior of apatite during crustal anatexis: equilibrium and kinetic considerations. *Geochimica et Cosmochimica Acta, 48*(7), 1467-1477.

Holland, T. J. B., & Powell, R. (1998). An internally consistent thermodynamic data set for phases of petrological interest. *Journal of metamorphic Geology, 16*(3), 309-343.

Holland, T. I. M., & Powell, R. (2001). Calculation of phase relations involving haplogranitic melts using an internally consistent thermodynamic dataset. *Journal of Petrology, 42*(4), 673-683.

Holub, F.V. (1989). Durbachite. In D.R. Bowes (Ed.), *Encyclopedia of Igneous and Metamorphic Petrology*. New York: Springer-Verlag Berlin Heidelberg.

Holub, F. V. (1997). Trace-element patterns in ultrapotassic rocks of the Bohemian Massif: implications for heterogeneity of their mantle sources. *Journal of the Czech Geological Society*, *42*(3), 9-0.

Holub, F.V. (2001). Ultrapotassic Intrusions of the Bohemian Massif: Insights into the Variscan Sub-continental Lithospheric Mantle? *Geolines, 13*, 61-62.

Hutchison, C. S. (2007). *Geological Evolution of South-East Asia Geological Society of Malaysia*. Kuala Lumpur: Geological Society of Malaysia.

Irvine, T., & Baragar, W. (1971). A guide to the chemical classification of the common volcanic rocks. *Canadian Journal of Earth Sciences*, *8*(5), 523-548.

Janoušek, V., Holub, F.V., Rogers, G. and Bowes, D.R., (1997). Two distinct mantle sources of Hercynian magmas intruding the Moldanubian unit, Bohemian Massif, Czech Republic. *Journal of the Czech Geological Society*, 42, 10-10.

Janoušek, V., Bowes, D. R., Rogers, G., Farrow, C. M., & Jelinek, E. (2000). Modelling diverse processes in the petrogenesis of a composite batholith: the Central Bohemian Pluton, Central European Hercynides. *Journal of Petrology*, *41*(4), 511-543.

Janoušek, V., Holub, F. V., & Gerdes, A., (2003). K-rich Magmatism in the Moldanubian Unit, Bohemian Massif—a complex story featuring variably enriched lithospheric mantle melts and their interaction with the crust. *Geolines*, 16, 48-49.

Janoušek, V. (2006). Saturnin, R language script for application of accessory-mineral saturation models in igneous geochemistry. *Geologica Carpathica*, *57*, 131-42.

Janoušek, V., & Holub, F. V. (2007). The causal link between HP-HT metamorphism and ultrapotassic magmatism in collisional orogens: case study from the Moldanubian Zone of the Bohemian Massif. *Proceedings of the Geologists Association, 118*, 75-86.

Janoušek, V., Holub, F. V., Rogers, G., & Bowes, D. R. (1997). Two distinct mantle sources of Hercynian magmas intruding the Moldanubian unit, Bohemian Massif, Czech Republic. *Journal of the Czech Geological Society, 42*(3), 10-10.

Johannes, W., & Koepke, J. (2001). Incomplete reaction of plagioclase in experimental dehydration melting of amphibolite. *Australian Journal of Earth Sciences, 48*(4), 581-590.

Jones, C. R. (1970). *The geology and mineral resources of the Grik area, Upper Perak.* Ipoh: Geological Survey Headquarters.

Kotkova, J., Schaltegger, U., & Leichmann, J. (2010). Two types of ultrapotassic plutonic rocks in the Bohemian Massif - Coeval intrusions at different crustal levels. *Lithos, 115*(1-4), 163-176.

Korotev, R. L. (2009). "Rare Earth Plots" and the Concentrations of Rare Earth Elements (REE) in Chondritic Meteorites. Retrieved 5, March, 2014, from http://meteorites.wustl.edu/goodstuff/ree-chon.htm

Kumar, S. C. (1985). The Enclaves of Peninsular Malaysian Granitoids. Unpublished doctoral dissertation, University of Malaya, Kuala Lumpur.

Kuno, H. (1959). Origin of Cenozoic petrographic provinces of Japan and surrounding areas. *Bulletin Volcanologique, 20*(1), 37-76.

Kusiak, M. A., Dunkley, D. J., Suzuki, K., Kachlík, V., Kędzior, A., Lekki, J., & Opluštil, S. (2010). Chemical (non-isotopic) and isotopic dating of Phanerozoic zircon—A case study of durbachite from the Třebíč Pluton, Bohemian Massif. *Gondwana Research, 17*(1), 153-161.

Kyaw Kyaw Nyein (2014). Petrology and Geochemistry of the Langkawi Granites, North of Peninsular Malaysia. Unpublished master dissertation, University of Malaya, Kuala Lumpur.

Langmuir, C. H., Vocke Jr, R. D., Hanson, G. N., & Hart, S. R. (1978). A general mixing equation with applications to Icelandic basalts. *Earth and Planetary Science Letters, 37*(3), 380-392.

Larsen, E. S. (1938). Some new variation diagrams for groups of igneous rocks. *The Journal of Geology, 46*, 505-520.

Liew, T. C. (1983). Petrogenesis of the Peninsular Malaysia granitoid batholith. Unpublished doctoral dissertation, University of Malaya, Kuala Lumpur.

Liew, T. C., & McCulloch, M. T. (1985). Genesis of granitoid batholiths of Peninsular Malaysia and implications for models of crustal evolution: Evidence from a Nd, Sr isotopic and U-Pb zircon study. *Geochimica et Cosmochimica Acta, 49*(2), 587-600.

Lee, C. P. (2009). Paleozoic Stratigraphy. In C. S. Hutchison & D. N. K. Tan (Eds.), *Geology of Peninsular Malaysia* (pp. 55-86). Kuala Lumpur: The University of Malaya and Geological Society of Malaysia.

LeFort, P. (1991). Enclaves of the Miocene Himalayan leucogranites. In J. Didier and B. Barbarin (1991) (Eds.), *Enclaves in Granite Petrology* (pp. 35-46). Amsterdam: Elsevier.

Le Maitre, R. W. (1976). The chemical variability of some common igneous rocks. *Journal of Petrology, 17*(4), 589-598.

Ludwig, K. R. (2003). Isoplot [computer software]. Berkeley: Berkeley Geochronology Center.

Mcdonough, W. F., & Sun, S. S. (1995). The Composition of the Earth. *Chemical Geology, 120*(3-4), 223-253.

Metcalfe, I. (1988). Origin and assembly of south-east Asian continental terranes. *Geological Society, London, Special Publications, 37*(1), 101-118.

Metcalfe, I. (2000). The Bentong-Raub Suture Zone. *Journal of Asian Earth Sciences, 18*(6), 691-712.

Metcalfe, I. (2011). Tectonic framework and Phanerozoic evolution of Sundaland. *Gondwana Research, 19*(1), 3-21.

Metcalfe, I. (2013). Gondwana dispersion and Asian accretion: Tectonic and palaeogeographic evolution of eastern Tethys. *Journal of Asian Earth Sciences, 66*, 1-33.

Miller, C. F., McDowell, S. M., & Mapes, R. W. (2003). Hot and cold granites? Implications of zircon saturation temperatures and preservation of inheritance. *Geology, 31*(6), 529-532.

Montel, J., Didier, J., and Pichavant, M. (1991). Origin of surmicaceous enclaves in intrusive granites. In J. Didier and B. Barbarin (1991) (Eds.), *Enclaves in Granite Petrology* (pp. 508-528). Amsterdam: Elsevier.

Oliver, G., Zaw, K., Hotson, M., Meffre, S., & Manka, T. (in press). U–Pb zircon geochronology of Early Permian to Late Triassic rocks from Singapore and Johor: A plate tectonic reinterpretation. *Gondwana Research*.

Parat, F., Holtz, F., Rene, M., & Almeev, R. (2010). Experimental constraints on ultrapotassic magmatism from the Bohemian Massif (durbachite series, Czech Republic). *Contributions to Mineralogy and Petrology, 159*(3), 331-347.

Paton, C., Hellstrom, J., Paul, B., Woodhead, J., & Hergt, J. (2011). Iolite: Freeware for the visualisation and processing of mass spectrometric data. *Journal of Analytical Atomic Spectrometry, 26*(12), 2508.

Peccerillo, A., & Taylor, S. R. (1976). Geochemistry of Eocene calc-alkaline volcanic rocks from the Kastamonu area, northern Turkey. *Contributions to mineralogy and petrology, 58*(1), 63-81.

Pichavant, M., Montel, J. M., & Richard, L. R. (1992). Apatite solubility in peraluminous liquids: Experimental data and an extension of the Harrison-Watson model. *Geochimica et Cosmochimica Acta, 56*(10), 3855-3861.

Raj, J. K., Tan, D. N. K. & Wan Hasiah Abdullah (2009). Cenozoic Stratigraphy. In C. S. Hutchison & D. N. K. Tan (Eds.), *Geology of Peninsular Malaysia* (pp. 133-173). Kuala Lumpur: The University of Malaya and Geological Society of Malaysia.

Rock, N. M., Bowes, D. R., & Wright, A. E. (1991). *Lamprophyres*. Glagsgow: Blackie.

Rollison, H (1993). *Using Geochemical Data: Evaluation, Presentation, Interpretation.* Singapore: Longman Scientific & Technical Limited.

Sacks, P. E., & Secor, D. T. (1990). Delamination in Collisional Orogens. *Geology, 18*(10), 999-1002.

Sauer, A. (1893). Der Granitit von Durbach im nordlichen Schwarzwald und seine Grenzfacies von Glimmersyenit (Durbachit). *Mitt Badisch Geol Landesanst, 2*, 233-276.

Scarrow, J. H., Bea, F., Montero, P., & Molina, J. F. (2009). Shoshonites, vaugnerites and potassic lamprophyres: similarities and differences between 'ultra'-high-K rocks. *Earth and Environmental Science Transactions of the Royal Society of Edinburgh, 99*, 159-175.

Searle, M. P., Whitehouse, M. J., Robb, L. J., Ghani, A. A., Hutchison, C. S., Sone, M., . . . Oliver, G. J. H. (2012). Tectonic evolution of the Sibumasu-Indochina terrane collision zone in Thailand and Malaysia: constraints from new U-Pb zircon chronology of SE Asian tin granitoids. *Journal of the Geological Society, 169*(4), 489-500.

Sevastjanova, I., Clements, B., Hall, R., Belousova, E. A., Griffin, W. L., & Pearson, N. (2011). Granitic magmatism, basement ages, and provenance indicators in the Malay Peninsula: Insights from detrital zircon U-Pb and Hf-isotope data. *Gondwana Research, 19*(4), 1024-1037.

Sláma, J., Košler, J., Condon, D.J., Crowley, J.L., Gerdes, A., Hanchar, J.M., Horstwood, M.S.A., Morris, G.A., Nasdala, L., Norberg, N., Schaltegger, U., Xchoene, B., Tubrett, M.N. and Whitehouse, M.J. (2007). Plešovice zircon-A new natural reference material for U–Pb and Hf isotopic microanalysis. *Chemical Geology, 249*, 1-35.

Stampfli, G. M., Hochard, C., Verard, C., Wilhem, C., & vonRaumer, J. (2013). The formation of Pangea. *Tectonophysics, 593*, 1-19.

Streckeisen, A. L. (1974). Classification and Nomenclature of Plutonic Rocks. Recommendations of the IUGS Subcommission on the Systematics of Igneous Rocks. Geologische Rundschau. *Internationale Zeitschrift für Geologie*, 63, 773-785.

Streckeisen, A., & Le Maitre, R. W. (1976). A chemical approximation to the modal QAPF classification of the igneous rocks. *Neues Jahrbuch für Mineralogie, Abhandlungen*, *136*, 169-206.

Sun, S. S., & McDonough, W. (1989). Chemical and isotopic systematics of oceanic basalts: implications for mantle composition and processes. *Geological Society, London, Special Publications*, *42*(1), 313-345.

Tafti, R., Mortensen, J. K., Lang, J. R., Rebagliati, M., & Oliver, J. L. (2009). Jurassic U-Pb and Re-Os ages for the newly discovered Xietongmen Cu-Au porphyry district, Tibet, PRC: implications for metallogenic epochs in the southern Gangdese belt. *Economic Geology, 104*(1), 127-136.

Vernon, R. H. (1984). Microgranitoid enclaves in granites-globules of hybrid magma quenched in a plutonic environment. *Nature*, *309*, 438-439.

von Raumer, J. F., Finger, F., Veselá, P., & Stampfli, G. (2013). Durbachites-Vaugnerites - a geodynamic marker in the central European Variscan orogen. *Terra Nova*, *0*, 1-11.

Weill, D. F., & Drake, M. J. (1973). Europium anomaly in plagioclase feldspar: experimental results and semiquantitative model. *Science*, *180*(4090), 1059-1060.

Wheller, G. E. (1986). Petrogenetic Studies of Basalt-Andesite -Dacite Volcanism at Batur Volcano, Bali, and the Causes of K-variation in Sunda- Banda Arc Basalts. Unpublished doctoral dissertation, University of Tasmania, Holbart.

White, R. W., Powell, R., & Holland, T. J. B. (2001). Calculation of partial melting equilibria in the system Na2O–CaO–K2O–FeO–MgO–Al2O3–SiO2–H2O (NCKFMASH). *Journal of Metamorphic Geology*, *19*(2), 139-153.

Wu, H. H., Tsai, Y. B., Lee, T. Y., Lo, C. H., Hsieh, C. H., & Van Toan, D. (2004). 3-D shear wave velocity structure of the crust and upper mantle in South China Sea and its surrounding regions by surface wave dispersion analysis. *Marine Geophysical Researches*, *25*(1-2), 5-27.

Appendix 1: Geochemistry data

Location	Bukit Berapit			Batu Kurau			Taiping
Label	BB-1	***BB-2***	***BB-3***	BK-1	BK-2	***BK-3***	T-1
Type	Melagranite						
(in wt. %)							
SiO_2	68.0	63.5	64.8	66.3	67.8	61.4	68.3
Al_2O_3	14.41	13.53	12.86	13.83	13.52	11.36	14.07
FeO est.	2.52	4.91	4.75	3.48	3.33	6.15	3.28
Fe_2O_3 est.	0.31	0.61	0.59	0.43	0.41	0.76	0.40
ΣFe_2O_3	3.11	6.05	5.86	4.29	4.11	7.58	4.04
CaO	2.83	1.75	1.45	2.67	3.08	5.55	3.31
MgO	1.83	3.66	3.51	2.70	2.50	6.39	1.94
Na_2O	2.63	1.61	1.35	1.84	2.01	1.20	2.77
K_2O	4.95	7.00	7.31	5.43	4.29	4.89	4.13
MnO	0.04	0.08	0.07	0.06	0.06	0.16	0.06
TiO_2	0.56	1.12	1.06	0.76	0.70	0.97	0.68
P_2O_5	0.20	0.38	0.35	0.28	0.26	0.36	0.21
Cr_2O_3	0.039	0.039	0.055	0.044	0.054	0.077	0.059
LOI	1.12	0.71	0.78	1.08	1.06	1.12	0.94
SUM	99.72	99.43	99.46	99.28	99.44	101.06	100.51
(in ppm)							
Cr XRF	266.84	266.84	376.31	301.05	369.47	526.83	403.68
Ba	742	368	379	991	677	987	532
Cs	21.0	49.9	51.7	17.1	16.3	12.5	38.8
Ga	17.9	20.8	18.0	17.7	17.4	16.1	18.3
Hf	9.0	15.3	13.5	11.1	9.5	11.4	9.3
Nb	23.8	44.7	45.2	24.9	23.4	27.6	29.8
Rb	306.4	610.3	617.8	350.1	303.5	321.0	290.3
Sr	238.8	100.3	93.0	264.7	261.9	165.1	237.2
Ta	3.1	6.0	5.0	2.6	2.8	2.1	5.7
Zr	291.0	500.2	514.8	387.3	365.1	392.2	286.9
Y	33.2	60.9	57.4	32.8	30.1	44.1	61.6
Th	69.0	92.3	85.0	60.2	61.8	107.6	42.8
U	22.2	35.9	34.7	16.3	17.5	18.1	13.9
Pb	16.2	31.3	13.2	11.4	11.0	11.3	23.0
La	75.8	17.5	17.0	55.4	62.7	61.8	51.2
Ce	162.9	50.7	49.4	112.5	125.8	129.8	111.6
Pr	18.31	8.17	7.45	13.71	15.06	15.45	13.84
Nd	63.0	38.1	35.5	54.7	66.4	60.6	56.3
Sm	11.71	12.25	12.34	10.63	10.92	13.51	14.02
Eu	1.46	0.59	0.67	1.66	1.47	1.22	1.33
Gd	8.63	11.58	10.64	8.13	7.54	10.36	12.86
Tb	1.27	1.81	1.76	1.15	1.04	1.52	2.12
Dy	6.96	10.26	9.53	6.10	5.65	7.22	12.00
Ho	1.24	2.28	2.19	1.13	1.13	1.64	2.07
Er	4.06	5.97	5.95	3.33	2.96	4.15	6.42
Tm	0.52	0.92	0.88	0.50	0.44	0.60	0.89
Yb	3.13	5.40	5.82	2.85	2.89	4.16	5.44
Lu	0.46	0.86	0.84	0.39	0.38	0.55	0.69
Co	6.0	14.0	11.0	9.8	9.8	18.4	8.9
Cu	7.8	4.3	6.4	10.9	10.6	11.2	50.0
V	61	113	107	78	79	104	67
Zn	29	66	56	39	36	42	46
Ni	14.8	26.8	27.5	23.7	22.3	52.9	19.6
Larsen DI	20.4	17.9	19.2	18.7	18.0	7.3	18.4
Kuno SI	14.9	20.6	20.0	19.5	19.9	33.0	15.5

Location	Baling-Gerik				Lenggong		
Label	***BG-1***	BG-2	***BG-3***	***BH1 3B***	BH1 4-5	***BH1 6A***	***BH1 8A***
Type	Melagranite						
(in wt. %)							
SiO_2	65.3	67.9	61.3	65.3	66.2	60.2	63.3
Al_2O_3	13.82	12.94	13.56	13.82	14.33	16.13	14.59
FeO est.	3.88	4.14	6.15	4.65	3.53	4.51	4.43
Fe_2O_3 est.	0.48	0.51	0.76	0.57	0.44	0.56	0.55
ΣFe_2O_3	4.79	5.10	7.59	5.74	4.36	5.56	5.46
CaO	2.93	2.73	3.04	2.84	2.91	3.41	3.21
MgO	3.12	3.06	5.11	3.47	2.84	3.63	3.55
Na_2O	2.07	2.14	1.90	1.89	2.13	2.37	1.94
K_2O	5.29	3.59	3.86	4.58	4.38	5.31	5.32
MnO	0.06	0.06	0.11	0.05	0.05	0.06	0.06
TiO_2	0.85	0.83	1.23	0.99	0.81	1.04	0.97
P_2O_5	0.33	0.31	0.58	0.37	0.32	0.39	0.38
Cr_2O_3	0.046	0.047	0.053	0.083	0.036	0.044	0.046
LOI	0.80	1.11	1.23	0.82	1.32	1.58	0.69
SUM	99.41	99.82	99.56	99.95	99.66	99.72	99.52
(in ppm)							
Cr XRF	314.73	321.57	362.63	567.89	246.31	301.05	314.73
Ba	1296	546	370	1157	1269	1620	1632
Cs	14.6	33.0	57.2	7.5	10.0	11.6	8.2
Ga	17.2	17.5	22.3	17.8	18.5	20.8	17.7
Hf	11.5	12.9	14.9	11.1	10.5	11.6	11.6
Nb	26.5	28.9	36.6	22.0	21.1	26.1	22.9
Rb	338.8	385.8	582.4	265.1	254.3	312.5	301.5
Sr	285.9	196.8	133.8	270.2	337.6	383.0	324.7
Ta	1.8	3.4	2.5	1.6	1.3	1.3	1.3
Zr	402.5	383.2	487.2	394.5	375.4	433.2	414.2
Y	32.7	33.7	46.7	22.1	23.0	25.4	22.1
Th	86.8	62.8	24.0	53.5	85.9	39.4	44.3
U	10.5	20.7	10.1	6.0	14.2	6.5	6.0
Pb	24.9	9.6	4.9	0.0	7.6	7.4	4.5
La	135.5	56.4	21.9	56.4	131.2	58.0	58.7
Ce	257.6	119.3	50.9	120.6	255.9	123.2	122.5
Pr	28.04	13.52	7.67	14.04	27.64	14.89	14.60
Nd	96.1	50.2	34.9	54.4	93.1	61.2	56.1
Sm	15.92	10.12	9.37	9.35	13.84	11.05	9.96
Eu	1.83	1.31	0.76	1.69	1.99	2.17	1.96
Gd	10.49	7.37	9.03	7.05	8.41	8.00	7.35
Tb	1.28	1.14	1.43	0.96	1.09	1.12	0.97
Dy	6.54	6.16	7.99	4.95	5.22	5.82	4.64
Ho	1.13	1.20	1.66	0.98	0.91	1.00	0.98
Er	3.00	3.74	4.89	2.20	2.29	2.74	2.18
Tm	0.46	0.53	0.65	0.30	0.33	0.33	0.31
Yb	2.67	3.38	4.20	1.93	1.73	2.14	1.81
Lu	0.33	0.51	0.58	0.26	0.24	0.30	0.27
Co	12.0	13.7	17.0	13.6	11.3	13.7	15.2
Cu	12.8	18.3	13.6	0.0	13.8	10.6	16.7
V	98	96	135	91	79	103	100
Zn	55	53	81	0	47	54	50
Ni	26.8	34.0	33.9	0.0	24.9	27.7	32.9
Larsen DI	17.1	16.3	10.0	15.4	17.2	13.8	15.2
Kuno SI	21.0	22.8	28.7	22.9	21.3	22.2	22.5

Location	Lenggong						
Label	***BH1 9A***	BH2 2B	BH2 3B	***BH2 5-6***	BH2 7B	***BH3 2B***	BH3 3B
Type	Melagranite						
(in wt. %)							
SiO_2	59.2	59.8	66.4	60.9	58.4	63.1	65.8
Al_2O_3	14.96	15.31	13.03	14.34	15.48	15.30	14.42
FeO est.	5.42	4.67	4.33	4.92	4.79	3.84	3.23
Fe_2O_3 est.	0.67	0.58	0.53	0.61	0.59	0.47	0.40
ΣFe_2O_3	6.69	5.76	5.34	6.07	5.91	4.74	3.98
CaO	4.76	4.25	2.83	3.85	4.81	3.16	2.24
MgO	4.90	5.76	4.95	6.06	6.05	3.02	2.57
Na_2O	2.18	2.50	2.03	2.07	2.50	2.01	1.62
K_2O	4.38	3.55	3.88	4.23	3.66	6.30	7.23
MnO	0.08	0.05	0.06	0.06	0.06	0.05	0.04
TiO_2	0.94	1.22	0.97	1.15	1.09	0.85	0.66
P_2O_5	0.46	0.62	0.26	0.42	0.41	0.33	0.27
Cr_2O_3	0.042	0.057	0.076	0.075	0.072	0.054	0.037
LOI	1.04	0.59	0.77	0.73	0.64	0.91	0.70
SUM	99.63	99.47	100.60	99.88	99.08	99.82	99.57
(in ppm)							
Cr XRF	287.36	389.99	519.99	509.73	492.62	369.47	253.15
Ba	1210	502	897	1088	940	1904	2240
Cs	8.6	14.4	13.6	12.5	11.5	12.5	12.7
Ga	19.9	22.3	17.7	19.8	20.3	18.4	16.4
Hf	13.7	17.2	9.0	13.4	13.7	10.4	10.1
Nb	27.7	35.0	28.3	30.5	26.0	22.7	19.3
Rb	275.3	328.1	300.0	319.3	291.1	334.5	331.7
Sr	321.1	319.4	273.7	330.7	446.3	328.6	305.6
Ta	1.8	2.4	1.9	2.0	1.6	1.4	1.1
Zr	491.7	599.1	328.5	477.8	500.5	362.4	342.9
Y	45.1	35.1	18.0	26.3	27.3	23.3	19.0
Th	104.8	31.6	147.0	49.3	52.7	22.3	31.9
U	10.8	14.7	8.3	7.6	6.2	5.4	5.9
Pb	7.0	3.4	7.5	4.2	4.2	11.4	20.8
La	238.3	56.3	55.4	73.9	108.3	28.8	34.0
Ce	478.7	134.1	117.5	157.0	215.1	63.9	72.0
Pr	53.50	16.94	13.63	18.25	24.18	8.18	8.85
Nd	185.2	68.4	52.0	67.6	90.7	35.3	35.1
Sm	27.26	13.81	8.77	11.94	13.49	7.43	7.16
Eu	3.02	1.87	1.66	2.02	2.49	2.01	1.84
Gd	16.79	10.50	5.88	8.58	8.69	6.09	5.70
Tb	2.10	1.44	0.80	1.13	1.11	0.90	0.82
Dy	10.12	7.46	3.75	5.65	5.77	4.47	4.04
Ho	1.58	1.34	0.70	1.04	0.99	0.94	0.69
Er	4.58	3.20	1.79	2.72	2.60	2.19	2.03
Tm	0.65	0.45	0.23	0.38	0.34	0.32	0.27
Yb	3.86	2.46	1.22	2.01	2.43	1.70	1.58
Lu	0.52	0.38	0.22	0.34	0.33	0.27	0.25
Co	20.4	19.2	16.1	19.9	19.7	11.4	9.7
Cu	30.5	13.0	14.3	14.0	14.7	12.4	12.9
V	115	142	85	122	121	81	66
Zn	50	56	53	54	47	57	47
Ni	41.8	69.9	58.6	69.8	74.2	28.6	24.8
Larsen DI	9.0	8.8	13.9	9.7	7.5	17.3	21.1
Kuno SI	27.9	33.8	31.5	33.9	34.4	19.3	17.1

Location	Lenggong						
Label	DH1 10A	Dh1 1516	***DH1 17A***	DH1 18A	DH1 19A	***DH1 1B***	***DH1 20A***
Type	Melagranite						
(in wt. %)							
SiO_2	63.7	64.1	65.5	63.0	61.9	62.3	62.5
Al_2O_3	15.34	14.25	13.18	15.78	14.75	15.19	15.17
FeO est.	3.52	4.55	4.18	3.14	4.83	3.96	3.63
Fe_2O_3 est.	0.43	0.56	0.52	0.39	0.60	0.49	0.45
ΣFe_2O_3	4.34	5.62	5.16	3.87	5.96	4.89	4.48
CaO	2.76	3.53	3.37	2.19	4.15	3.22	2.74
MgO	2.74	3.72	3.38	2.47	4.02	3.24	3.03
Na_2O	1.99	2.11	1.73	1.70	2.22	1.96	1.71
K_2O	6.69	3.93	4.52	8.78	3.93	6.24	6.74
MnO	0.05	0.06	0.06	0.04	0.06	0.05	0.05
TiO_2	0.78	0.99	0.97	0.64	1.11	0.89	0.81
P_2O_5	0.31	0.41	0.37	0.25	0.43	0.35	0.33
Cr_2O_3	0.049	0.050	0.041	0.043	0.045	0.041	0.038
LOI	0.88	1.15	1.45	0.76	1.00	0.81	1.61
SUM	99.63	99.85	99.73	99.52	99.58	99.18	99.21
(in ppm)							
Cr XRF	335.26	342.10	280.52	294.21	307.89	280.52	260.00
Ba	2210	920	1277	3075	924	1995	2399
Cs	12.6	21.1	13.8	14.9	14.5	11.6	8.6
Ga	17.5	19.3	15.8	15.4	19.3	17.8	16.5
Hf	9.4	12.4	12.1	8.2	13.8	12.0	10.6
Nb	20.2	24.2	23.8	17.2	27.3	22.4	18.9
Rb	342.8	365.1	311.9	396.3	336.3	339.3	377.0
Sr	356.2	312.8	281.9	385.8	316.3	358.3	379.4
Ta	1.2	1.5	1.4	1.3	1.5	1.5	1.1
Zr	349.6	453.4	433.0	288.9	493.7	424.8	359.6
Y	23.7	33.9	25.6	21.9	29.7	25.2	20.4
Th	63.5	87.1	51.7	42.2	48.0	65.1	44.1
U	7.4	8.0	6.9	5.6	5.5	6.8	4.9
Pb	13.3	10.9	9.3	13.2	7.5	9.1	22.1
La	83.7	193.5	88.1	76.7	98.1	142.5	88.5
Ce	170.3	377.5	180.5	155.8	200.0	276.5	175.7
Pr	19.06	40.69	20.18	17.37	21.99	29.99	19.35
Nd	68.7	139.1	72.5	59.0	80.8	100.6	68.1
Sm	10.63	19.30	11.51	9.98	13.10	14.51	11.05
Eu	2.09	2.24	1.84	2.24	2.06	2.23	2.23
Gd	7.38	12.16	8.41	6.80	9.77	8.70	7.24
Tb	1.00	1.47	1.04	0.89	1.16	1.09	0.89
Dy	5.20	7.44	5.47	4.45	5.80	5.22	4.72
Ho	0.82	1.21	0.95	0.80	1.01	0.92	0.68
Er	2.10	3.23	2.52	2.07	2.72	2.43	1.93
Tm	0.34	0.43	0.32	0.29	0.41	0.33	0.26
Yb	1.69	2.56	2.13	1.67	2.23	1.94	1.52
Lu	0.26	0.37	0.28	0.22	0.35	0.30	0.30
Co	12.6	14.0	15.0	16.0	15.3	14.3	10.7
Cu	13.7	15.2	15.9	15.5	14.5	10.9	11.2
V	82	108	102	65	112	91	85
Zn	44	53	53	37	57	47	50
Ni	25.3	33.1	30.6	27.1	33.2	27.1	25.0
Larsen DI	18.9	13.5	15.4	22.0	11.6	16.6	18.2
Kuno SI	17.8	25.0	23.6	15.0	25.8	20.4	19.5

Location				Lenggong			
Label	DH1 21B	***DH1 23B***	***DH1 24A***	DH1 27A	***DH1 2B***	***DH1 3A***	DH1 4B
Type				Melagranite			
(in wt. %)							
SiO_2	59.4	61.6	62.5	65.8	65.4	65.4	67.3
Al_2O_3	15.27	15.27	14.62	14.29	13.76	13.81	14.55
FeO est.	5.53	4.20	4.27	3.70	4.08	4.39	2.71
Fe_2O_3 est.	0.68	0.52	0.53	0.46	0.50	0.54	0.33
ΣFe_2O_3	6.82	5.18	5.27	4.56	5.03	5.41	3.34
CaO	4.69	3.06	3.38	3.73	3.23	3.18	2.85
MgO	4.73	3.38	3.52	2.92	3.20	3.47	1.94
Na_2O	2.31	2.08	2.04	2.45	1.98	1.94	2.18
K_2O	4.07	6.04	5.21	3.49	4.60	4.70	5.67
MnO	0.08	0.06	0.05	0.05	0.06	0.06	0.03
TiO_2	1.27	0.86	0.94	0.81	0.88	0.95	0.62
P_2O_5	0.49	0.36	0.38	0.30	0.36	0.36	0.26
Cr_2O_3	0.042	0.041	0.036	0.039	0.064	0.039	0.050
LOI	0.82	0.79	0.63	0.84	0.93	0.67	0.92
SUM	99.99	98.72	98.58	99.28	99.49	99.99	99.71
(in ppm)							
Cr XRF	287.36	280.52	246.31	266.84	437.89	266.84	342.10
Ba	901	1777	1439	689	1366	1266	1727
Cs	15.3	9.6	9.3	15.0	9.8	12.2	8.9
Ga	21.4	16.8	17.6	17.3	17.6	18.0	15.8
Hf	16.2	9.5	9.3	9.9	11.6	12.6	8.0
Nb	31.7	19.5	20.8	23.5	21.9	25.5	16.8
Rb	359.2	294.6	280.7	241.8	289.4	312.0	273.3
Sr	317.7	297.6	280.4	271.6	300.1	275.2	341.7
Ta	1.6	0.9	1.4	2.1	1.4	1.6	1.1
Zr	576.0	361.3	340.7	354.2	417.1	459.0	302.0
Y	29.9	22.4	24.0	31.6	24.1	23.5	17.4
Th	42.5	79.4	63.8	68.9	57.5	52.3	38.4
U	6.1	6.2	6.6	11.6	5.9	6.9	7.3
Pb	8.8	10.0	6.6	6.7	15.7	9.8	16.4
La	77.1	139.3	126.2	181.9	54.8	43.3	39.5
Ce	163.1	277.2	261.7	371.7	112.9	94.3	82.6
Pr	18.97	28.69	27.26	38.12	13.33	11.64	9.68
Nd	72.1	98.0	92.4	122.3	51.2	44.9	36.3
Sm	13.20	13.85	13.70	17.73	9.29	8.98	6.80
Eu	2.02	1.91	1.86	1.73	1.84	1.73	2.04
Gd	9.95	8.62	8.92	10.43	7.14	7.23	5.24
Tb	1.25	1.02	1.08	1.33	1.05	0.96	0.71
Dy	6.36	4.74	5.18	6.86	4.96	5.11	3.50
Ho	1.16	0.79	0.86	1.15	0.95	0.98	0.71
Er	2.87	2.18	2.18	3.05	2.22	2.41	1.71
Tm	0.38	0.32	0.29	0.43	0.31	0.34	0.30
Yb	2.20	1.51	2.03	2.46	1.93	1.98	1.59
Lu	0.34	0.26	0.27	0.34	0.27	0.30	0.25
Co	17.6	12.0	12.3	10.0	13.1	14.4	9.6
Cu	16.4	12.1	13.1	12.5	16.2	17.2	8.6
V	142	89	95	79	97	88	59
Zn	65	54	55	44	53	54	37
Ni	37.5	28.9	29.3	25.7	33.6	31.0	20.3
Larsen DI	8.9	15.9	14.9	15.1	15.9	15.5	20.6
Kuno SI	27.3	20.8	22.6	22.4	22.3	23.1	15.1

Location				Lenggong
Label	***DH1 6B***	***DH1 8A***	***DH1 9A***	Dh1 1112
Type		Melagranite		
(in wt. %)				
SiO_2	64.4	64.2	64.6	63.5
Al_2O_3	14.67	15.06	14.26	14.53
FeO est.	3.87	3.82	3.95	4.31
Fe_2O_3 est.	0.48	0.47	0.49	0.53
ΣFe_2O_3	4.77	4.71	4.87	5.32
CaO	3.31	3.25	3.22	3.54
MgO	3.07	2.99	3.21	3.36
Na_2O	2.07	2.20	2.01	2.08
K_2O	5.26	5.44	4.89	4.05
MnO	0.05	0.05	0.05	0.06
TiO_2	0.88	0.85	0.90	0.96
P_2O_5	0.33	0.34	0.38	0.38
Cr_2O_3	0.043	0.042	0.034	0.048
LOI	0.86	0.80	1.05	1.76
SUM	99.71	99.93	99.47	99.56
(in ppm)				
Cr XRF	294.21	287.36	232.63	328.42
Ba	1558	1689	1229	1211
Cs	10.7	13.0	12.9	27.4
Ga	18.3	18.5	18.5	19.0
Hf	11.9	10.6	14.0	12.4
Nb	20.9	23.0	23.3	24.9
Rb	317.7	319.3	356.8	294.7
Sr	331.1	338.6	345.2	310.6
Ta	1.1	1.3	1.8	1.7
Zr	433.7	404.6	504.4	433.0
Y	22.6	26.1	26.6	30.9
Th	40.0	64.7	81.6	74.6
U	6.8	9.8	10.1	13.7
Pb	11.8	9.8	8.9	15.4
La	59.7	87.8	74.0	154.4
Ce	121.2	176.2	147.4	310.3
Pr	14.13	19.52	16.96	33.08
Nd	55.2	66.9	62.1	113.5
Sm	9.35	10.93	10.69	16.85
Eu	2.02	2.01	1.98	2.03
Gd	7.16	8.06	7.92	10.80
Tb	0.95	1.04	1.05	1.30
Dy	4.98	5.48	5.14	6.49
Ho	0.79	0.92	0.94	1.10
Er	2.27	2.34	2.70	2.91
Tm	0.30	0.34	0.33	0.40
Yb	1.75	2.37	2.15	2.38
Lu	0.26	0.29	0.28	0.34
Co	12.0	13.1	12.0	13.0
Cu	14.3	15.0	12.5	11.6
V	88	83	90	98
Zn	48	47	48	55
Ni	26.9	28.8	27.3	30.5
Larsen DI	16.5	16.8	16.0	14.0
Kuno SI	20.8	20.0	22.1	23.4

Appendix 2: Apatite saturation thermometry

Sample	A/CNK	P_2O_5 (wt. %)	Temp. (°C) Harrison and Watson (1984)	Temp. (°C) Bea et al. (1992)
BB-1	0.97	0.20	958.41	-
BB-2	**1.01**	0.38	-	981.06
BB-3	**1.01**	0.35	-	986.72
BK-1	**1.01**	0.28	-	976.47
BK-2	1.00	0.26	987.36	-
BK-3	0.65	0.36	957.27	-
T-1	0.94	0.21	967.18	-
BG-1	0.96	0.33	990.54	-
BG-2	**1.05**	0.31	-	973.02
BG-3	**1.06**	0.58	-	969.53
BH1 3B	**1.04**	0.37	-	967.65
BH1 4-5	**1.06**	0.32	-	947.14
BH1 6A	**1.02**	0.39	-	936.97
BH1 8A	0.99	0.38	986.70	-
BH1 9A	0.88	0.46	963.72	-
BH2 2B	0.98	0.62	1014.78	-
BH2 3B	**1.03**	0.26	-	950.58
BH2 5-6	0.96	0.42	971.46	-
BH2 7B	0.92	0.41	937.40	-
BH3 2B	0.96	0.33	965.88	-
BH3 3B	0.99	0.27	970.76	-
DH1 1B	0.96	0.35	964.24	-
DH1 2B	0.98	0.36	1002.90	-
DH1 3A	0.98	0.36	1002.90	-
DH1 4B	0.98	0.26	982.15	-
DH1 6B	0.97	0.33	980.62	-
DH1 8A	0.98	0.34	982.24	-
DH1 9A	0.99	0.38	1001.27	-
DH1 10A	0.99	0.31	964.72	-
Dh1 1112	**1.02**	0.38	-	969.64
Dh1 1516	**1.01**	0.41	-	998.33
DH1 17A	0.95	0.37	1007.57	-
DH1 18A	0.97	0.25	929.78	-
DH1 19A	0.95	0.43	987.23	-
DH1 20A	**1.01**	0.33	-	954.33
DH1 21B	0.91	0.49	975.22	-
DH1 23B	0.98	0.36	959.67	-
DH1 24A	0.97	0.38	977.48	-
DH1 27A	0.98	0.30	983.86	-

The temperature ranges from 1012.5 °C to 1092.9 °C. Average: 1058.8 °C

Appendix 3: LA ICP-MS U–Pb geochronology data for BB-1

Zircon	U (ppm)	Th (ppm)	Pb (ppm)	Th/U	$^{207}Pb/^{235}U$	2σ (abs)	$^{206}Pb/^{238}U$
BB-1_1	2030	1600	524	0.79	0.239	0.071	0.0351
BB-1_2	1678	505	154	0.30	0.2401	0.071	0.035
BB-1_3	1098	197.3	64.1	0.18	0.238	0.069	0.03497
BB-1_4	**1260**	**980**	**310**	**0.78**	**0.2494**	**0.073**	**0.0363**
BB-1_5	1536	890	290	0.58	0.2441	0.073	0.0352
BB-1_6	870	419	132.5	0.48	0.2445	0.072	0.03507
BB-1_7	345.9	117.6	35.7	0.34	0.2487	0.072	0.03387
BB-1_8	886	100.8	33.1	0.11	0.2404	0.07	0.03442
BB-1_9	566	526	164.4	0.93	0.2558	0.073	0.03395
BB-1_10	919	123.6	38.5	0.13	0.2477	0.07	0.03415
BB-1_11	478	219.6	62.5	0.46	0.244	0.071	0.03367
BB-1_12	667	156.6	47.9	0.23	0.2516	0.073	0.03399
BB-1_13	727	85.4	23.6	0.12	0.2487	0.072	0.0346
BB-1_14	844	113	31.8	0.13	0.2426	0.072	0.0343
BB-1_15	873	468	124.5	0.54	0.2482	0.073	0.03418
BB-1_16	971	127.2	46.3	0.13	0.2417	0.07	0.03437
BB-1_17	706	204.8	83.2	0.29	0.2424	0.071	0.03418
BB-1_18	1141	319	149	0.28	0.2396	0.07	0.0347
BB-1_19	1148	655	440	0.57	0.273	0.076	0.03462
BB-1_20	591	256.4	185.5	0.43	0.242	0.069	0.0345

2σ (abs)	Rho	$^{207}Pb/^{206}U$	2σ (abs)	$^{206}Pb/^{238}U$ age	2σ (abs)	$^{207}Pb/^{235}U$ age	2σ (abs)
0.0011	0.71394	0.0496	0.014	223.5	6.9	217.7	58
0.001	0.69225	0.0503	0.014	221.5	6.3	218.8	59
0.00094	0.58687	0.0489	0.014	221.9	5.9	216.7	56
0.0011	**0.69498**	**0.0505**	**0.014**	**229.4**	**6.7**	**225.6**	**59**
0.0012	0.70372	0.0501	0.014	223	7.6	220.9	60
0.00098	0.45165	0.0505	0.014	222.1	6.1	221.5	59
0.00087	0.47694	0.0511	0.014	214.6	5.4	224.8	59
0.00098	0.58764	0.0492	0.014	218	6.1	218.7	57
0.00084	0.42281	0.052	0.014	215.1	5.2	229.8	60
0.00078	0.59373	0.05	0.014	216.4	4.9	224.8	58
0.0008	0.64896	0.05	0.014	213.3	5	220.8	57
0.00086	0.64686	0.0505	0.014	215.3	5.4	227.6	59
0.00093	0.59436	0.05	0.014	219.2	5.8	225.5	59
0.00093	0.62704	0.0495	0.014	217.1	5.8	220.1	58
0.00091	0.68067	0.0507	0.014	216.5	5.7	224.9	59
0.00092	0.61887	0.0501	0.014	217.7	5.7	219.9	57
0.00083	0.50727	0.0513	0.014	216.9	5.2	220.8	57
0.00082	0.64045	0.0501	0.014	219.8	5.1	217.1	57
0.00079	0.36901	0.057	0.015	219.3	4.9	239	53
0.001	0.49919	0.0513	0.014	218.7	6.4	220	56

*Bold: rejected

Appendix 4: Perple_X model data

	Greywacke from Clemens et al. (2011)	Minette from Rock (1991)
SiO_2	70.35	51.1
Al_2O_3	14.24	7.6
MgO	2.22	11.4
CaO	2.64	4.8
Na_2O	3.06	0.65
K_2O	2.11	7.3
TiO_2	0.8	4.1
FeO	5.38	7.8
H_2O	0.6	3.2

Mix greywacke (75%) and minette (25%)

	Greywacke from Clemens et al. (2011)	Minette from Rock (1991)	Mixture
SiO_2	70.35*(0.75)	51.18*(0.25)	65.5375
Al_2O_3	14.24*(0.75)	7.6*(0.25)	12.58
MgO	2.22*(0.75)	11.4*(0.25)	4.515
CaO	2.64*(0.75)	4.8*(0.25)	3.18
Na_2O	3.06*(0.75)	0.65*(0.25)	2.4575
K_2O	2.11*(0.75)	7.3*(0.25)	3.4075
TiO_2	0.8*(0.75)	4.1*(0.25)	1.625
FeO	5.38*(0.75)	7.8*(0.25)	5.985
H_2O	0.6*(0.75)	3.2*(0.25)	1.25

Appendix 5: Thin section preparation

Collected melagranite samples will then undergo processing into thin section for petrographic analysis. The thin section making process employs methods from Buehler (2004), described in the following section:

1. The sample rock is first cut into small (small enough to fit on the prepared glass slide) rectangle blocks (sometimes called as "chip"). Then the block is grinded to produce a flat, smooth surface, free from any obvious deformation. This will help the block to cement properly onto the glass slide later on.
2. The block is then heated up (using a hot plate) and glued to the glass slide using a batch of epoxy (usually two parts epoxy with one part hardener).
3. After the epoxy is cured, the excess rock block is cut off, leaving a thin slice of rock with the thin section.
4. The thin slice of rock that is left on the slide is grinded to the correct thickness (estimated during the grinding process with the help of a microscope. Acceptable thickness is about 30 μm, with near perfect parallelism)

Note: Appendix 1 calculation formula are shown below

1. When Fe_2O_3 needs to be estimated from an analysis that lists only total iron oxide, a useful convention is to set $Fe_2O_3^{est} = 0.1 \times \Sigma Fe_2O_3$
2. $FeO^{est} = (\Sigma Fe_2O_3 - Fe_2O_3^{est})/1.11$
3. Cr (in ppm) = Cr2O3 (in wt. %) × 0.6842 × 10000
4. Larsen differentiation index (DI) = $(1/3SiO_2 + K_2O) – (FeO + MgO + CaO)$
5. Kuno solidification index (SI) =

   $100 \times (MgO / (MgO + Fe_2O_3 + FeO + Na_2O + K_2O))$